

MAPK9: Ein neuer Regulator des Triglyzerid-Stoffwechsels, entdeckt durch siRNA Screening

DISSERTATION

zur Erlangung des akademischen Grades

Doctor rerum naturalium
(Dr. rer. nat.)

vorgelegt

der Fakultät Mathematik und Naturwissenschaften
der Technischen Universität Dresden

von

Vinciane Grimard

geboren am 30. Oktober 1978 in Brüssel

Gutachter:

Prof. Dr. Gerhard Rödel
Prof. Dr. Walter Nickel
Dr. Christoph Thiele

Eingereicht am 25. Juni 2007

Tag der Verteidigung am 4. Oktober 2007

Faculty of Sciences
Dresden University of Technology

**MAPK9:
A New Regulator of Triglyceride
Metabolism revealed by siRNA Screening**

Thesis presented for
the obtention of the academic degree
Doctor rerum naturalium (Dr. rer. nat.)

Vinciane Grimard

Summary

Lipid homeostasis is an essential factor for proper function both at the level of a cell and of an organism. Dysregulation of this process is responsible for some of the major health concerns of our societies such as obesity and atherosclerosis. Considering the wide variety of lipids and the high dynamic of the system, it is clear that regulation is required to keep the appropriate balance between the different lipids. Although a few regulation pathways are already characterized, some others still wait to be discovered. In order to unravel new players involved in lipid regulation, a screening procedure was developed combining RNA interference in HeLa cells and thin layer chromatography. Thereby, it is possible to monitor modifications of lipid composition resulting from siRNA knock-down. Furthermore, the potential of mass spectrometry as a lipid analysis tool in large-scale studies was evaluated.

This method was then applied to an essential family of regulatory proteins, the kinases. Lipid composition of 600 kinases knock-downs was analyzed. Mostly, variations in triglyceride and cholesterol levels were observed, suggesting that these lipids are more subject to variation in the cells. Unfortunately, it appears that the screen suffered from a high-rate of off-targets effects, implying that most of the phenotypes observed can't reliably be linked to the corresponding kinase knock-downs.

However, several interesting conclusions can still be derived from this screen. First, it was observed that several siRNA induce a decrease in cholesterol, which is coupled to accumulation of a new lipid. Several lines of evidence suggest that this new lipid is in fact a methylated sterol precursor such as lanosterol or demethylsterol. Previously, HMG-CoA reductase was considered as the rate-limiting enzyme of cholesterol biosynthesis and the major regulated step of this process. These data show that another major regulation step occurs more downstream in the pathway at the level of methylated cholesterol precursors.

Furthermore, MAPK9 was identified as a new regulator of triglyceride homeostasis at the cellular level. Upon MAPK9 knock-down, an increase in triglyceride content was observed both by thin layer chromatography and mass spectrometry. Accordingly, these cells present an increase in lipid droplets, the cellular organelles responsible for triglyceride storage. Sty1 was also identified as the functional homolog of MAPK9 in *S. pombe* for this process, as similar increase in triglyceride and lipid droplets is observed in a deletion strain for this gene. Although more detailed studies will be necessary to unravel the molecular mechanism of this process, these data suggest the evolutionary conserved implication of the MAP kinase pathway in the regulation of lipid storage both in humans and in yeasts.

Outline

Introduction

At the crossroad between lipids and diseases	06
- Obesity, diabetes and the metabolic syndrome: a rising Concern	08
- Atherosclerosis: when lipids cause inflammation	10
A wide variety of lipids – A wide variety of functions	12
- The fatty acids and glycerolipids	12
- The glycerophospholipids	13
- The sphingolipids	14
- The sterols	15
Lipid turnover in the body	17
Cellular regulation of lipids	19
- A cholesterol sensor: the SREBP pathway	19
- The nuclear hormone receptors LXR and PPAR	20
- A new class of metabolic regulators: the microRNAs	22

Aim of the thesis 24

Material and Methods 26

Human cells	27
Yeast cells	37

Results 39

The development of a method	40
- RNA interference: a powerful tool	40
- RNA interference applied to the study of lipid metabolism	41
- Finding the controls	47
- Signal normalization	49
- Mass spectrometry: an alternative method to study lipid composition	50
The kinase screen	55
- The preparation of the screen	55
- The screen	57
- Validation of the screen	63
MAPK9: A potential regulator of triglycerides metabolism	69
- Phenotypic characterization	70
- Sty1: a potential homolog of MAPK9 in <i>S. pombe</i>	75

Discussion 80

Off-target effects	82
Regulation of cholesterol metabolism	84
Regulation of triglyceride metabolism	85

Abbreviations 87

List of figures – List of Tables	90
Bibliography	92
Acknowledgements	104
Certificate	105

Introduction

In today's society, awareness has raised on the importance of lipids in health issues. People caring about a healthier diet have come to know the existence of specific lipids as important factors for their health, following the appearance of their names on packages of many dietary or even cosmetic products. On the other hand, most of the rising health concerns in developed countries have been linked to imbalance in lipid intake and regulation. Among others, we can mention obesity and the metabolic syndrome, diabetes or atherosclerosis, as consequences of the often too rich diet that has become a standard in the US, but also, increasingly, in Europe (Murray & Lopez 1997). Furthermore, the occurrence of these pathologic states is rapidly increasing in developing countries for it appears that an insufficient nutrition during early infancy, or even pregnancy, predisposes to these disorders at later stages of life (Caballero 2005). It is therefore essential to unravel the molecular basis of these diseases as well as the more general cellular factors that trigger lipid dysregulation.

The first part of this introduction will therefore be dedicated to the current knowledge of the molecular basis of these major diseases, with a focus on the role of lipids in these processes. A general introduction on the different roles of lipids in our body and the main factors that control their regulation both at the organism and cellular levels will follow.

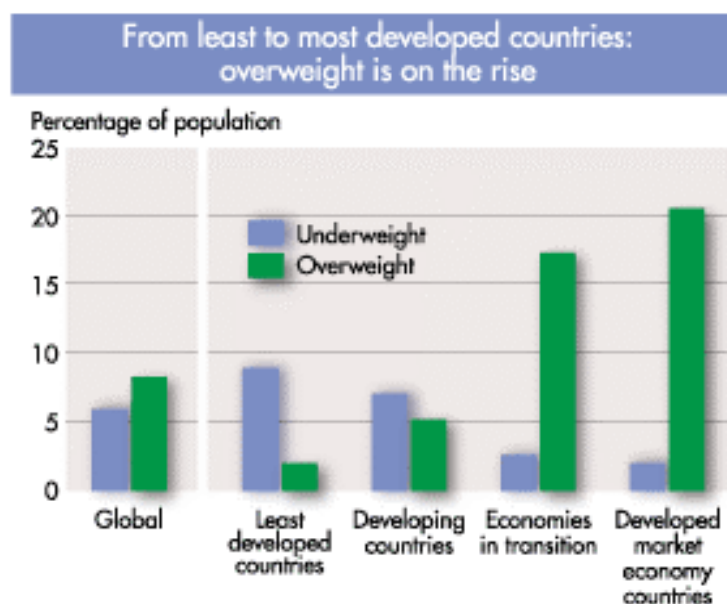


Figure 1: Increase of overweight population in developing countries.
Source: World Health Organization (WHO), 2000

At the Crossroad between Lipids and Diseases

Numerous diseases have been linked to dysregulation of specific or more general lipid-related processes. The complete overview of these diseases is beyond the focus of this thesis. However, the following chapters will focus on the most common ones, which present a major challenge for today's public health systems.

Obesity, Diabetes and the Metabolic Syndrome: a rising concern

Obesity derives from overnutrition (Stein & Colditz 2004), resulting in excessive energy storage, mostly in adipose tissues, in the form of specific lipids, called triglycerides. Adipose tissues are formed of specialized cells, the adipocytes. These cells contain a high number of lipid droplets, cellular organelles specialized in lipid storage. They consist of a core of triglycerides (TAG) and cholesterol esters (CE) surrounded by a phospholipid monolayer (Tauchi-Sato et al 2002). These lipids can be mobilized in case of energy shortage and metabolized to serve as fuel for the Krebs cycle and the production of ATP.

Triglycerides represent the densest form of energy storage and are therefore preferred for long-term storage. In the past, food availability could be limited and the accumulation of lipids was then used as an energetic reserve in case of food shortage. Nowadays, although the availability of food is not limiting anymore in westernized societies, the body has kept this important security system. However, energy expenditure doesn't always compensate for energy intake, resulting over time in weight gain. Only very fine perturbation of the energy balance can result in large fluctuations in body weight. As an example, as little as 25 excessive calories per day (or an apple every three days) can give rise to a 50 kg excess weight at the age of 40. The transition to severe overweight, called obesity, is defined by a body mass index (BMI) exceeding 30 kg/m^2 (Stein & Colditz 2004).

In the US, more than 20% of adults are obese. Although the number is still lower in Europe, it is clearly rising. The caloric imbalance typical for obesity results from a combination of genetic and environmental factors. For example, mutations in genes controlling appetite, like the various adipokines and their corresponding receptors, are known to induce the disease (Tartaglia et al 1995, Zhang et al 1994). However, such mutations have only been found in 5% of obese individuals so far. This suggests that, like many pathologic conditions, obesity more likely results from interactions between multiple mutated genes, as well as from independent factors, such as calorie-rich food availability, decreased physical activity, increased marketing, stress and aging population. The main drawback of obesity is that it predisposes the individuals to various health problems, such as the metabolic syndrome, which is characterized by the development of type 2 diabetes, high blood pressure, elevated cholesterol and triglycerides blood levels, as well as increased probability for atherosclerosis and thrombosis (Reaven 1988).

Increased weight gain and concomitant development of visceral fat often induces an inflammatory response characterized by the overproduction of tumor necrosis factor alpha (TNF α) (Kahn et al 2006). Concomitantly, the fatty acids released by the adipocytes induce accumulation of fatty acid metabolites. These conditions lead to phosphorylation of insulin-receptor substrate 1 (IRS1) and decreased ability to activate the downstream insulin signaling (Aguirre et al 2002). In healthy individuals, this will be compensated by increased insulin production in the pancreas. However, in about one third of obese people, the pancreatic β -cells fail to counteract the insulin resistance, resulting in increased triglyceride hydrolysis by adipocytes, reduced glucose uptake and storage in muscles and liver, and consequent elevated glucose plasma level, a condition known as type 2 diabetes (Kahn et al 2006).

Conversely, insulin resistance is responsible for hyperlipidemia (Avramoglu et al 2006). Lipoprotein lipase is activated by insulin, while ApoB lipoprotein particles production by hepatocytes, in particular very-low density lipoproteins (VLDL), is inhibited by insulin. Consequently, insulin resistance will result in elevated triglycerides level in the form of ApoB lipoprotein particles in the plasma. Furthermore, the release of fatty acids from adipocytes will be enhanced in the absence of insulin, thus further increasing lipid blood level. Taken together, this results in an intricate interconnection between diabetes, insulin resistance and obesity.

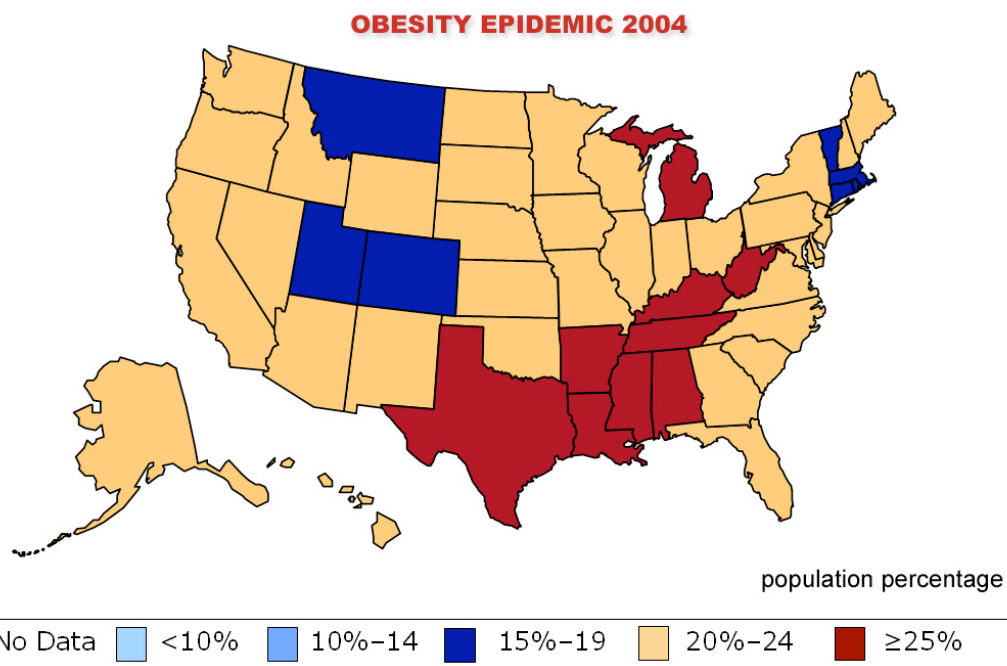


Figure 2: Obesity in the United States in 2004.
Source: Behavioral Risk Factor Surveillance System (BRFSS)

Although prevention of the disease via a healthy nutrition and an active life style would be the best way to decrease obesity occurrence, treatment of the already present pathologic condition appears as a major goal of today's health research. The best cure to obesity is a combination of an energy-limited diet and increased

exercise. However, if this efficiently results in weight loss, more than 80% of the individuals will regain weight after the treatment. This is most probably due to the already existing dysregulation of adipokines metabolism, such as resistance to leptin, the main regulator of long-term appetite control. Therefore, medication is often necessary. The most common drug prescribed is Orlistat, which decreases intestinal fat absorption via inhibition of the pancreatic lipase. However, better understanding of the molecular basis of the disease could lead to the development of additional drugs. In the most advanced cases, weight loss surgery can be performed. This includes stomach size restriction, biliopancreatic diversion or removal of portion of the intestine. However, these surgeries are often inducing complications, and do not guarantee weight loss and reversal of the metabolic syndrome.

Atherosclerosis: when lipids cause inflammation

Atherosclerosis is a progressive disease characterized by the thickening and hardening of the arterial blood vessels. The initial step of atherogenesis consists in accumulation of lipids, mostly in the form of low-density lipoproteins (LDL), in the arterial wall. The exact molecular trigger of this event is not clear. One hypothesis would be that genes with anti-oxidative properties contain shear-stress response elements in their promoter, which are activated by the pulsative laminar blood flow, therefore protecting against oxidative stress (Topper & Gimbrone 1999). However, at branch points of arteries, the disturbed blood flow doesn't trigger the anti-oxidative genes as efficiently, predisposing these sites to lesion formation. Oxidation of LDL results then in an inflammatory response, production of various leukocytes adhesion molecules such as vascular cell adhesion molecule-1 (VCAM-1), and recruitment of circulating monocytes (Dansky et al 2001). The monocytes migrate through the endothelial monolayer that lines the arterial lumen, towards the innermost layer of the arterial wall, the tunica intima (Li & Glass 2002, Libby 2002). There, they differentiate into macrophages and express scavenger receptor proteins able to recognize the modified LDL and promote their internalization (Kunjathoor et al 2002). Upon excessive internalization, macrophages are slowly turning into foam cells (so called because of their foamy appearance under the microscope due to accumulation of cytoplasmic lipid droplets) (Libby 2002). This lesion is called the fatty streak. Conversely, high-density lipoproteins (HDL) can promote efflux of cholesterol from the foam cells, thereby decreasing the lesion (Li & Glass 2002).

As the inflammation increases, vascular smooth muscle cells migrate from the tunica media, the next arterial layer, towards the lesion. There, they further proliferate and also accumulate cholesterol, becoming foam cells as well (Li & Glass 2002). Foam cells then eventually die, generating a necrotic core and extracellular lipid deposits which further propagate the inflammatory process. The formation of the plaque and consequent thickening of the arterial wall is first compensated by artery enlargement, but ultimately induce a narrowing of the vessel lumen, decreasing blood supply to the target organs. This usually remains asymptomatic.

However, upon plaque rupture, platelets adhere to the lesion, leading to obstruction of the bloodstream, thrombosis and in the worst case, myocardial infarction (Libby 2002).

In this context, the reduction of lipid accumulation in the circulation and in macrophages appears as an essential process to protect against cardiovascular diseases, one of the major causes of death in our society.

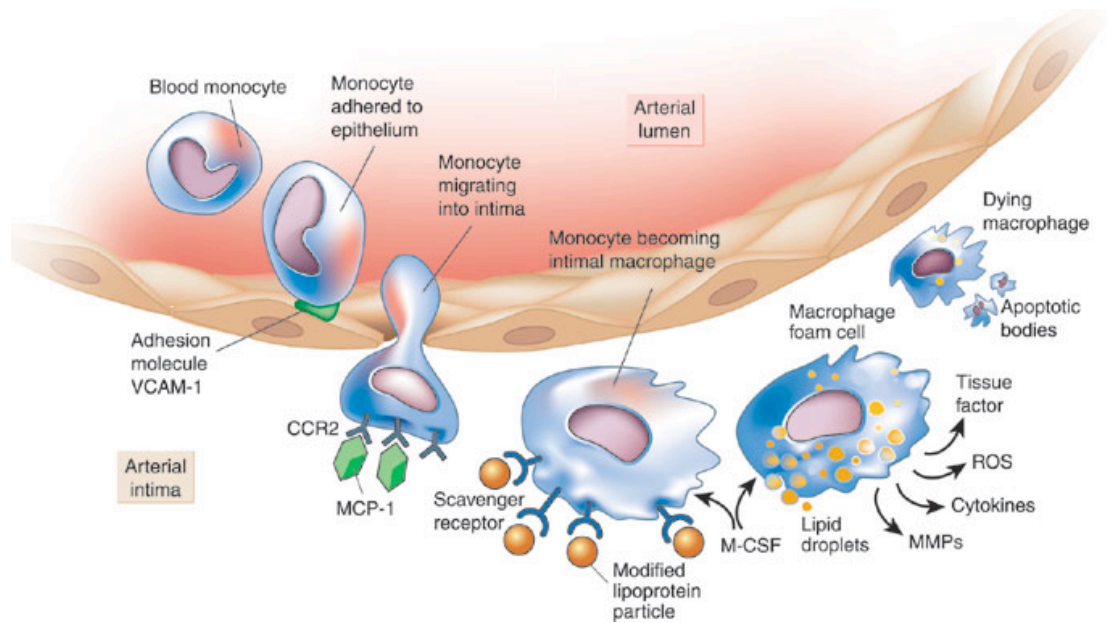


Figure 3: The early steps of atherosclerosis (Libby 2002). Oxidation of LDL promotes inflammation and differentiation of monocytes into foam cells.

A wide variety of Lipids – A wide variety of Functions

For long, lipids have been considered mostly as inert material performing two major functions: a source of energy, allowing the cell to produce the ATP necessary for its biological functions, as well as the main structural constituent of membranes, protecting the inside of the cell from the external milieu as well as allowing compartmentalisation of the different organelles.

However, more recent studies have brought to light an enormous variety of functions that are performed by lipids. This can, in part, explain the existence of hundreds or even thousands different lipid species in a cell (Fahy et al 2005).

Because of this wide variety, recent efforts have brought to the generation of a comprehensive classification system, defining eight lipid categories (Fahy et al 2005). However, the next chapter will focus only on the major types of lipids found in human cells and their main biological functions.

The Fatty Acids and Glycerolipids

Fatty acids consist in a long carbon chain, generally ending with a carboxyl group (Fahy et al 2005). The carbon chain can either be saturated with hydrogen atoms, or contain double bonds. It is then called unsaturated. The most common ones are palmitic acid, a saturated chain of 16 carbon atoms and oleic acid, a mono-unsaturated chain of 18 carbon atoms. However, a vast variety of fatty acids exists differing by the length of the carbon chain and the number and position of unsaturations. Because the free form of the fatty acid is toxic, owing to its detergent-like properties, it is generally coupled to coenzymeA (CoA), forming the fatty acylCoA, a highly reactive molecule that can be easily coupled to other lipid moieties to form more complex lipids. Up to three fatty acids can be coupled to glycerol via ester linkages to form mono-, di- and triacylglycerol respectively. Again, the possible combination of different fatty acids to the glycerol backbone will give rise to a wide variety of lipid species.

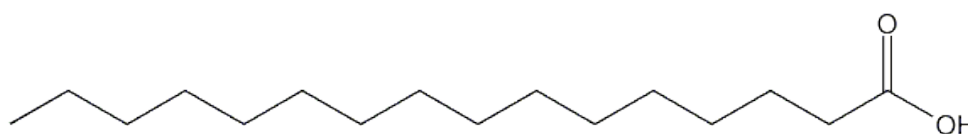


Figure 4: Example of a fatty acid structure: palmitic acid.

Triacylglycerol (TAG) is the major storage form of lipids and is mainly found in specific storage organelles called lipid droplets (Brown 2001). However, in case of energy need, the fatty acids can easily be released by hydrolysis. They are then transported to the peroxisomes or the mitochondria where they can serve as substrate for β -oxidation, a process ultimately leading to the generation of ATP.

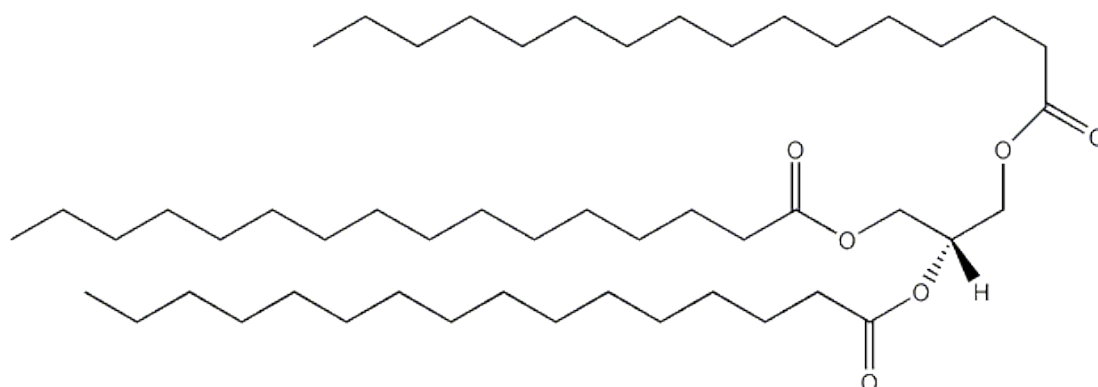


Figure 5: Example of a triacylglycerol structure: tripalmitoylglycerol.

Diacylglycerol (DAG) is the basic building block of glycerophospholipid and is therefore a major intermediate of their synthesis. It can also be released during signaling events, where it acts as a potent second messenger, activating members of the protein kinase C family (Bell et al 1986).

In addition, fatty acids can be used to modify protein, serving as a membrane anchor, a process known as palmitoylation or myristoylation, depending of the acyl moiety (Linder & Deschenes 2007). They also interact with transcription factors, thereby influencing gene expression (Kliwer et al 1997).

The Glycerophospholipids

Glycerophospholipids are the major constituents of membranes (Fahy et al 2005). They are formed from a glycerol backbone linked to two fatty acids. The third hydroxyl group is then linked to a phosphate group, forming phosphatidic acid. Additional molecules can in turn be linked to the phosphate moiety (Fahy et al 2005). They will define the phospholipid classes. The most common head group is choline, but other molecules like ethanolamine, serine or inositol are also common headgroups.

These lipids will organize themselves in bilayer structures, such as the cellular membranes, with their hydrophobic fatty acyl chains pointing inwards, while the more polar headgroups localize at the interface with the aqueous environment. Depending on the nature of the acyl chains, the fluidity of the membrane will vary, more saturated fatty acids giving rise to a tighter packing and less flexibility. This modulation of membrane fluidity is essential to accommodate proteins or for the fission and fusion events that the membranes undergo.

In addition, the different classes of phospholipids have been associated to different cellular events. Phosphatidylcholine (PC) has been shown to specifically interact with several proteins, such as the enzyme 3-hydroxybutyrate dehydrogenase (Loeb-Hennard & McIntyre 2000), and to be essential for their function. It is also the precursor of the platelet-activating factor, the first biologically active phospholipid identified (Bussolino & Camussi 1995). Phosphatidylethanolamine (PE) has been shown to act as a chaperone for the proper folding of the lactose permease in *E.coli* (Bogdanov et al 2002). Phosphatidylserine (PS) is a well-known marker in apoptosis, where it moves from the inner to the outer leaflet of the plasma membrane (Schlegel et al 1996). Phosphatidylinositol (PI) can be further phosphorylated at various positions on its inositol ring, and the resulting molecules serve as specific markers for the various membranes of the secretory pathway, helping in the recruitment of specific proteins at the proper location (De Matteis et al 2002). Cardiolipin (CL), a unique phospholipid with four fatty acid chains localizes specifically to the mitochondria, where it acts as an essential cofactor for several enzymes involved in oxidative phosphorylation, like the cytochrome C oxidase (Robinson 1993).

Although this list is far from being exhaustive, it gives an idea of the pleiotropic functions that can be performed by phospholipids in addition to their well-known structural role.

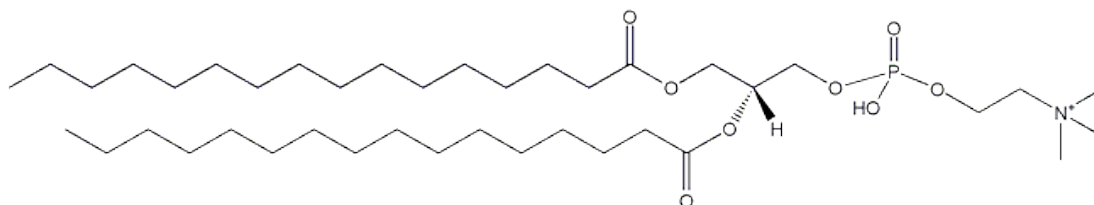


Figure 6: Example of a phospholipid structure: dipalmitoylphosphatidylcholine.

The Sphingolipids

Sphingolipids are a particular type of lipids that use a sphingoid base, such as sphingosine, as primary building block. They can be coupled to fatty acids via an amide bond to form ceramide, while their free hydroxyl group can be linked to phosphoryl or carbohydrate moieties (Fahy et al 2005).

Sphingomyelin (SM), that contains a choline group like PC, is mostly found in the outer leaflet of the plasma membrane, where it interacts with other lipids, like cholesterol and saturated phospholipids, to form membrane microdomains. These

microdomains are generally enriched in specific proteins and have been implicated in various biological events such as endocytosis (Simons & Ikonen 1997).

Several intermediates of sphingolipid metabolism have been involved in signaling pathways. For example, ceramide has been shown to induce apoptosis and cell death (Lakics & Vogel 1998) while sphingosine-1-phosphate promotes cell division and proliferation (Maceyka et al 2002). The balance between these two intermediates is therefore essential in the regulation of cell fate (Maceyka et al 2002).

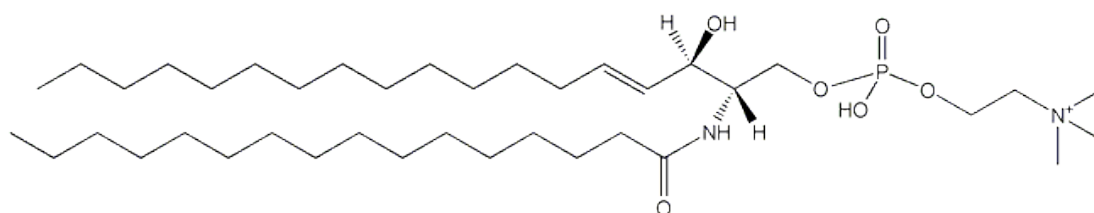


Figure 7: Example of a sphingolipid structure: palmitoylsphingomyelin.

The Sterols

Sterols are totally different in structure from the other types of lipids described above. They are characterized by a four rings core structure, which can be modified by several functional groups differentiating the individual sterols (Fahy et al 2005). Cholesterol is the main sterol found in human cells. In its free form, it localizes within membranes and modulates their fluidity. It is a major constituent of some lipid membrane microdomains, where it interacts with sphingolipids (Simons & Ikonen 1997). Because of its intrinsic toxicity, cholesterol is esterified for storage or transport purposes. This form is mostly found in lipid droplets and lipoprotein particles.

In addition to its structural role, cholesterol is the precursor of numerous other bioactive lipids like steroid hormones, oxysterols and bile acids (Fahy et al 2005). It can also be linked to protein, like the morphogen Hedgehog (Porter et al 1996), where it serves as a membrane anchor for this protein, similarly to palmitoylation.

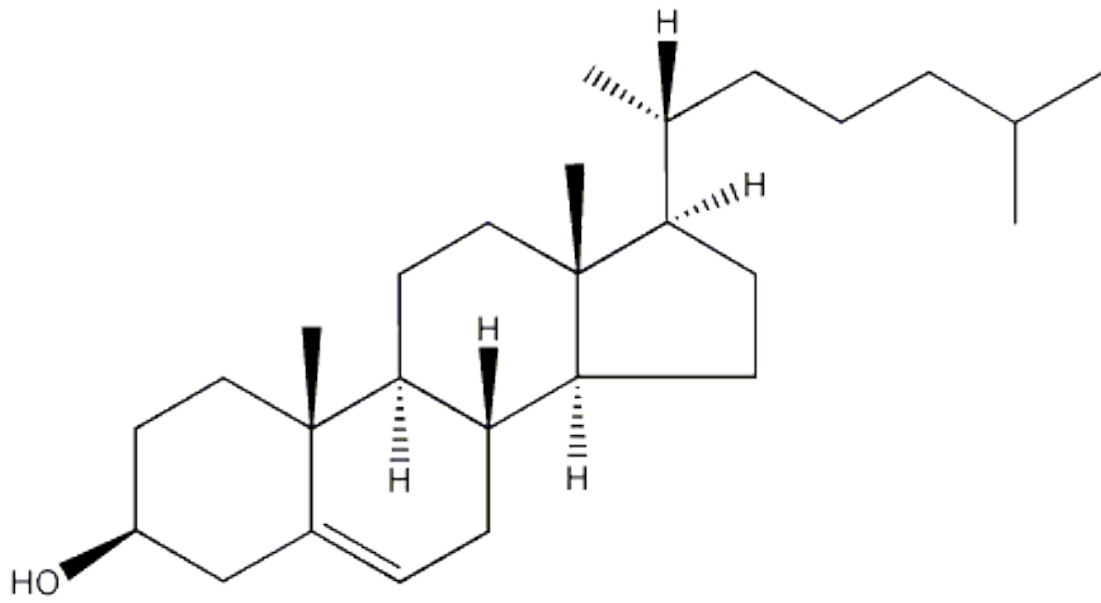


Figure 8: Example of a sterol structure: cholesterol.

Lipid Turnover in the body

Lipids in our organism are either synthesized *de novo*, or taken up from nutritional sources at the level of the intestine. Then, transport of lipids through the body is achieved by lipoprotein particles, which consist of a core of triglycerides and cholesterol esters surrounded by a lipid monolayer and stabilized by apolipoproteins (Olofsson & Boren 2005).

In the intestine, fatty acids, triglycerides and cholesterol are loaded onto ApoB48-containing lipoprotein particles, called chylomicrons, which are then transported to the liver through the intestinal lymph (Olofsson & Boren 2005). Lipids can also be directly produced by the liver, which releases cholesterol and triglycerides onto ApoB100-containing lipoprotein particles, called VLDL (Olofsson & Boren 2005). These particles transport triglycerides and cholesterol towards receiving tissues throughout the body. Upon interaction with the receiving cells, the lipoprotein lipase hydrolyzes their triglyceride content. The released free fatty acids can then be taken up by the receiving cells (Verges 2005). As a consequence, lipoprotein particles become smaller and cholesterol-rich. These particles are known as intermediate density lipoproteins (IDL). Further metabolizing of triglycerides by the hepatic lipase then generates LDL (Verges 2005). LDL can be either taken up by cells that require cholesterol, through interaction with the LDL receptors and subsequent internalization, or recycled to the liver. Eventually, they can also become the target of macrophages, inducing atherogenesis (Li & Glass 2002).

The liver and the intestine also release in the blood circulation ApoA1, which is responsible for the reverse cholesterol transport to the liver and ultimately for cholesterol clearance. The ATP-binding cassette transporter ABCA1 interacts with ApoA1 and facilitates cholesterol efflux from the liver and other tissues. The cholesterol loading of ApoA1 forms the nascent HDL (Lewis & Rader 2005). Lecithin-cholesterol acyltransferase (LCAT), which is present on the particle, then esterifies cholesterol, generating mature HDL particles (Lewis & Rader 2005). Several proteins, such as scavenger receptor B1 and ABCG1, promote further cholesterol loading of HDL (Ji et al 1997, Wang et al 2004). The circulating enzyme cholesteryl ester transfer protein (CETP) in turn triggers the exchange of cholesterol and triglycerides between HDL and LDL particles (Lewis & Rader 2005). Alternatively, HDL particles can either interact with scavenger receptor B1 on the hepatocytes, removing cholesterol from the particle, or be fully catabolized by the liver or the kidneys (Lewis & Rader 2005).

In the liver, cholesterol is converted into bile acids through multiple successive steps generating a soluble, detergent-like molecule that can be secreted into the bile. Since mammalian cells are unable to degrade the steroid nucleus of cholesterol, this constitutes the major pathway for cholesterol clearance (Repa & Mangelsdorf 2000). The bile acid synthesis is controlled by the cytochrome P450 enzyme CYP7A, which catalyzes the first and rate-limiting step of the conversion (Repa & Mangelsdorf 2000). The release of cholesterol and bile acids into the bile is

then achieved via several transporters like ABCG5 and ABCG8, as well as the multidrug transporter Mdr2 (Beaven & Tontonoz 2006).

Fatty acids are mostly taken up by muscles and adipocytes. In the muscle cells, fatty acids are degraded via β -oxidation in the mitochondria, generating ATP necessary for their activity. In adipocytes, fatty acids are converted to TAG and stored in lipid droplets, from which they get released in case of energy shortage. Upon fatty acid uptake, adipocytes also release leptin, a hormone that signals to the hypothalamus and thereby induces satiety (Campfield et al 1995, Pelleymounter et al 1995). In addition, leptin inhibits lipid biosynthesis and excessive lipid uptake by non-adipose tissues to protect them from the deleterious effects of elevated lipid levels (Unger 2003). The lipotoxicity of fatty acids in these cells seem to be mainly the result of their degradation via non-oxidative pathways, inducing, among other effects, the production of ceramide, a secondary messenger able to induce apoptosis (Unger & Orci 2002).

Cellular Regulation of Lipids

As it has been mentioned above, cells contain a wide variety of lipid species, the individual nature of each being essential for various cellular functions. These lipids can either be obtained from external sources and be distributed throughout the body by lipoproteins, or they can be synthesized *de novo* by the cells. Although most of the *de novo* lipid synthesis occurs in the liver, each cell possesses the active machinery to synthesize lipids. The lipid pool of a cell is therefore very dynamic. To keep a proper balance between the individual lipids in a cell, regulation of this complex system appears essential. Several regulation processes are already partially characterized and the next chapter will focus on the current knowledge on the most relevant ones.

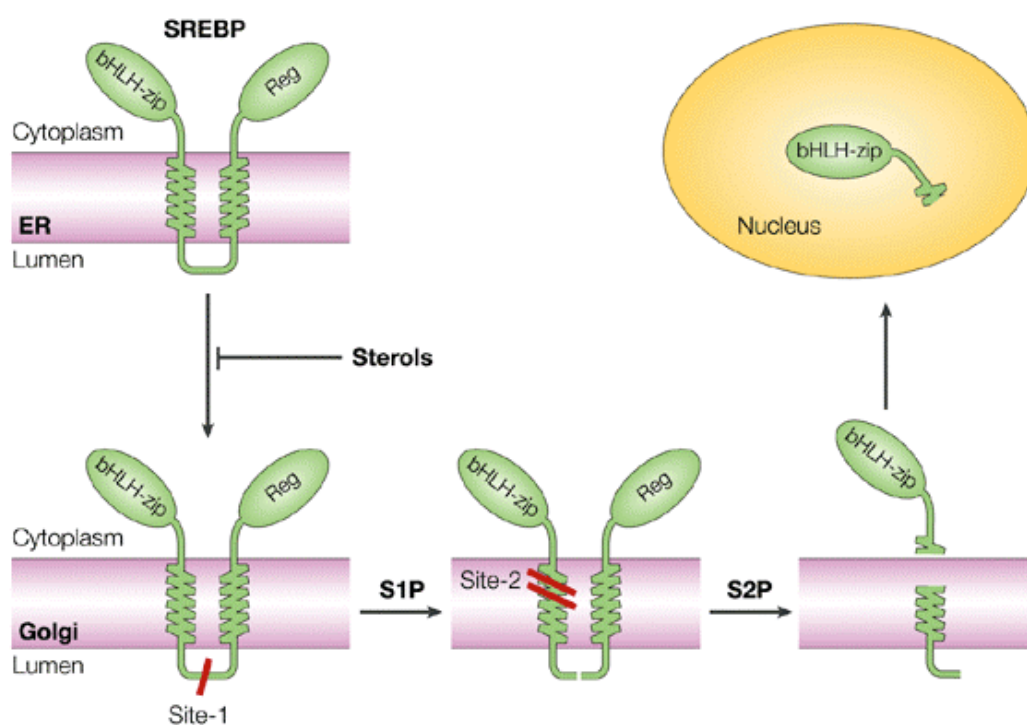
A Cholesterol Sensor: The SREBP pathway

In 1993, Briggs and colleagues identified a transcription factor, a basic helix-loop-helix leucine zipper, able to activate gene transcription in a cholesterol dependent manner by interacting with sterol regulatory element (SRE) found in the promoter of its target genes (Briggs et al 1993, Wang et al 1993). Since then, tremendous efforts have been made to understand the mechanism governing the action of these SRE binding proteins (SREBP). Two different SREBP genes are present in mammalian cells, encoding for three different isoforms. As SREBP-2 mostly regulates genes involved in cholesterol biosynthesis and uptake, SREBP1a and 1c are more involved in the regulation of fatty acid synthesis (Rawson 2003). However, the product of these genes is much longer than the nuclear form that was initially discovered. They encode for a precursor protein containing two transmembrane domains that localizes in the endoplasmic reticulum (ER). SREBP interacts there with another membrane protein, SREBP-cleavage-activating protein (SCAP) (Hua et al 1996). SCAP is necessary for the transport of SREBP to the Golgi apparatus, where SREBP can be further processed (Nohturfft et al 2000). SCAP contains eight membrane-spanning helices, five of which form the sterol-sensing domain. Upon interaction with cholesterol, SCAP modifies its conformation (Brown et al 2002) and interacts with insulin induced genes (Insig) proteins, which retain the SCAP-SREBP complex in the ER (Yang et al 2002b). However, when the cholesterol level decreases, this interaction is impaired and the complex can partition in COPII vesicles and travel to the Golgi (Espenshade et al 2002). There, SREBP is successively cleaved by Site-1 protease (S1P) in its luminal loop (Duncan et al 1997) and by Site-2 protease (S2P) in its N-terminal transmembrane helices (Rawson et al 1997), releasing a transcription factor fragment that is transported to the nucleus by importin β (Lee et al 2003a) to induce target genes expression.

In addition to its action as a retention factor, Insig also acts at another level of cholesterol regulation. HMG-CoA reductase is the enzyme responsible for the formation of mevalonate, the rate-limiting step of sterol biosynthesis (Goldstein & Brown 1990). It is transcriptionally regulated by SREBP. But in addition, it contains,

like SCAP, a sterol-sensing domain driving its interaction with Insig upon binding with sterols, in particular with the cholesterol precursor lanosterol (Sever et al 2003, Song et al 2005a). Insig favors its ubiquitylation and subsequent proteolytic degradation (Song et al 2005b). Insig is thereby involved at two different levels in down-regulation of sterol biosynthesis, although the molecular mechanisms seem very different in both cases.

Interestingly, SREBP homologues have been found in all the metazoan genomes sequenced so far, even in the species auxotroph for cholesterol (Rawson 2003). For example, in *Drosophila*, the SREBP-SCAP system has been shown to respond to the level of PE, rather than cholesterol (Dobrosotskaya et al 2002), and to regulate several genes implicated in fatty acids and phospholipids biosynthesis, suggesting a broader spectrum of possible regulation by this system.



Nature Reviews | Molecular Cell Biology

Figure 9: Two-steps processing of SREBP (Rawson 2003).

The Nuclear Hormone Receptors LXRs and PPARs

Nuclear hormone receptors are transcription factors that are activated upon binding of small lipophilic ligands (Whitfield et al 1999). Several members of this protein family have been shown to regulate lipid metabolism, in particular the liver X receptors (LXR) and the peroxisome proliferator-activated receptors (PPAR).

Most of the members of this family were initially cloned on the basis of sequence homology with the steroid hormone receptors. They were referred to as orphan receptors, because of the absence of any known physiological ligand. But in 1997, Lehmann et al. identified oxysterols as potent regulators of LXR (Lehmann et al 1997). Oxysterols are oxygenated sterols that are formed as by-products of cholesterol, bile acids or steroid hormones biosynthesis (Olkonen & Levine 2004). They are therefore good markers for cholesterol accumulation. Upon interaction with LXR, they induce recruitment of coactivators and expression of several genes implicated in reverse cholesterol transport and cholesterol clearance (Kalaany & Mangelsdorf 2006, Zelcer & Tontonoz 2006). There are two LXR genes. While LXR β is ubiquitously expressed, LXR α is mostly found in the liver (Repa & Mangelsdorf 2000). However, they have very similar structure and activities (Zelcer & Tontonoz 2006).

Among the genes that are up-regulated by LXR, one can find ABCA1 (Repa et al 2000b) and ABCG1 (Venkateswaran et al 2000), two ABC transporters facilitating cholesterol loading on HDL, and thereby clearance of cholesterol from peripheral tissues. In particular, their action on cholesterol clearance from macrophages gives LXR a protective role against atherosclerosis. This is further promoted by up-regulation of various genes implicated in lipoprotein remodeling (Kalaany & Mangelsdorf 2006, Zelcer & Tontonoz 2006). But the anti-atherogenic action of LXR is probably not limited to the regulation of cholesterol metabolism, since they have also been shown to down-regulate several inflammatory genes, probably by competition with other transcription factors for coactivators or via down-regulation of the NF κ B pathway (Zelcer & Tontonoz 2006). However, LXR also activates SREBP1c, thereby inducing lipogenesis (Repa et al 2000a). This may be a way to protect from cholesterol overload by allowing cholesterol esterification and storage (Goldstein et al 2006).

LXR also activates ABCG5 and ABCG8 (Repa et al 2002). These two proteins form a heterodimer that limits the absorption of cholesterol and phytosterols in the gut, probably by pumping them out of the cells (Lee et al 2001). They also promote cholesterol efflux from hepatocytes into the bile (Yu et al 2002). Similarly, CYP7A, the rate-limiting enzyme of bile acid synthesis, is also a target of LXR in mice, however not in humans (Chiang et al 2001, Peet et al 1998).

The other important nuclear hormone receptors implicated in lipid metabolism are PPARs. Three isoforms exist: PPAR α , PPAR γ and PPAR δ (Li & Glass 2004). They are activated by a wide variety of fatty acids, with overlapping specificity between the isoforms (Berger & Moller 2002). Contrary to the analogous functions of the two LXR isoforms, the different PPARs are implicated in different metabolic processes. For example, PPAR α up-regulates fatty acid oxidation through the transcriptional activation of several enzymes of this pathway (Chawla et al 2001b). It also up-regulates ABCD2 and ABCD3, two ABC transporters implicated in the transport of fatty acids to peroxisomes (Fourcade et al 2001). The general outcome of PPAR α activation is therefore a decrease in triglyceride level. On the contrary, PPAR γ

promotes fat storage through up-regulation of adipocyte differentiation factors, lipogenic enzymes and genes involved in fatty acid uptake (Beaven & Tontonoz 2006, Chawla et al 2001b). Activation of PPAR γ is also critical for glucose homeostasis (Li & Glass 2004), in particular through the up-regulation of the insulin-dependent glucose transporter GLUT4 (Wu et al 1998). In addition, an interesting crosstalk is observed with the LXR pathway, since PPAR γ , as well as PPAR α , induce LXR α , thereby activating lipogenesis and the reverse cholesterol pathway (Chawla et al 2001a, Chinetti et al 2001). The role of PPAR δ is less well understood, but it seems to be mostly implicated in the regulation of fatty acid oxidation (Wang et al 2003). It has also been shown to regulate the production of myelin, an insulating phospholipid layer surrounding the axons of some neurons (Berger & Moller 2002).

A New Class of Metabolic Regulators: The microRNAs

MicroRNAs (miRNA), a new class of regulatory molecules, have been implicated in the regulation of lipid metabolism. MiRNAs are short non-coding RNA molecules that can bind to partially complementary mRNA, inducing their translational repression and eventually their degradation, ultimately leading to depletion of the target protein (Bartel 2004, Kim & Nam 2006). More than 300 miRNAs sequences have been identified so far in the human genome (Kim & Nam 2006, Krutzfeldt & Stoffel 2006). The function of most of them is still unknown, but several have been implicated in the regulation of development, differentiation and metabolism (Krutzfeldt & Stoffel 2006). The first study implicating miRNAs in lipid metabolism was carried out in *Drosophila* (Xu et al 2003). Overexpression of *drosophila* miR-14 induces a decrease in triglyceride level. However, the mechanism of this down-regulation was not determined. Conversely, depletion of *drosophila* miR-278 also induces a decrease in triglyceride level, suggesting an important role for miRNAs in the regulation of triglyceride metabolism (Teleman et al 2006). Although no homolog of these miRNAs has been found in mammals, other miRNAs have been implicated in the regulation of adipocyte differentiation (miR-143 (Esau et al 2004)) and cholesterol homeostasis. Two studies (Esau et al 2006, Krutzfeldt et al 2005) have shown that depletion of miR-122 induces a decrease in plasma cholesterol level in mice (figure 10, right), probably owing to an observed decrease in the expression of cholesterol biosynthetic genes such as HMG-CoA reductase and mevalonate kinase. However, the mechanism by which miRNAs could activate gene expression is currently unknown. In addition, Esau et al. showed a comparable modulation of triglyceride level, and down-regulation of the fatty acid synthase and other lipogenic genes in miR-122 depleted hepatocytes (Esau et al 2006).

Since the function of most miRNAs is still unknown, it is likely that more will be implicated in the regulation of lipid metabolism. Systematic identification of miRNAs expressed in liver and adipocytes have been carried out recently (Esau et al 2004, Fu et al 2005, Kajimoto et al 2006), suggesting new potential candidates for such regulators.

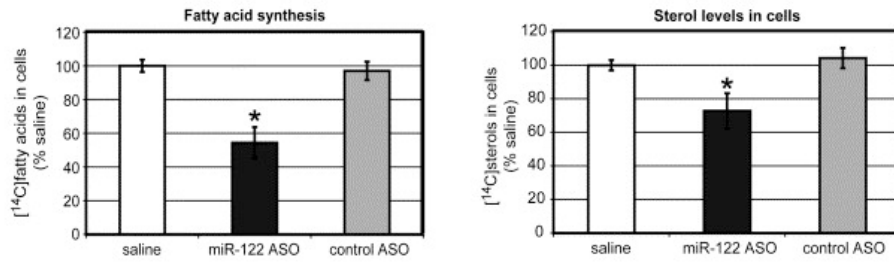


Figure 10: Decrease in fatty acid synthesis and cholesterol levels upon miR-122 depletion (denoted by ASO) (Esau et al 2006).

Aim

Aim of the thesis

The cell is a very dynamic system, continuously exchanging information and molecules with its surrounding, and among them, lipids. As it has been pointed out in the introduction, the importance of lipids goes far beyond their structural role in membranes. It is therefore essential to keep a proper balance between the wide variety of lipid entities present in the cells. To achieve this, cells developed tight regulation systems.

Although some regulation processes have been already uncovered and are beginning to be understood, these would be insufficient to fully regulate such a complex cellular lipid homeostasis. It is therefore highly expected that other regulation systems still need to be unraveled. This is precisely the aim of this thesis.

Therefore, the first goal of this thesis is the design of a screening procedure that allows identification of such regulators. Systematic knock-down of individual genes can be achieved using a recently discovered cellular process, RNA interference. Combining this technique with lipid analysis methods appears as a good way to monitor variation of lipid composition upon gene knock-downs.

Then, this procedure can be applied to the study of gene families that potentially play a role in lipid regulation. In particular, kinases appear as good candidates for such regulators, considering their wide implication in the regulation of other biological processes.

Finally, the results of the screen are analyzed, and the most promising candidates further characterized, leading to the potential identification of new regulators of lipid homeostasis.

Material and Methods

Material and Methods: Human cells

Material

Dulbecco's modified Eagle's medium with high glucose and sodium pyruvate (DMEM), Opti-MEM, Fetal Bovine Serum (FBS) and trypsin were obtained from Gibco (Karlsruhe, Germany). Delipidated FBS was prepared as described previously (Thiele et al 2000). Briefly, lipids were extracted from FBS using successively a diisopropylether/butanol 2:1 mix and pure diisopropylether. Then, the upper phase was dialyzed against phosphate buffered saline (PBS). After several dialysis steps, delipidated FBS was filter-sterilized and kept frozen until use.

Lipid standards were from Sigma (St. Louis, MO), except phosphatidylserine (PS), sphingomyelin (SM), phosphatidylinositol (PI) and glucosylceramide which were from Avanti (Alabaster, AL), cholesterol ester from AppliChem (Darmstadt, Germany), oleate from Acros (Geel, Belgium), ceramide from Matreya biochemicals (Pleasant Gap, PA), lophenol from ResearchPlus (Manasquan, NJ), desmosterol and epoxycholesterol from Steraloids (Newport, RI). ¹⁴C-acetate was obtained from Amersham (Freiburg, Germany) and ³H-oleate from Hartmann Analytic (Braunschweig, Germany).

The siRNA kinase library was obtained from Ambion (Austin, TX). Other siRNAs were also from Ambion, unless mentioned otherwise and are described in table 1. EsiRNAs were a kind gift from Dr. R. Kittler (Kittler et al 2004).

Real-Time PCR primers were from Biospring (Frankfurt, Germany). Sequences can be found in table 2. Rabbit polyclonal antibody against IKK1 was from Santa Cruz (Heidelberg, Germany). Rabbit polyclonal antibody against JNK2 and mouse monoclonal antibody against phospho-JNK were from Cell Signaling Technologies (Danvers, MA). Rabbit polyclonal antibodies against ATGL and HSL were from Cayman chemical (Ann Harbor, MI). Horseradish peroxidase (HRP)-conjugated donkey anti-mouse and donkey anti-rabbit immunoglobulin G (IgG) secondary antibodies were from Jacksons Immunological (West Grove, PA).

Cell culture

Hela cells and A431 cells were cultured in DMEM supplemented with 10% FBS. Cells were passaged regularly using trypsin to maintain them in exponential growth phase and were tested for the absence of mycoplasma on a regular basis (Stratagene, Amsterdam, The Netherlands).

Table 1: List of siRNAs used in this work (except the kinase library).

Gene	ID number	Company	RefSeq Number	Other names used in the thesis or sequences
ALS2CR2	1171	Ambion	NM_018571	siRNA1 (screen), O1
ALS2CR2	1266	Ambion	NM_018571	siRNA2 (screen), O2
ALS2CR2	1361	Ambion	NM_018571	siRNA3 (screen), O3
ATR	82	Ambion	NM_001184	siRNA1 (screen), O1
ATR	103302	Ambion	NM_001184	siRNA2 (screen), O2
CASK	446	Ambion	NM_003688	siRNA1 (screen), O1
CASK	447	Ambion	NM_003688	siRNA2 (screen), O2
CASK	448	Ambion	NM_003688	siRNA3 (screen), O3
CASK	139314	Ambion	NM_003688	siRNA1 (new), N1
CASK	139315	Ambion	NM_003688	siRNA2 (new), N2
CASK	139316	Ambion	NM_003688	siRNA3 (new), N3
CASK	109507D02	Invitrogen	NM_003688	
CASK	109507D04	Invitrogen	NM_003688	
CASK	109507D05	Invitrogen	NM_003688	
CASK	SI02223368	Qiagen	NM_003688	
CASK	SI02223375	Qiagen	NM_003688	
CKMT2	175	Ambion	NM_001825	siRNA1 (screen), O1
CKMT2	176	Ambion	NM_001825	siRNA2 (screen), O2
CKMT2	177	Ambion	NM_001825	siRNA3 (screen), O3
CSF1R	641	Ambion	NM_005211	siRNA1 (screen), O1
CSF1R	642	Ambion	NM_005211	siRNA2 (screen), O2
CSF1R	643	Ambion	NM_005211	siRNA3 (screen), O3
CSF1R	146601	Ambion	NM_005211	siRNA1 (new), N1
CSF1R	146602	Ambion	NM_005211	siRNA2 (new), N2
CSF1R	146603	Ambion	NM_005211	siRNA3 (new), N3
CSNK1G2	115	Ambion	NM_001319	siRNA1 (screen), O1
CSNK1G2	116	Ambion	NM_001319	siRNA2 (screen), O2
CSNK1G2	117	Ambion	NM_001319	siRNA3 (screen), O3
EG5	custom	Ambion	NM_004523	CUGAAGACCUGAAGACAAUtt AUUGUCUUCAGGUCUUCAGtt
EPHB3	529	Ambion	NM_004443	siRNA1 (screen), O1
EPHB3	530	Ambion	NM_004443	siRNA2 (screen), O2
EPHB3	531	Ambion	NM_004443	siRNA3 (screen), O3
FLT1	190	Ambion	NM_002019	siRNA1 (screen), O1
FLT1	191	Ambion	NM_002019	siRNA2 (screen), O2
FLT1	192	Ambion	NM_002019	siRNA3 (screen), O3
IKK1 (CHUK)	112	Ambion	NM_001278	siRNA1 (screen), O1
IKK1 (CHUK)	113	Ambion	NM_001278	siRNA2 (screen), O2
IKK1 (CHUK)	114	Ambion	NM_001278	siRNA3 (screen), O3
IKK1 (CHUK)	145720	Ambion	NM_001278	siRNA1 (new), N1
IKK1 (CHUK)	145721	Ambion	NM_001278	siRNA2 (new), N2
IKK1 (CHUK)	145722	Ambion	NM_001278	siRNA3 (new), N3
LAK	1075	Ambion	NM_025144	siRNA1 (screen), O1
LAK	1076	Ambion	NM_025144	siRNA2 (screen), O2
LAK	103610	Ambion	NM_025144	siRNA3 (screen), O3
LCK	668	Ambion	NM_005356	siRNA1 (screen), O1
LCK	669	Ambion	NM_005356	siRNA2 (screen), O2
LCK	670	Ambion	NM_005356	siRNA3 (screen), O3
LCK	143990	Ambion	NM_005356	siRNA1 (new), N1
LCK	143991	Ambion	NM_005356	siRNA2 (new), N2
LCK	143992	Ambion	NM_005356	siRNA3 (new), N3

Gene	ID number	Company	RefSeq Number	Other names used in the thesis or sequences
LCK	SI00075992	Qiagen	NM_005356	
LCK	SI00075999	Qiagen	NM_005356	
LCK	SI00076006	Qiagen	NM_005356	
MAP3K4	1470	Ambion	NM_005922 NM_006724	siRNA1 (screen), O1
MAP3K4	1564	Ambion	NM_005922 NM_006724	siRNA2 (screen), O2
MAP3K4	1654	Ambion	NM_005922 NM_006724	siRNA3 (screen), O3
MAP3K4	144116	Ambion	NM_005922 NM_006724	siRNA1 (new), N1
MAP3K4	144117	Ambion	NM_005922 NM_006724	siRNA2 (new), N2
MAP3K4	144118	Ambion	NM_005922 NM_006724	siRNA3 (new), N3
MAPK9	1452	Ambion	NM_139070 NM_139069 NM_002752 NM_139068	siRNA1 (screen), O1
MAPK9	1547	Ambion	NM_139070 NM_139069 NM_002752 NM_139068	siRNA2 (screen), O2
MAPK9	1637	Ambion	NM_139070 NM_139069 NM_002752 NM_139068	siRNA3 (screen), O3
MAPK9	142316	Ambion	NM_139070 NM_139069 NM_002752 NM_139068	siRNA1 (new), N1
MAPK9	142317	Ambion	NM_139070 NM_139069 NM_002752 NM_139068	siRNA2 (new), N2
MAPK9	142318	Ambion	NM_139070 NM_139069 NM_002752 NM_139068	siRNA3 (new), N3
MAPK9	SI00300797	Qiagen	NM_139070 NM_139069 NM_002752 NM_139068	
MAPK9	SI02222913	Qiagen	NM_139070 NM_139069 NM_002752 NM_139068	
NFKB1	5213	Ambion	NM_003998	
NFKB2	115299	Ambion	NM_002502	
NFKB2	143618	Ambion	NM_002502	
NFKB2	143619	Ambion	NM_002502	

Gene	ID number	Company	RefSeq Number	Other names used in the thesis or sequences
PDXK	440	Ambion	NM_003681	siRNA1 (screen), O1
PDXK	441	Ambion	NM_003681	siRNA2 (screen), O2
PDXK	442	Ambion	NM_003681	siRNA3 (screen), O3
PDXK	139305	Ambion	NM_003681	siRNA1 (new), N1
PDXK	139306	Ambion	NM_003681	siRNA2 (new), N2
PDXK	139307	Ambion	NM_003681	siRNA3 (new), N3
PDXK	109507E01	Invitrogen	NM_003681	
PDXK	109507E04	Invitrogen	NM_003681	
PDXK	109507E05	Invitrogen	NM_003681	
PDXK	SI00054593	Qiagen	NM_003681	
PDXK	SI00054600	Qiagen	NM_003681	
PDXK	SI00288071	Qiagen	NM_003681	
PHKG2	50	Ambion	NM_000294	siRNA1 (screen), O1
PHKG2	51	Ambion	NM_000294	siRNA2 (screen), O2
PHKG2	52	Ambion	NM_000294	siRNA3 (screen), O3
PHKG2	110737	Ambion	NM_000294	siRNA1 (new), N1
PHKG2	118254	Ambion	NM_000294	siRNA2 (new), N2
PHKG2	118293	Ambion	NM_000294	siRNA3 (new), N3
PRKCL1	312	Ambion	NM_213560 NM_002741	siRNA1 (screen), O1
PRKCL1	313	Ambion	NM_213560 NM_002741	siRNA2 (screen), O2
PRKCL1	314	Ambion	NM_213560 NM_002741	siRNA3 (screen), O3
PRKWNK1	1174	Ambion	NM_018979	siRNA1 (screen), O1
PRKWNK1	1269	Ambion	NM_018979	siRNA2 (screen), O2
PRKWNK1	1364	Ambion	NM_018979	siRNA3 (screen), O3
RIPK4	1177	Ambion	NM_020639	siRNA1 (screen), O1
RIPK4	1272	Ambion	NM_020639	siRNA2 (screen), O2
RIPK4	1367	Ambion	NM_020639	siRNA3 (screen), O3
RIPK4	113612	Ambion	NM_020639	siRNA1 (new), N1
RIPK4	113613	Ambion	NM_020639	siRNA2 (new), N2
RIPK4	133160	Ambion	NM_020639	siRNA3 (new), N3
ROCK2	595	Ambion	NM_004850	siRNA1 (screen), O1
ROCK2	596	Ambion	NM_004850	siRNA2 (screen), O2
ROCK2	597	Ambion	NM_004850	siRNA3 (screen), O3
ROCK2	137769	Ambion	NM_004850	siRNA1 (new), N1
ROCK2	137770	Ambion	NM_004850	siRNA2 (new), N2
ROCK2	137771	Ambion	NM_004850	siRNA3 (new), N3
ROCK2	109507E07	Invitrogen	NM_004850	
ROCK2	109507E10	Invitrogen	NM_004850	
ROCK2	109507E11	Invitrogen	NM_004850	
ROCK2	SI02223746	Qiagen	NM_004850	
ROCK2	SI02223753	Qiagen	NM_004850	
SOAT1	4490	Ambion	NM_003101	siRNA1
SOAT1	4586	Ambion	NM_003101	siRNA2
SOAT1	4679	Ambion	NM_003101	siRNA3
TRIO	848	Ambion	NM_007118	siRNA1 (screen), O1
TRIO	849	Ambion	NM_007118	siRNA2 (screen), O2
TRIO	103343	Ambion	NM_007118	siRNA3 (screen), O3
TRIO	103427	Ambion	NM_007118	siRNA1 (new), N1

Table 2: List of RT-PCR primers used in this work.

gene	forward primer	reverse primer
SOAT1	CACGTTCTGGACTTGTCTGTTAC	TCAGGGAGCTACCCAATCTTCA
GAPDH-1	TCGACAGTCAGCCGCATCT	CCCCATGGTGTCTGAGCG
GAPDH-2	CAAGGTCATCCATGACAACCTTG	GGCCATCCACAGTCTTCTGG
tubulin	ACTGGCATCCTGCTTTCCAGT	GGCTCTGTAGCTCCCCATGTACT
IKK1	CAAGATGGGGAGACTTCAGC	ATTGCCCTGTTCTCATTG
ATR	CACCACCAGACAGCCTACAA	AACATCACCTTGGACCAGA
TRIO	AAGCAGCAGCAGTAGCAACA	TTTGAACGACCTCTCCTTGG
RIPK4	AGGATGAGGACCAGTGGACA	GAGGCGTTCTTCTCCAACAG
PRKWNK1	AACCAGCAGCACAAACTG	ATCTGTGAATGTGCCCTTCC
ROCK2	TAAGGAAAACCCAGGCAGAA	TAACTTGGCAGTCTCCAGCA
CASK	GAGATTCCCCTTCCACTTCC	TCGTCCTTTTGGTTGGGTAG
MAPK9	CTGCGTCACCCATACATCAC	CTTTCTTCCAACCTGGGCATC
PDXK	CGTGTGTGATCCAGTCTTGG	CGGCACCACTTTTTCTTTGT
MAP3K4	CAGGAGCAGACATCCAGTCA	TGGCATTGCTTATCCTGTTG
AGPAT	GCATCATCGGCTGGTTCGTG	TGCTCTGGTGGTTGGAGACG
LIPIN1	GCAGAAGAACCCAGAAATGC	TCAATGGGCTGGACTCTTTC
ATGL	CGGGTCACCAACACCAGCATC	ACATCTCTCGCAGCACCAGGG
HSL	CAGTTCACGCCTGCCATCCG	CGTTTGTAGTGCTCCCCGAAGG

siRNA transfection

4000 HeLa cells were plated in 80 μ l growth medium in each well of a 96 well-plate 20h before transfection. Oligofectamine (Invitrogen, Karlsruhe, Germany) was mixed with Opti-MEM medium in a 1:6.5 ratio and incubated for 5'. For each well, 10pmole siRNA were mixed with 17 μ l Opti-MEM medium and 3 μ l of the oligofectamine mix prepared above. The siRNA mix was incubated for 20' to allow formation of the cationic liposome/RNA complex and then added to the cells. For the screen, the transfection procedure was automated and performed on a Tecan Freedom Evo workstation (Tecan, Mannedorf, Switzerland) under sterile conditions. 100 μ l fresh growth medium was added to the cells 4h after transfection (except for the screen). Except indicated otherwise, growth medium was exchanged 48h after transfection for 100 μ l DMEM medium supplemented with 10% delipidated FBS. For lipid analysis by Thin Layer Chromatography (TLC), 2 μ Ci of ¹⁴C-acetate were added in each well 56h after transfection. Lipid extracts or cells were harvested 72h after transfection.

esiRNA transfection

2000 HeLa cells were plated in 100 μ l growth medium in each well of a 96 well-plate 20h before transfection. Oligofectamine was mixed with serum-free DMEM medium in a 1:6 ratio and incubated for 5'. For each well, 25ng esiRNA were mixed with 7 μ l Opti-MEM medium and 3 μ l of the oligofectamine mix prepared above. The esiRNA mix was incubated for 20' to allow formation of the cationic liposome/RNA complex and then added to the cells. 100 μ l fresh growth medium was added to the cells 4h

after transfection. Except indicated otherwise, growth medium was exchanged 48h after transfection for 100µl DMEM medium supplemented with 10% delipidated FBS. For lipid analysis by TLC, 2µCi of ¹⁴C-acetate were added in each well 56h after transfection. Lipids were extracted 72h after transfection.

One-phase lipid extraction and TLC analysis

Lipids were extracted directly from the wells using 15µl MeOH/CHCl₃ 5:1, unless indicated otherwise. Samples were applied onto the TLC plates (Merck, Darmstadt, Germany) using either capillaries or a multichannel pipette (Eppendorf, Hamburg, Germany). TLC plates were developed in a glass chamber containing EtOH/water/triethylamine/CHCl₃ 50/10/35/35 till 2/3 of the plate, dried and then further developed with hexane/ethylacetate 5:1 till the top of the plate. Radioactive samples were visualized by exposure on a phosphoimager plate for 1 to 3 days and subsequent reading by the phosphoimager (Fuji, Dusseldorf, Germany). Non-radioactive samples were revealed by charring with 20% H₂SO₄ aqueous solution and heated up to 250°C.

Bligh and Dyer lipid extraction

Cells were scraped in 1ml PBS, supplemented with 0.5mM MgCl₂ and CaCl₂ and transferred to a tube containing 4ml MeOH/CHCl₃ 2:1. Samples were mixed and centrifuged at 4000g on a multifuge 3 S-R (Heraeus Holding, Hanau, Germany). Supernatant was transferred to a fresh tube, then 1ml of 20mM acetic acid and 1ml CHCl₃ were added. Samples were mixed and centrifuged again at 4000g. The organic phase was transferred to a new tube and 50µl of 1M citric acid and 2ml CHCl₃ were added to the aqueous phase. Samples were mixed and centrifuged again at 4000g. The organic phases were combined and evaporated under a stream of nitrogen. Dried lipids were dissolved in 30µl MeOH/CHCl₃ 1:2.

Lipid profile comparison and quantification

For analysis of the TLC plates, the radioactive signal revealed by the phosphoimager was initially analyzed using the *Image Gauge* software (Fuji, Dusseldorf, Germany). Individual lipid intensity profiles were recovered via this program and then transferred to the *Graph Explorer* software designed by Yannis Kalaidzidis. For profile comparison, lipid intensities were normalized on the level of PC. When necessary, alignment of the profiles was performed. For quantification, the different peaks were fitted using Gaussian curves. The area below the different curves was retrieved and transferred to *Excell* (Microsoft, Munich, Germany). There, results were normalized on the total lipid signal. In the case of the specific analysis of cholesterol ester levels in SOAT1 knock-down, only the peaks corresponding to

TAG and cholesterol ester were fitted and their ratio was normalized to the ratio of the non-transfected negative control.

Clustering

The different phenotypes were first converted into a numerical representation. For each lipid peak, a phenotype readily visible on the TLC plate was assigned a value of 3 while a phenotype revealed by profile comparison was assigned a value of 2. The numerical table was loaded into *CUPID* and clustered by k-means clustering using Pearson correlation. Annotation was performed using *CUPID* and corrected manually when needed.

Protein quantification

To test the potential of protein determination methods in the context of the screening assay, bovine serum albumin (BSA, AppliChem, Darmstadt, Germany) solutions of various concentrations (containing up to 10µg BSA) were analyzed in the presence or absence of 2% sodium dodecyl sulfate (SDS, Serva, Heidelberg, Germany). In addition, different amount of cells were plated in 96 well-plates and grown for 20h, lipids were extracted using MeOH/CHCl₃ 5:1 as described above before protein determination. Cells were then treated with 10µl SDS 2%. For the Bradford assay (Sigma, St. Louis, MO), 200µl of a 1/15 diluted Bradford solution was added on the BSA standard solution or on the cells and, after 10' incubation, absorbance was measured at 570 nm on a Digiscan 400 microplate reader (Asys, Dornstadt, Germany). For the BCA assay (Perbio, Bonn, Germany), 200µl of the BCA mix was added to the samples and, after 30' incubation at 37°C, absorbance was measured at 550 nm. For the fluorescamine assay, 100µl sodium borate 0.1M pH 8.9 and 20µl fluorescamine (0.25 mg/ml, Sigma, St. Louis, MO) were added to the samples and fluorescence was measured using a Fluoroskan Ascent CF microplate reader (Thermo Labsystems, Vantaa, Finland) with excitation at 380 nm and emission at 485 nm.

DNA quantification

After lipid extraction, 200µl of propidium iodide (3µg/ml, Sigma, St. Louis, MO) were added to the wells and incubated in the dark for 3h, unless indicated otherwise. Fluorescence emission was measured using a Fluoroskan Ascent CF microplate reader (Thermo Labsystems, Vantaa, Finland) with excitation at 530 nm and emission at 620 nm.

Treatment with kinase inhibitors or chemicals

For inhibition of IKK, parthenolide (Biomol International, Exeter, United Kingdom) was added to the cells at the indicated concentrations 24h before lipid extraction. For lipid analysis by TLC, 2 μ Ci of 14 C-acetate were added in each well 6h later.

For inhibition of JNK, SP600125 (Sigma, St. Louis, MO) was added to the cells at the indicated concentrations 24h before lipid extraction. For lipid analysis by TLC, 2 μ Ci of 14 C-acetate were added in each well 6h later.

For rescue of the PDXK knock-down, pyridoxal phosphate (Sigma, St. Louis, MO) was added to the cells 48h after transfection with a pool of three siRNA sequences against PDXK. Concentrations of pyridoxal phosphate were varied between 0.01 and 100 μ M. For lipid analysis by TLC, 2 μ Ci of 14 C-acetate were added in each well 6h later. Lipids were extracted 72h after transfection.

Oleate feeding

Oleate was added to the cells 4h after transfection to a final concentration of 50 μ M. In addition, 1 μ Ci of 3 H-oleate was added in each sample. Lipids were extracted as described above 48h after transfection and resolved by TLC. The TLC plate was then dipped in LumaSafe solution (Lumac-LSC, Groningen, The Netherlands) and exposed on MP films (Amersham, Freiburg, Germany) for 6h at -80°C.

JNK activation

UV activation of JNK was achieved by 10' irradiation using a 200 W high-pressure Oriol Photomax mercury lamp (Newport, Irvine, CA), which filter out wavelengths shorter than 310 nm. Prior to irradiation, growth medium was removed from the cells and replaced by TBS. Cells were kept on ice during irradiation to avoid overheating of the samples. Then, cells were transferred back to their growth medium and kept at 37°C for 20' prior protein extraction using Laemmli buffer.

Anisomycin activation of JNK was achieved by addition of anisomycin (Sigma, St. Louis, MO) to a final concentration of 250ng/ml directly in the growth medium. Cells were further grown for 2h prior protein extraction using Laemmli buffer.

Mass spectrometry

For MS analysis on the Esi-Qq-ToF mass spectrometer, cells were extracted in 30 μ l MeOH/CHCl₃ 5:1 supplemented with 5mM ammonium acetate. Aliquot from these samples were analyzed in negative ion mode on a QSTAR Pulsar/QqTOF mass

spectrometer (MDS Sciex, Concord, Canada). Ionization voltage was set to -0.9kV and gas pressure to 0.1psi. Then, the rest of the samples was dried under a stream of nitrogen and lipids were re-suspended in 50 μ l MeOH/CHCl₃ 2:1. Then, samples were re-extracted after addition of 50 μ l H₂O. The organic phase was then recovered and analyzed by MS using the same settings as above. Spectra were obtained by Christer Ejsing.

For MS analysis on the Orbitrap mass spectrometer, lipid extracts were obtained either 72h after siRNA transfection or 3.5h after addition of 10 μ M of a fatty acid, namely myristate, palmitate or oleate. Lipids were extracted using 100 μ l MeOH/CHCl₃ 5:1 and the extract was transferred to a 1.5ml Eppendorf tube (Eppendorf, Hamburg, Germany). 100 μ l of chloroform and 100 μ l H₂O were added, tubes thoroughly vortexed and centrifuged at 1000g. The organic phase was transferred into a new tube and dried down in a SpeedVac. Samples were then resuspended in 100 μ l MeOH/CHCl₃/isopropanol 2:1:4 supplemented with 7.5mM ammonium acetate. Mass spectrometric analysis was performed on a LTQ Orbitrap (ThermoElectron, San Jose, CA) equipped with a NanoMate HD robotic nanoflow ion source (Advion BioSciences Ltd, Ithaca, NJ) with 4.1 μ m nozzle diameter chip. NanoMate HD was operated in positive ion mode at an ionization voltage of 1.05kV and gas pressure of 1psi. MS/MS experiments on the LTQ Orbitrap were performed using collision-induced dissociation in the linear ion trap. Using *QualBrowser 2.0* software (ThermoElectron, San Jose, CA), each survey spectrum was converted into a peak list, which reported *m/z*, absolute intensity, relative intensity (normalized to the most abundant peak) and the sum composition for each peak detected with a signal-to-noise ratio above 6. The peak list was further imported by *MarkerView* software (MDS Sciex, Concord, Canada) for Principal Component Analysis (PCA). Spectra were obtained by Dominik Schwudke.

RNA extraction and Real-Time PCR

Cells in a 96 well-plate were rinsed with PBS and then resuspended in 100 μ l buffer RLT (Qiagen, Hilden, Germany). For each sample, lysates from three wells were pooled together. The lysate was then homogenized by centrifugation through a QIAshredder column (Qiagen, Hilden, Germany). RNA was isolated using the RNeasy kit (Qiagen, Hilden, Germany) according to the manufacturers protocol. Finally, RNA was eluted in 30 μ l RNase-free water (Qiagen, Hilden, Germany). To remove DNA contamination, 3 μ l 10x DNase buffer (0.4M Tris, 0.1M NaCl, 60mM MgCl₂ in RNase-free water, pH 7.5) and 1 μ l RNase-free DNase I (10U/ μ l, Boehringer Ingelheim, Ingelheim, Germany) were added to the RNA solution and incubated at 37°C for 30', then at 65°C for 20', cooled on ice and spun down. Then, 11 μ l RNA were heated to 70°C for 10' to destroy secondary structure, cooled on ice for 2' and spun down. For reverse transcription, 4 μ l reverse-transcriptase (RT) buffer (Promega, Mannheim, Germany), 0.4 μ l dNTP Mix (Fermentas, Burlington, Canada), 0.6 μ l oligodT primers (Promega, Mannheim, Germany), 1 μ l RNase inhibitor (Promega, Mannheim, Germany) and 2 μ l H₂O were added to each sample. Before

adding the reverse transcriptase, 1µl was removed from each sample and mixed with 9µl H₂O, to be used as a non-template control during Real-Time PCR. 1µl reverse transcriptase (Promega, Mannheim, Germany) was then added in each sample tube and reverse transcription was carried out at 37°C for 60'.

For Real-Time PCR, 2,5µl cDNA were mixed with 2,5µl forward and reverse primer mix (1µM each) and 5µl SYBR green mix (ABgene, Hamburg, Germany). Primers are listed in table 2. Real-Time PCR was carried out on an Mx3000 instrument (Stratagene, Amsterdam, The Netherlands) using an annealing temperature of 60°C. The house-keeping genes tubulin or GAPDH were used for normalization.

SDS-page and western blotting

After the addition of Laemmli sample buffer, samples were subjected to 3 cycles of heating at 95°C for 5' and sonication for 1' in a Sonorex super 10P sonicator bath (Bandelin, Berlin, Germany). Samples were resolved by SDS-PAGE on mini-gels with various acrylamide percentages and then proteins were transferred from the gels onto nitrocellulose using a semi-dry blot system (Bio-Rad, Munich, Germany).

Blocking was performed for 1h at room temperature or overnight at 4°C in PBS or TBS supplemented with 0.2% Tween and 5% milk (Heirlar, Radolfzell, Germany) or 4% BSA (AppliChem, Darmstadt, Germany). Incubations with both primary and secondary antibodies were performed at room temperature for 2h and 1h respectively in the same solution as for the blocking. After each antibody incubation, blots were extensively washed in PBS or TBS supplemented with 0.2% Tween. Signal was detected using ECL or ECL+ (Amersham, Freiburg, Germany).

Bodipy staining and microscopy

4000 A431 cells were plated in 400µl growth medium in each well of a 24 well-plate 20h before transfection. For each well, 14pmole siRNA were mixed with 100µl Opti-MEM medium and 6µl Hiperfect (Qiagen, Hilden, Germany). The siRNA mix was incubated for 10' to allow formation of the cationic liposome/RNA complex and then added to the cells. 48h after transfection, the growth medium was exchanged for growth medium supplemented with 20µM oleate or for DMEM supplemented with 10% delipidated FCS. 72h after transfection, cells were rinsed once with PBS and fixed with 5% formaldehyde in PBS for 1h at room temperature. Cells were rinsed once again with PBS and Bodipy493/503 (MoBiTec, Göttingen, Germany) was added to the cells at a final concentration of 2µg/ml. Staining was performed in the dark for 1h at room temperature. After extensive rinses with PBS, cells were mounted on slides using 6µl Mowiol (CalBiochem, La Jolla, CA). Images were acquired on a Zeiss Axiovert 200 inverted confocal microscope (Jena, Germany) equipped with a 63x Plan-Apochrom oil objective. Images were acquired by Julia Massier.

Material and Methods: Yeast cells

Material

Sty1 deletion strain of *S. Pombe* (JM1160, L972h⁻ sty1::ura4 leu1-32 ura4-D18 ade6) and its parent wild-type strain (PR109, L972h⁻ leu1-32 ura4-D18) were a kind gift from Dr. J. B. Millar. The wild-type strain L972h⁻ and the strain expressing a GFP-tagged C-truncated NADPH-reductase (PG 2747, CRL126 h⁹⁰ leu1-32 ura4-D18 ade6-216 D817GFP/Leu2) were a kind gift from Dr. I. M. Tolic-Nørrelykke.

Yeast culture

Yeast cells were grown in rich medium (YES) supplemented with 225mg/l uracil, adenine and L-leucine (Sigma, St. Louis, MO) (Forsburg & Rhind 2006), either on agar plate at 30°C or in liquid cultures in a shaking incubator at 30°C and 200rpm.

Glucose depletion

Yeast cells were grown till an optical density (OD) of 0.4 at 600 nm. Cell pellets were obtained by centrifugation, rinsed once with and re-suspended in either Edinburgh minimal medium (EMM2) supplemented with 225mg/l uracil, adenine and L-leucine (Sigma, St. Louis, MO) (Forsburg & Rhind 2006) or, for glucose-free conditions, in the same medium where glucose was replaced by the same quantity of sorbitol (Sigma, St. Louis, MO). Cells were further grown in these conditions for 1h. For lipid analysis by TLC, 1μCi/ml of ³H-oleate was added to the yeast sample during that time.

Nile Red staining and microscopy

Yeast cell pellets were obtained by centrifugation of 2ml culture, re-suspended in 0.5ml PBS supplemented with 3μg Nile Red (Sigma, St. Louis, MO) and incubated 10' in the dark at room temperature and 1000rpm. Cells were rinsed twice in PBS and re-suspended in 200μl PBS. 2μl were used for microscopy. Images were acquired on an Olympus AX70 upright microscope (Hamburg, Germany) equipped with a 100x UplanApo oil objective and a CCD camera controlled with the *Metavue* software (Universal Imaging Corporation, Downingtown, PA).

Lipid extraction and TLC

Yeast cell pellets labeled with ³H-oleate were obtained by centrifugation of 5ml culture and rinsed twice in H₂O. The pellets were then resuspended in 1ml

MeOH/CHCl₃ 2:1. Samples were homogenized by vigorous beating in the presence of glass beads (Sigma, St. Louis, MO) for 2'. After centrifugation, supernatant was transferred to a new tube with 400µl of 50mM citric acid and 600µl CHCl₃. The organic phase was transferred to a new tube and evaporated under a stream of nitrogen. Lipids were then re-suspended in 30µl MeOH/CHCl₃ 2:1 and applied on the TLC plate using a capillary. Lipids were separated by TLC as described above. The TLC plate was then dipped in LumaSafe solution (Lumac LSC, Groningen, Netherlands) and exposed on MP films (Amersham, Freiburg, Germany) for 16h at -80°C.

GFP fluorescence microscopy

Lectin BS-I (Sigma, St. Louis, MO) was spread on a coverslip, which was then glued to the bottom of a microscopy dish. 5µl of yeast culture were added on the lectin and allowed to settle for 5'. Then the dish was filled with the appropriate culture medium. Images were acquired on a Zeiss Axioplan 2 MOT upright microscope (Jena, Germany) equipped with a 100x Plan Neofluar oil objective and a CCD camera controlled with the *Metavue* software (Universal Imaging Corporation, Downingtown, PA).

Growth curve

Cells were grown in the indicated medium and OD was measured at 600 nm on a Ultrospec 3100 pro spectrophotometer (Biochrom, Cambridge, United Kingdom) at various time points. When OD was above 1, yeast cultures were diluted 5x and the measured OD was then multiplied 5x to ensure linearity of the measurement.

Results

The development of a method

The initial step towards a better understanding of lipid homeostasis regulation is the identification of candidate genes implicated in this process. When absent or mutated, these genes would affect the lipid composition of a cell. Therefore, it was necessary to design a method that could monitor such changes.

Systematic deletion or mutation in mammalian cells are still very demanding techniques, and are therefore not suitable for any large-scale analysis. More recently, the discovery of RNA interference (RNAi) (Elbashir et al 2001a, Fire et al 1998), as a tool to specifically decrease the expression level of any gene, has opened new possibilities for large-scale analysis of gene function (Carpenter & Sabatini 2004, Dorsett & Tuschl 2004).

Therefore, RNAi can be used to specifically knock-down a range of potential regulators of lipid metabolism. Subsequent analysis of lipid composition of the resulting knock-downs would allow the identification of genes affecting lipid homeostasis.

Different methods can be used for subsequent lipid analysis. Among them, both the classical thin layer chromatography (TLC) technique and mass spectrometry (MS) were evaluated.

RNA interference: A powerful tool

Previously, post-transcriptional gene silencing in plants and quelling in fungi have shown the existence of a homology-based gene silencing mechanism in cells (Mol et al 1990, Romano & Macino 1992, Wassenegger et al 1994). However, the trigger of this process was not clear. In 1998, Fire et al. made a major observation, for which they were awarded the Nobel Prize last year. They realized that injection of long double-strand RNA (dsRNA) in *C. elegans* potently and specifically results in genetic interference with the corresponding gene (Fire et al 1998). These long dsRNA molecules are processed inside the cells to 21 nucleotides (nt) long small interfering RNA (siRNA), through the action of a ribonuclease type III enzyme called Dicer (Bernstein et al 2001). But, in mammalian system, long dsRNAs induce an interferon response, leading to unspecific inhibition of protein translation (Gil & Esteban 2000). However, in 2001, Elbashir et al. showed that direct introduction of chemically synthesized siRNAs bypasses the interferon response, promoting specific knock-down of the targeted gene (Elbashir et al 2001a).

Once in the cell, the siRNA molecules are incorporated into a RNA-induced silencing complex (RISC) (Hammond et al 2000). This complex is able to recognize the perfectly matching messenger RNA (mRNA) and to induce the cleavage of that molecule (Elbashir et al 2001b, Hammond et al 2000), thereby impairing expression of the corresponding gene.

RNA interference applied to the study of lipid metabolism

siRNAs are 21 nt dsRNA duplexes that contain 2 nt overhangs with a 5'-phosphate and a 3'-hydroxyl termini (Elbashir et al 2001b). These features are characteristic of the cleavage by an RNaseIII enzyme, like Dicer, and are required for proper recognition by the RISC complex (Ma et al 2004, Ma et al 2005, Parker et al 2005). A (almost) perfect complementarity to their target sequence is necessary to induce mRNA cleavage. However, different sequences targeting a same gene can have different effectivity (Harborth et al 2001, Harborth et al 2003, Holen et al 2002), and although some characteristics have been linked to better silencing efficiency (Mittal 2004, Reynolds et al 2004), this variation is still not fully understood. It is therefore often necessary to test several siRNAs differing in sequence to find a potent one. An alternative is to use a mix of enzymatically-processed siRNAs, which are formed by in vitro-cleavage of long dsRNAs by Dicer (Kawasaki et al 2003, Myers et al 2003) or *E.coli* RNaseIII enzymes (Yang et al 2002a).

In this study, both chemically synthesized and RNaseIII-processed siRNAs were used. The RNA interference process was coupled to the analysis of lipid composition. The general scheme of the method is shown in figure 11. A more detailed description of its optimization can be found below.

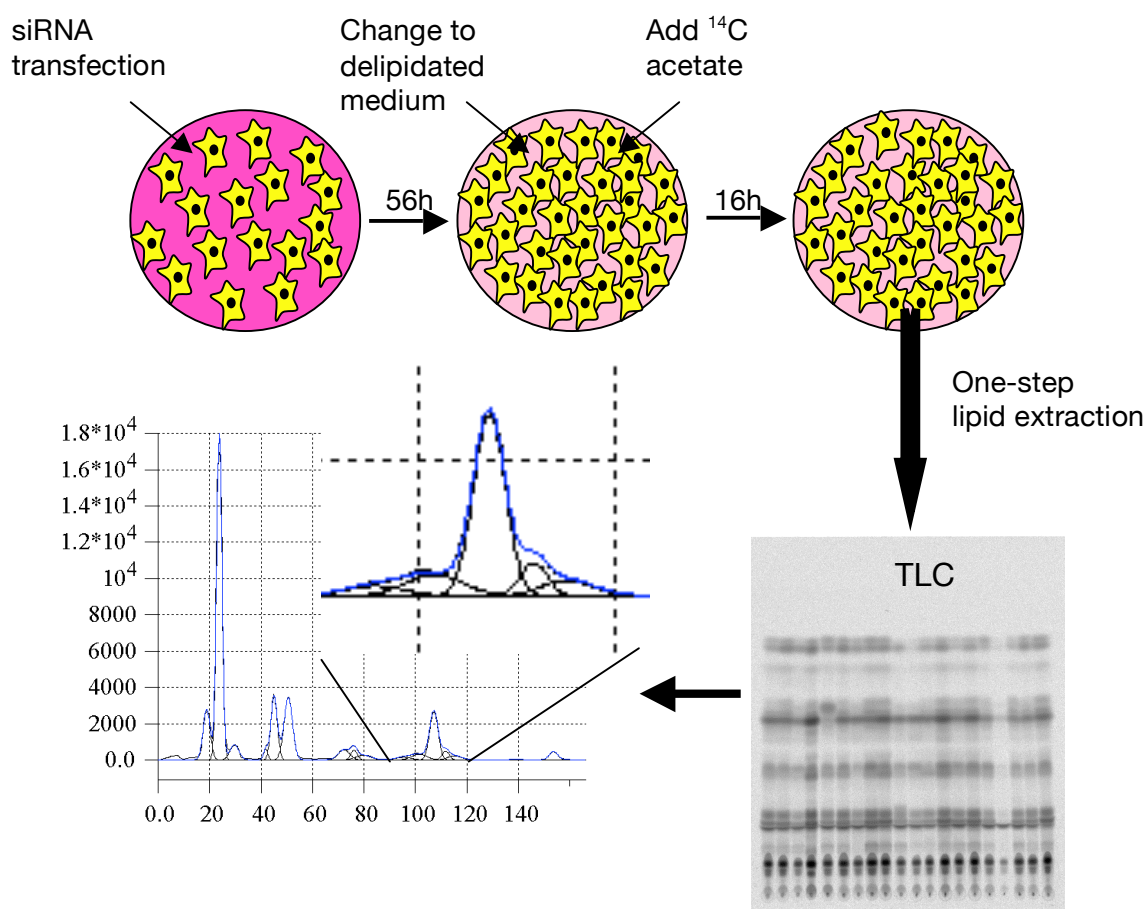


Figure 11: Schematic representation of the method.

SiRNAs can be delivered into cells via lipophilic transfection or via electroporation. However, on basis of previous experience from colleagues and robotic limitations in case of large-scale studies, the lipophilic transfection reagent oligofectamine was selected. Hela cells were used as a model cell line, because of its recognized ease of transfection, an important factor for large-scale analysis.

The efficiency of the knock-down depends not only on the mRNA degradation as such, but also on the turnover of the already existing proteins. Therefore, effective knock-down of a protein may require 72h (Elbashir et al 2002, Jackson et al 2006). Therefore, this time point was selected for harvesting the cells for lipid analysis.

To promote lipid synthesis, cells are placed in lipid-free condition 24 hours before harvesting. This is achieved by the use of a growth medium containing delipidated FBS (Thiele et al 2000). 16 hours before harvesting, radioactive acetate is added into the wells. Acetate is the building block of all the major lipids in the cell (figure 12). The use of radioactive acetate therefore results in labeling of all newly synthesized lipids.

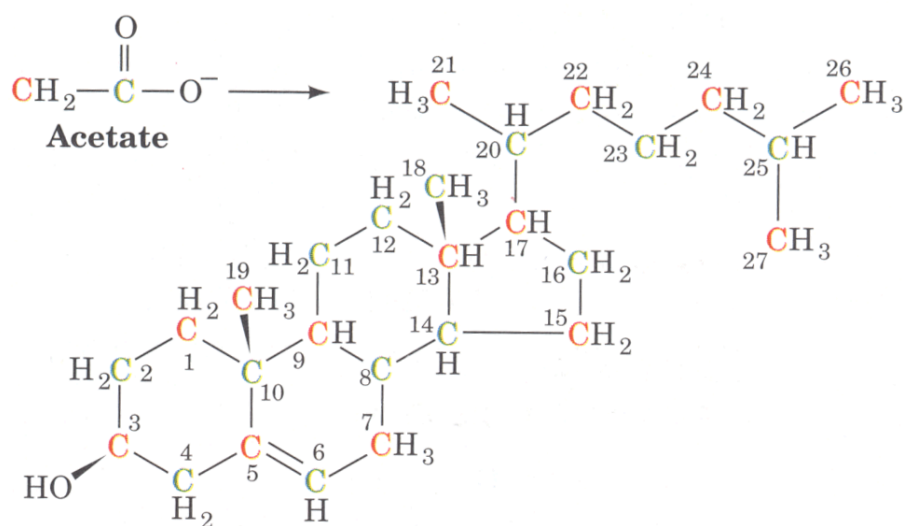


Figure 12: Incorporation of acetate into cholesterol. The red and green carbon atoms depicted in the molecule of cholesterol are derived through biosynthesis from the carbon atom depicted in the same color in the acetate molecule.

At the time point of harvesting, cells are rinsed and lipids are directly extracted using a one-phase system. Different compositions of the extraction solution were tested, namely MeOH, MeOH/CHCl₃ 5:1 and MeOH/CHCl₃ 3:1. As shown in Fig. 3.3, no major difference in efficiency was observed using either MeOH or MeOH/CHCl₃ 5:1 for the lipid extraction. The use of a higher ratio of CHCl₃ however decreased the efficiency of the extraction. In addition, the one-phase method was compared to the classical 'Bligh and Dyer' two-phases lipid extraction system (Bligh & Dyer 1959), and again no significant difference was observed. The influence of increasing amount of radioactive acetate on the staining was also tested. Although labeling with 1μCi/well gives a weaker staining, similar output signals were obtained using 2μCi or more (figure 13). Therefore, addition of 2μCi ¹⁴C-acetate per well, and a one-

phase lipid extraction, namely MeOH/CHCl₃ 5:1, were chosen to obtain the best lipid signal.

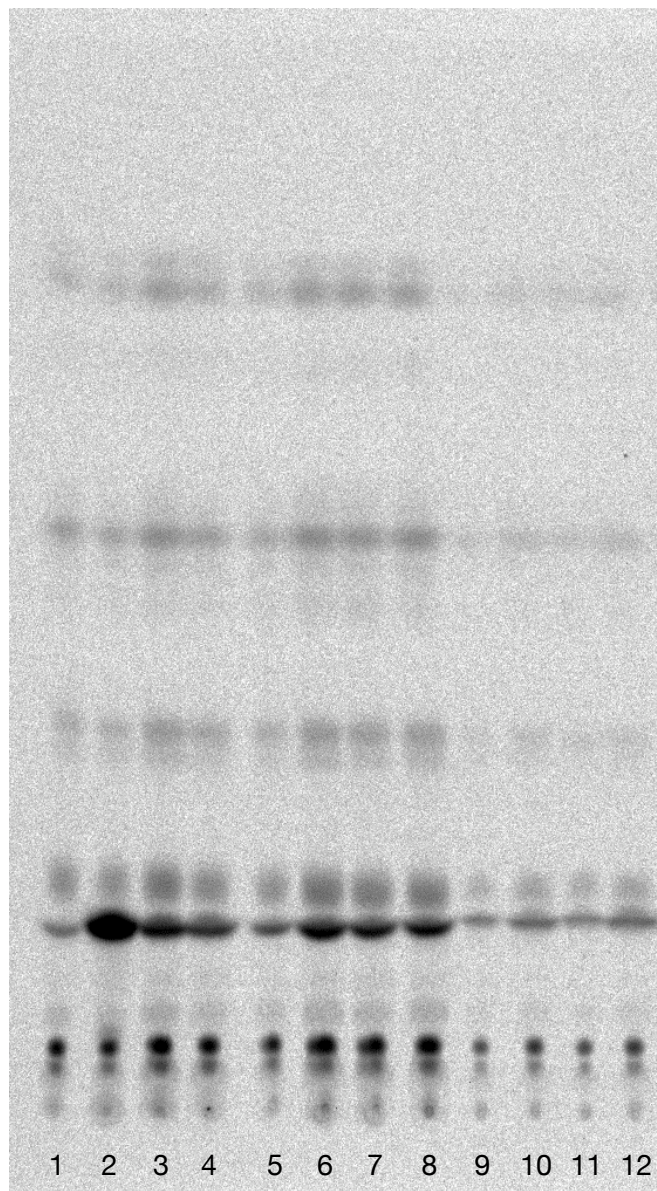


Figure 13: Test of extraction and labeling conditions.

¹⁴C-labeled lipids from Hela cells were extracted using MeOH (lane 1-4), MeOH/CHCl₃ 5:1 (lane 5-8) and MeOH/CHCl₃ 3:1 (lane 9-12) after labeling with various amounts of radioactivity (1μCi in lanes 1, 5 and 9, 2μCi in lanes 2, 6 and 10, 3μCi in lanes 3, 7 and 11 and 4μCi in lanes 4, 8 and 12). Signal was visualized upon exposure on phosphoimager plate.

The lipid extracts are then separated on a TLC plate using a two-solvent system as described previously (Kuerschner et al 2005). However, to improve the separation of the different classes of phospholipids, the possibility to increase the hydrophilicity of the first solvent was tested (data not shown). The chosen composition was finally EtOH/H₂O/triethylamine/CHCl₃ 50:10:35:35. To further improve the resolution, high

performance TLC (HPTLC) plates or pre-concentrative migration were tested, but no convincing results were obtained.

To identify the different lipid bands and further confirm that this system allows good separation of all the major lipid classes, standards of these lipids were run in this system and their migration was compared with the Hela cells lipid extract (figure 14).

In the case of acetate labeling, the radioactive signal can be visualized upon exposure on a phosphoimager plate. Then, a lipid intensity profile of the different lanes is obtained. Thanks to the software *Graph Explorer* developed in-house by Yannis Kalaidzidis (Kalaidzidis et al 1997), it is now possible to directly compare profiles or quantify the individual bands. Conversely to previously existing quantification programs, the lipid bands are fitted with Gaussian curves, taking into account the overlapping of different classes of lipids that are insufficiently resolved by the chromatography itself. This therefore strongly improves the reliability of the results. However, attempts to automate the quantification procedure were unsuccessful, limiting the use of quantification to the analysis of a small number of samples.

Finally, the effect of the transfection reagent on lipid composition was also tested. The lipid composition of wild type untreated cells or cells treated with oligofectamine were compared using both TLC and MS analysis. A similar lipid pattern was observed by TLC for both untransfected and mock-transfected cells (figure 16, lanes 1 and 15). For the MS analysis, untransfected and mock transfected cells were compared to cells treated with siRNA inducing a known change in lipid composition, as determined previously by TLC (data not shown). The MS analysis was performed by Dominik Schwudke and the MS data were then processed by Principal Component Analysis (PCA) as described previously (Schwudke et al 2007). As it can be seen in the PCA plot (figure 15), the mock transfected and untransfected samples, as well as the samples treated with a siRNA which didn't induce any change in lipid composition cluster together, while the siRNA inducing either an increase in SM or an increase in TAG are found in a completely different area of the plot. This confirms by an independent method that no major change in lipid composition is induced by the oligofectamine treatment, confirming that this transfection reagent can be used despite its lipidic nature.

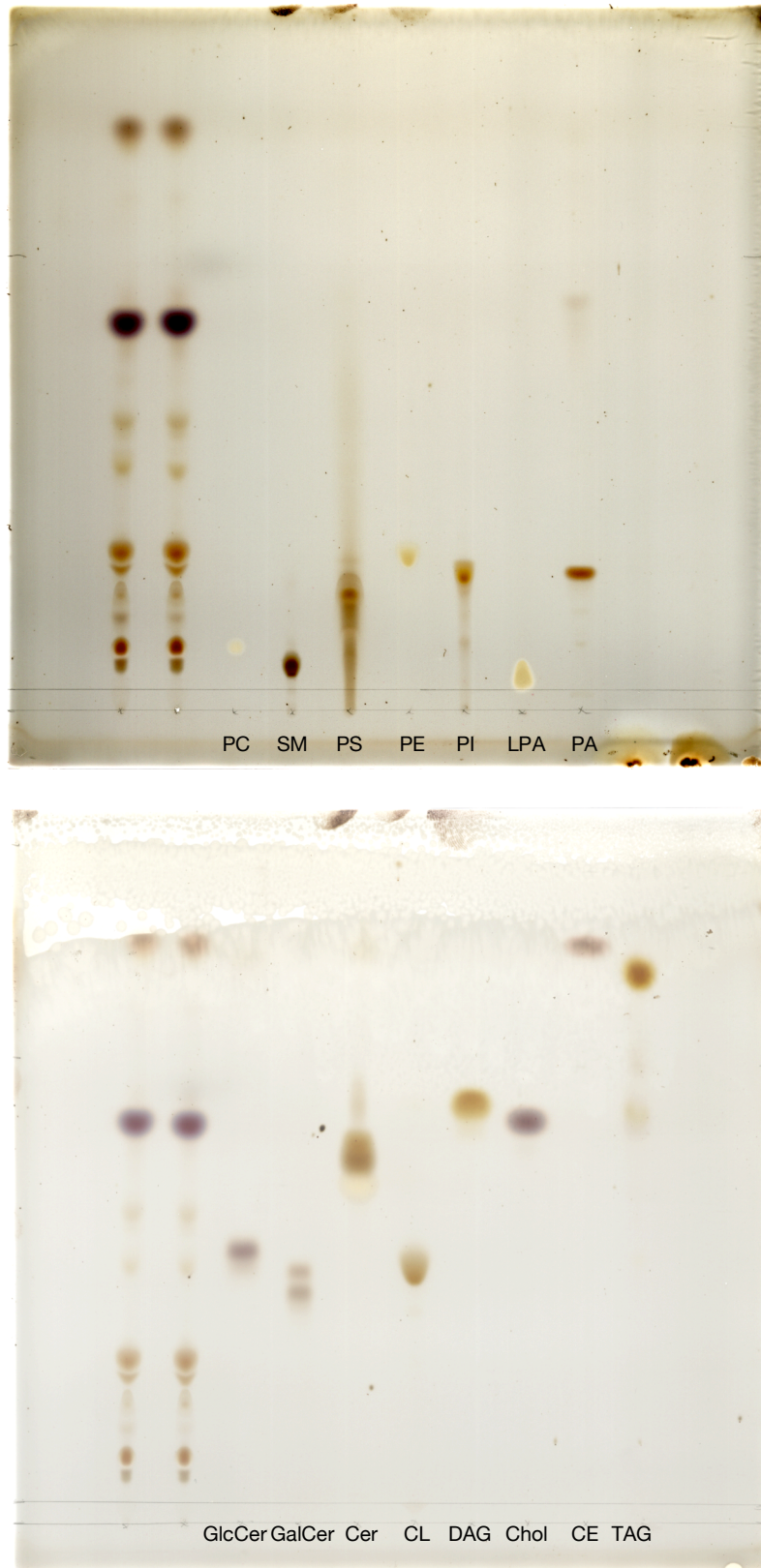


Figure 14: TLC with standard lipids.

Different standard lipids indicated in the picture were applied on a TLC plate and submitted to our two-solvents running system. Their migration can be compared to the corresponding bands in the HeLa cells lipid extracts (the two first lanes of each plate) in order to identify the nature of the different lipids separated by this system. Lipids were visualized by charring with H_2SO_4 .

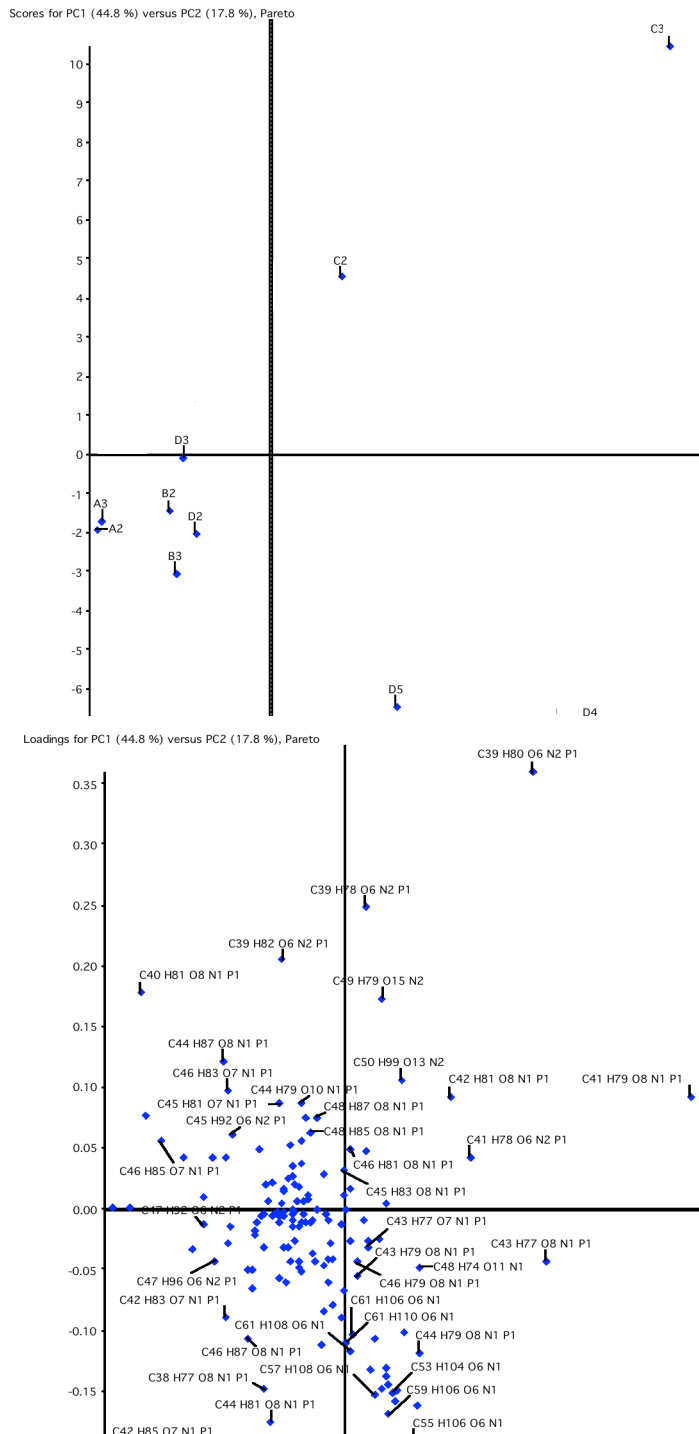


Figure 15: Effect of oligofectamine on lipid composition as determined by MS.

(a) The PCA plot was built on the basis of the individual mass signals obtained during the MS experiment. A2/3: untreated cells, B2/3: mock transfection. C2/3: siRNA inducing an increase in SM, D2/3: siRNA inducing no lipid modification, D4/5: siRNA inducing an increase in TAG.

(b) Loading plot: each chemical formula stands for the corresponding lipid species, and inform on its weight in the positioning of the samples into the PCA plot.

Finding the controls

Appropriate controls are essential in the design of large-scale experiments. As negative controls, mock transfection was used as well as transfection with siRNA that would not target any gene in the genome, like F-luciferase, neomycin or the scrambled silencer siRNAs S2, S5 and S6.

As a positive control to test transfection efficiency, the previously characterized Eg5 gene was selected (Harborth et al 2001, Weil et al 2002). This gene encodes for a kinesin related protein implicated in mitosis. Upon knock-down, cells arrest in mitosis, and ultimately die. This results in the round appearance of the cells and, on a TLC plate, in the absence of radioactive signal.

To find appropriate positive controls related to lipid metabolism, enzymes of the lipid biosynthetic pathway were analyzed. For this purpose, endoribonuclease-prepared siRNA (esiRNA) (Yang et al 2002a), derived from a library generated by Ralf Kittler (Kittler & Buchholz 2003), were used. In brief, cDNA clones were used as a starting material, from which dsRNAs were generated and then cleaved in small fragments by *E.coli* RNaseIII.

Among all the proteins tested, only the knock down of the sterol O-acyl transferase (SOAT1) was inducing a visible phenotype. SOAT1, sometimes better known as Acyl-Coa:cholesterol acyltransferase (ACAT1), is responsible for the esterification of cholesterol. Knock-down of this gene effectively induces a decrease in cholesterol ester level (figure 16).

Further quantification of the lipid profiles generated by the different knock-downs demonstrates that upon esiRNA treatment against the PI synthase, a small decrease in PI level is also observed (figure 17).

Although phenotypes could have been expected for other knock-downs, there may be several possible explanations. First, this can result from a poor effectiveness of some of the esiRNAs, or a slow turnover of the corresponding protein. In addition, as most of the genes tested were enzymes, a small quantity of protein left could be sufficient to perform its function and maintain lipid homeostasis (Harborth et al 2001). Furthermore, redundancy in the lipid biosynthetic pathway could also account for absence of phenotype in some knock-downs.

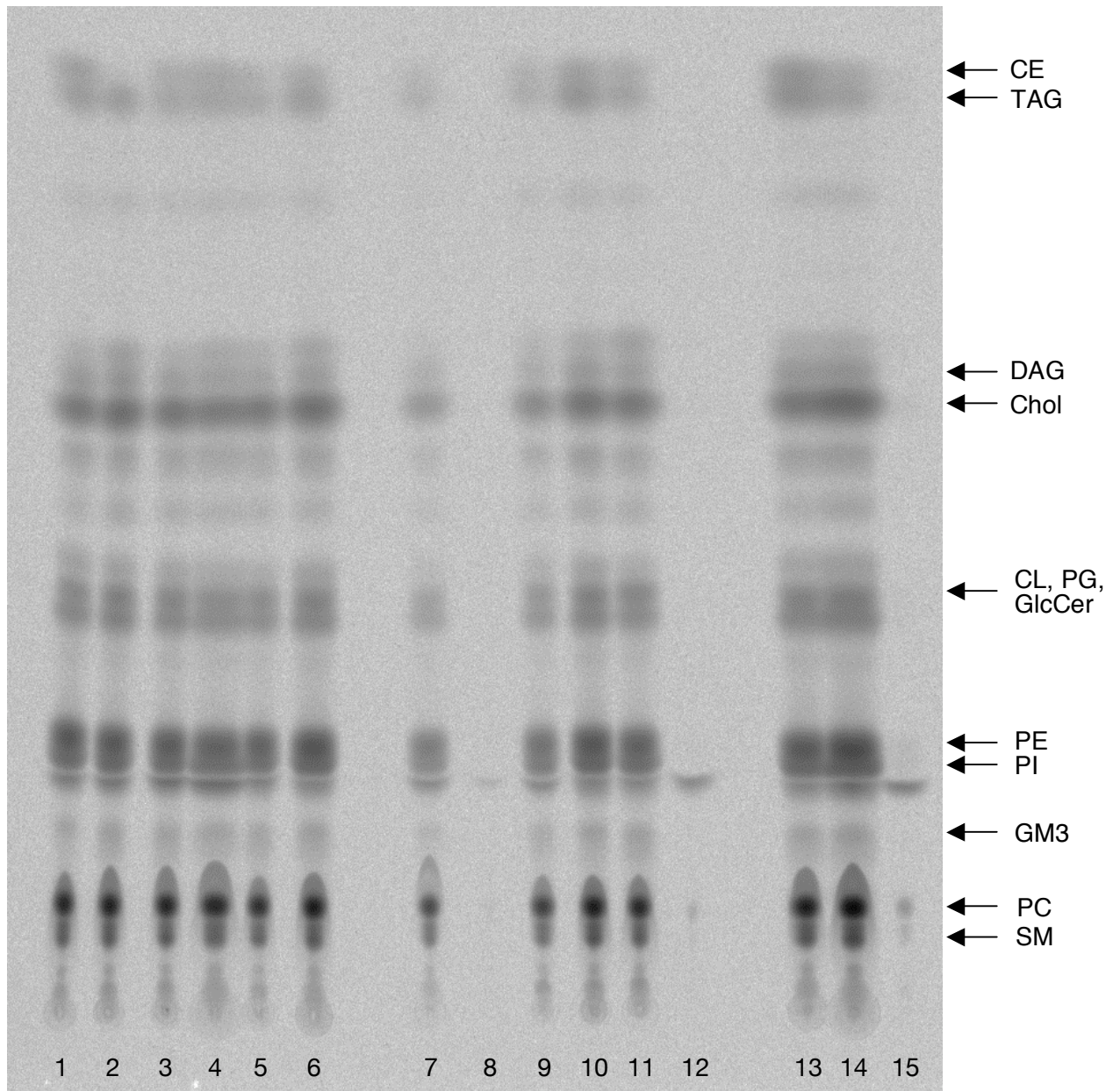


Figure 16: TLC analysis of lipid extracts of esiRNA knock-downs.

¹⁴C-labeled lipid extracts from HeLa cells treated with esiRNA against the following genes: (1) no transfection, (2) SOAT1, (3) FATP3, (4) FATP5, (5) mevalonate kinase, (6) DGAT2, (7) squalene synthase, (8) PI synthase, (9) SPT2, (10) CTP-cytidyltransferaseB, (11) SPT1, (12) Eg5, (13) F-luc, (14) R-luc, (15) mock transfection. The positions of the different lipid classes on the plate are indicated on the right of the plate. Radioactive signal was visualized upon exposure on phosphoimager plate.

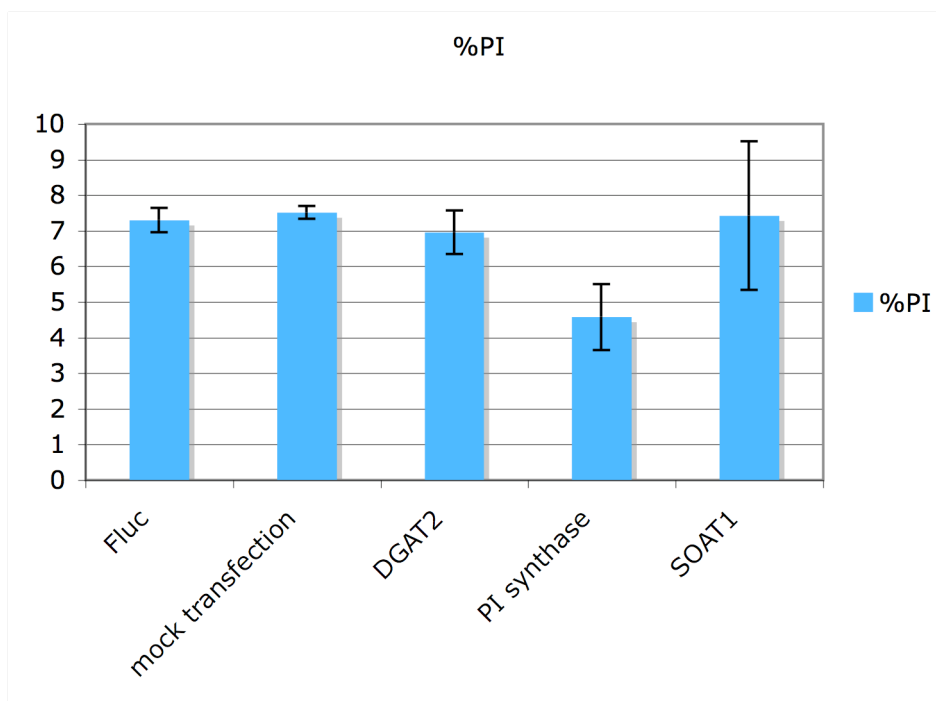


Figure 17: Decrease of PI levels in the PI knock-down.

Upon Gaussian fitting of the lipid profiles, the percentage of PI relative to the total amount of lipid was determined for the PI synthase knock-down and compared to mock transfection, the negative control F-luciferase and the knock-down of the unrelated enzymes DGAT2 and SOAT1.

Signal normalization

SiRNA transfection can induce toxicity and thereby cell death. To be able to compare the lipid signal of different samples, normalization is necessary. In case of complete quantification of the profiles, normalization to total lipid signal was achieved. However, this requires fitting of all the bands and is therefore not appropriate for large-scale analysis. To overcome this problem, normalization was done to the most abundant lipid, PC, for profile comparisons. From the initial studies, PC appeared to be less subject to level variation than some other lipids. Furthermore, variation in PC would still be visible by the resulting increase or decrease in all the other lipid classes after normalization.

This normalization method however limits the observations to variations in the level of specific lipids and modification of total lipid synthesis or degradation would not be detectable. Normalization to the cell number could overcome this limitation. Therefore, several protein quantification tools were evaluated for use directly in the wells after lipid extraction. However, this often led to interference with the SDS used to redissolve the protein (for the Bradford assay), or to an overestimation of protein levels at low cell numbers (for the BCA and fluorescamine assays). This effect is probably due to the presence of bovine serum albumin (BSA) in the serum. Because

of its hydrophobicity, BSA easily sticks to the walls of the wells and thereby impairs cellular protein determination.

Better results however were obtained using propidium iodide to evaluate the total DNA content of a well (figure 18). A linear signal could be obtained after long incubation of the dye with the cells to allow saturation of the signal. Although this method was not precise enough to normalize the lipid signal, it could be used to identify strong variation in total lipid synthesis upon specific knock-down.

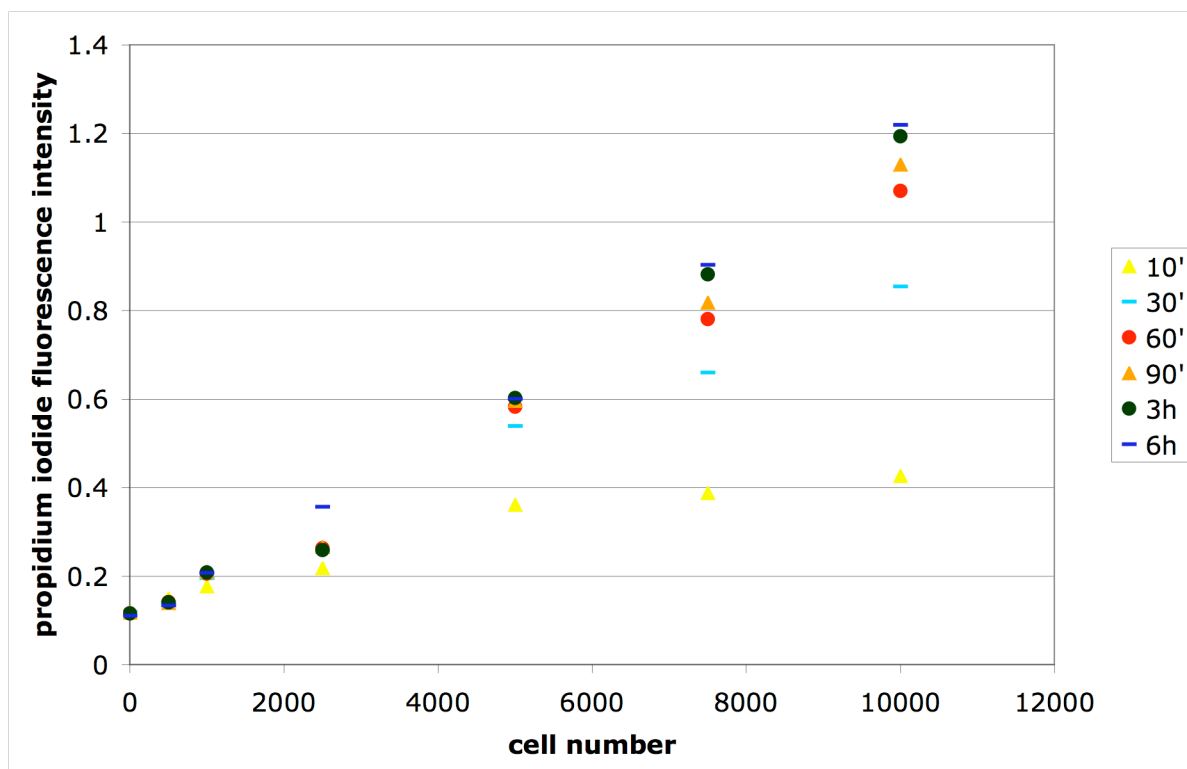


Figure 18: Propidium iodide fluorescence intensity in function of the number of cells plated. Cells were plated 16h before measurement. Fluorescence intensity was measured at 620 nm at different time points. Linearity was observed after 3h or 6h of incubation with the dye.

Mass spectrometry: An alternative method to study lipid composition

In the past few years, mass spectrometry appeared as a powerful tool to study biological molecules. Proteomics efficiently used this technique to decipher the protein content of specific cells or organelles (Peng & Gygi 2001). More recently, there has been a rising interest in the use of mass spectrometry as a tool to analyze lipid composition (Brugger et al 1997, Han & Gross 2003, Schneiter et al 1999). The potential of this method to study the lipid composition of the knock-downs was therefore investigated.

While TLC analysis is limited to the study of newly synthesized lipids that have been labeled with radioactive acetate, MS doesn't require any labeling and generate

therefore a profile of all the lipids present in a sample at a given time point. In addition, MS analysis enables not only identification of the different lipid classes but distinguishes between several species differing by their fatty acid composition and therefore by their mass. This allows therefore a more precise overview of the lipid composition of a sample. However, since several species from different classes may have very similar masses (Schwudke et al 2007), there may be some uncertainty on the nature of certain lipid peaks, which could only be revealed by further fragmentation of these lipids and subsequent MS analysis, a method known as MS/MS. Nevertheless, the use of mass spectrometer with high mass accuracy, such as the Orbitrap instrument (Hu et al 2005), partially overcomes this problem (Schwudke et al 2007). The other limitation of mass spectrometry is the difficulty to analyze neutral lipids, like sterols, which are of major importance in cells. This can be overcome by derivatisation (Liebisch et al 2006), a process that adds a charge to the molecule. However, this is difficult to perform in the context of the analysis of a large number of samples and limits therefore large-scale lipid analysis by MS to the study of charged lipids.

Therefore TLC analysis and mass spectrometry can be viewed as complementary techniques in the generation of the lipid profile of biological samples.

So far, large-scale analysis by mass spectrometry was limited by the manual injection of the sample in the electrospray ion source. However, the introduction of the robotic nanoflow ion source Nanomate, which allows automatic injection of samples from a 96 well-plate, increases the potential of this technique for large-scale analysis (Schultz et al 2000).

To evaluate the potential of the method in the context of the screening procedure developed above, lipid extracts generated by one-phase extraction of Hela cells in 96 well-plate were applied to MS analysis on a Esi-QqTof mass spectrometer (Chernushevich et al 2001). Unfortunately, as shown in figure 19 a, this gave rise to very noisy spectra, probably due to the concomitant extraction of a large number of compounds generally removed by a two-phase extraction. Accordingly, spectra generated after two-phase extraction of the same sample contain much less contaminating peaks (figure 19 b.). More hydrophobic extraction solutions were further tested, to limit the extraction of some contaminating hydrophilic compounds, but this didn't improve sufficiently the quality of the spectra (data not shown). The use of MS analysis was therefore limited for this study to the characterization of samples that would be selected after TLC analysis.

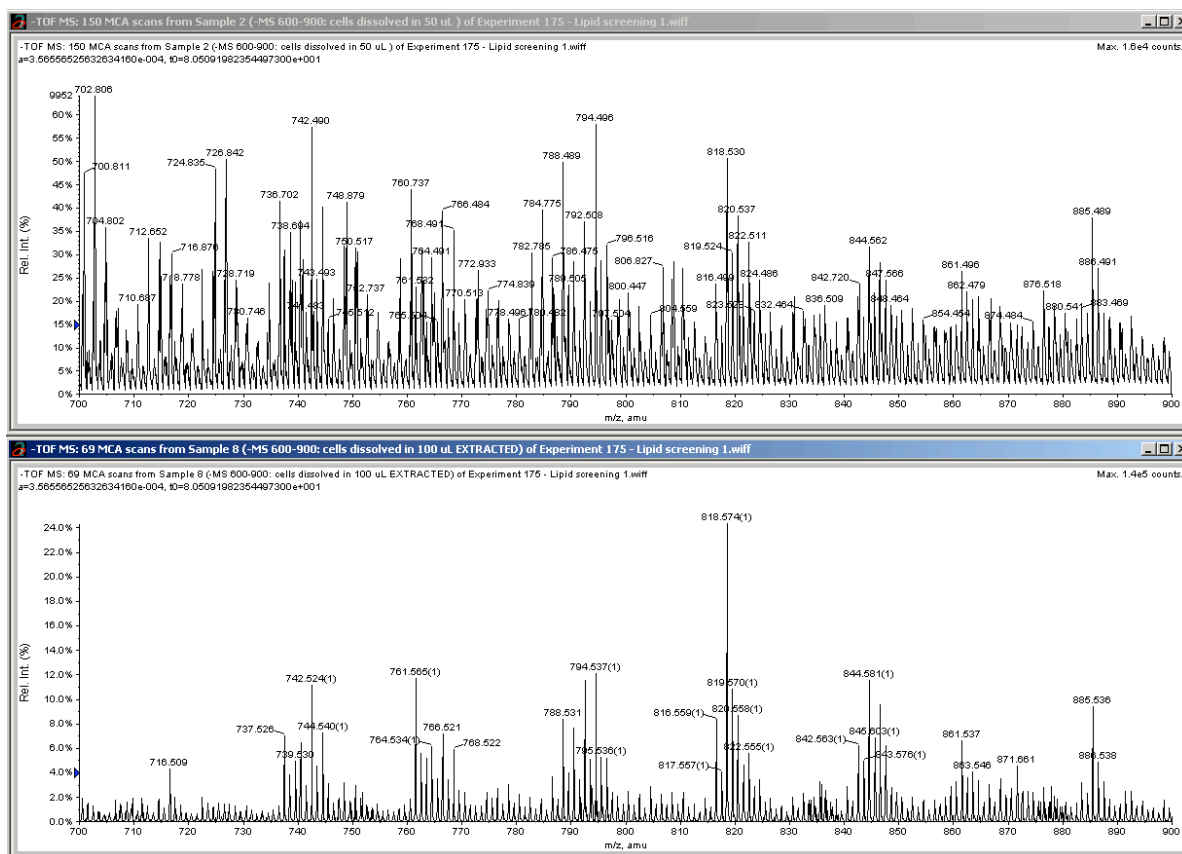


Figure 19: Esi-MS analysis of lipid extracts from HeLa cells obtained either by (a) one phase lipid extraction in a well of a 96 well-plate using MeOH/CHCl₃ 2:1 supplemented with 5 mM ammonium acetate or (b) after subsequent addition of water and two-phase extraction of the same sample. Spectra were generated by Christer Ejsing on a Esi-QqToF mass spectrometer.

MS spectra enable identification of a large number of individual species, and, as a result, give rise to a large number of data. It is therefore wise to simplify the dataset in order to identify variation in lipid composition between several samples. To do so, Schwudke et al. developed a method based on principal component analysis (PCA) (Schwudke et al 2007). Briefly, this method reorganizes the individual variables – here the signal of each individual mass – into a new set of variables called principal components. By giving different weight to each original variable, the method can extract similarities and differences between the samples. The first principal components (PC1 and PC2) will thereby contain the information on the major differences between the samples. These samples can then be plotted in function of their principal components. Samples of similar lipid composition will then be found in the same area of the PCA plot, while samples having a different lipid composition will be located somewhere else. The PCA loading plot informs on the influence of lipid species of a given mass to the position of a sample on the PCA plot. Thereby, one can find back which lipids may be responsible for the difference.

The method was tested by analyzing perturbations of the lipidome of HeLa cells upon addition of specific fatty acids in the cell culture medium. Then, the samples were analyzed by MS on a LTQ-orbitrap mass spectrometer (Hu et al 2005) by

Dominik Schwudke and the resulting data sets, comprising 262 mass signals, were submitted to PCA analysis (figure 20). Using the PCA loading plot, it is possible to identify the lipid species of a given mass whose intensity was specifically modified in the different samples. Further MS/MS analysis of the corresponding peaks confirmed that addition of myristate, palmitate or oleate specifically induce an increase in the PC and TAG species harboring the corresponding fatty acid (table 3).

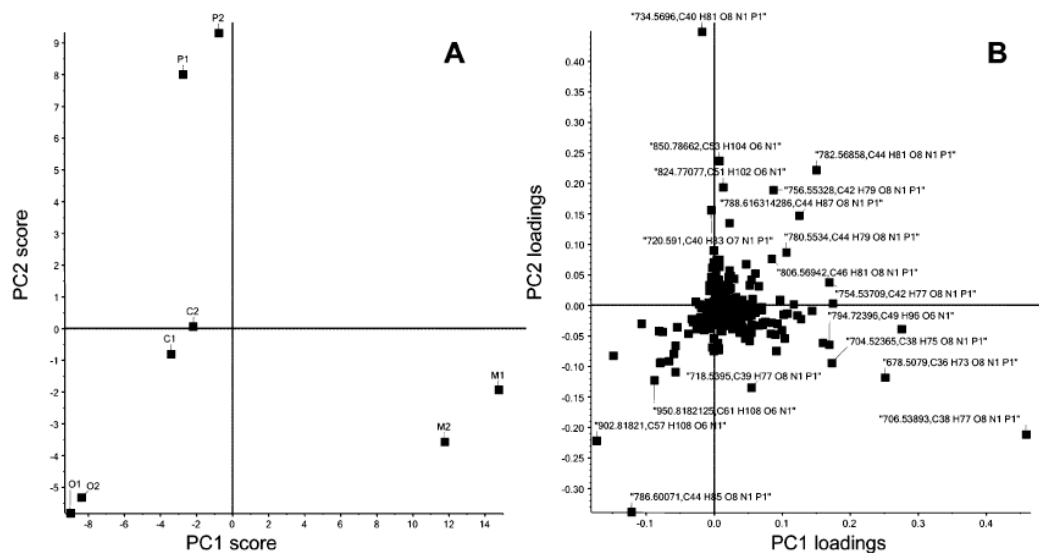


Figure 20: Principal Component Analysis (PCA) of 262 individual mass detected in HeLa cells feeding experiments.

(A) PCA plot (B) PCA loading plot. M1, M2 stand for two independent experiments with addition of myristic acid; O1, O2: of oleic acid; P1, P2: of palmitic acid; C1, C2: controls, no extra fatty acid added.

This method appears therefore as a good tool to characterize the variation in lipid composition that can arise from RNA interference of certain genes and can be utilized for secondary analysis of potential hits.

Table 3: Lipid species whose abundance was specifically increased by spiking fatty acids, as revealed by Principle Component Analysis. M1, M2 myristic acid added (FA 14:0); O1, O2 oleic acid added (FA 18:1); P1, P2 palmitic acid added (16:0), C1, C2: controls. Relative intensities are presented in percentage normalized to the most abundant lipid sum composition $C_{42}H_{83}O_8N_1P_1$, subsequently identified as PC 34:1.

m/z	Sum Composition	Lipid	M1	M2	O1	O2	P1	P2	C1	C2
706.5389	C38 H77 O8 N1 P1	PC 14:0/16:0	54.3	50.7	13.7	13.4	14.1	14.1	15.7	16.1
704.5237	C38 H75 O8 N1 P1	PC 14:0/16:1	7.9	7.3	2.0	2.0	1.7	1.8	2.5	2.6
678.5079	C36 H73 O8 N1 P1	PC 14:0/14:0	13.3	10.8	0.6	0.5	0.4	0.5	0.7	0.7
794.7240	C49 H96 O6 N1	TAG 14:0/14:0/18:1; TAG 14:0/16:0/16:1	6.5	4.3	0.2	0.2	0.5	0.3	0.1	0.1
786.6007	C44 H85 O8 N1 P1	PC 18:1/18:1	45.0	44.3	54.2	54.6	39.5	41.1	45.1	44.7
902.8182	C57 H108 O6 N1	TAG 18:1/18:1/18:1	1.4	1.4	12.3	14.3	1.9	2.6	2.3	1.9
876.8024	C55 H106 O6 N1	TAG 16:0/18:1/18:1	3.3	3.1	10.1	11.6	5.6	6.6	3.9	3.2
734.5696	C40 H81 O8 N1 P1	PC 16:0/16:0	34.2	35.8	32.8	31.5	53.3	46.6	37.4	37.7
824.7708	C51 H102 O6 N1	TAG 16:0/16:0/16:0	1.2	0.9	0.2	0.2	4.6	3.1	0.4	0.3
850.7866	C53 H104 O6 N1	TAG 16:0/16:0/18:1	3.3	2.8	2.2	2.4	7.9	7.1	1.6	1.4

The Kinase Screen

After development of the method, it was possible to apply it to the study of protein families whose members could potentially be implicated in lipid homeostasis. Kinases have been previously implicated in the regulation of numerous processes and appear therefore as obvious candidates in the study of lipid regulation.

SiRNA libraries against kinases have been developed and made commercially available. The siRNA library used was designed by Ambion and targets 600 kinases, each of them with three siRNA sequences. Individual siRNA sequences vary in efficiency in a manner not yet fully understood. In order to ensure a sufficient efficiency for each kinase, the screen was performed using a pool of the three individual sequences, hypothesizing that at least one of them would be sufficiently potent to reach a good knock-down efficiency.

The preparation of the screen

Because of the large number of samples, the screen was performed in collaboration with the Technology Development Studio (TDS), using their robotic equipment for transfection.

Since the method was initially developed using esiRNAs, the reproducibility of the positive control SOAT1 was tested using siRNAs. The efficiency of the knock-down was monitored by Real-Time PCR using either individual siRNA or a pool of the three sequences available. The best knock-down efficiency was obtained using the siRNA pool, although the individual sequence 1 was much less efficient than the two others (figure 21). Then, the potency of these siRNAs to decrease cholesterol ester level was tested by TLC. Both the individual sequence 2 and the pooled sequences gave rise to a strong decrease in cholesterol esters, while the individual sequences 1 and 3 induced only a moderate decrease (figure 22). Taken together, these results confirm that the use of a pool of individual sequences ensures a good knock-down efficiency without need for testing individual sequences.

As a last control, SOAT1 mRNA level and cholesterol ester level were monitored after robotic transfection for the negative control S2 and the positive control SOAT1. Similar results as for manual transfection were obtained (results not shown), confirming that robotic transfection was suitable for our assay.

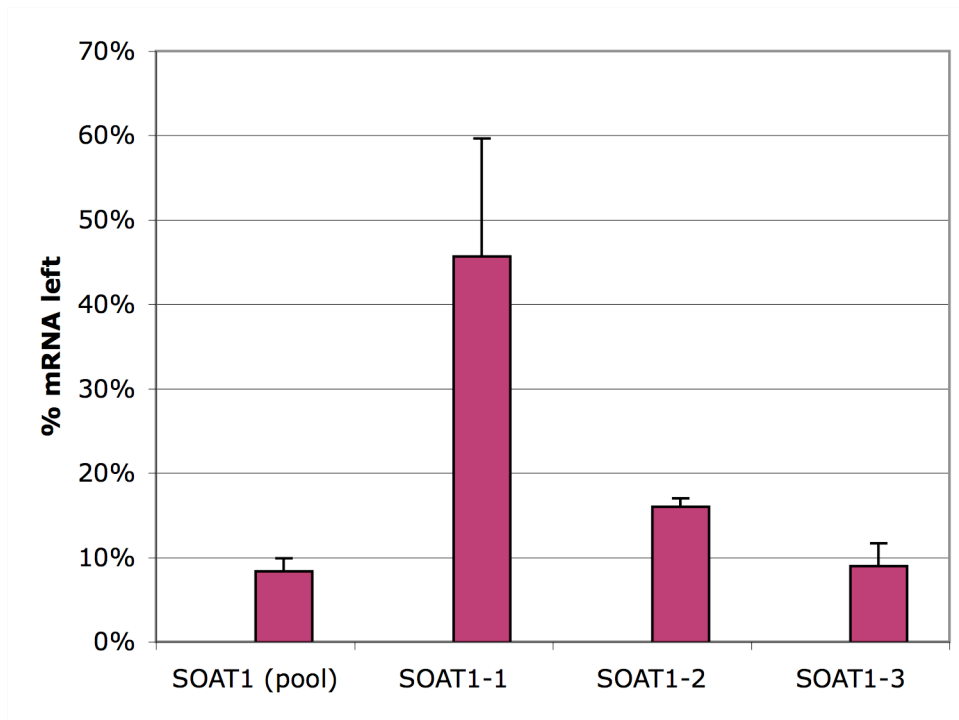


Figure 21: Decrease in SOAT1 mRNA level upon siRNA treatment. Percentage of SOAT1 mRNA level left 72h after siRNA treatment in the siRNA knock-downs relative to mock transfection and neomycin siRNA negative controls. Values are normalized to tubulin mRNA level to account for variation of total mRNA. Error bars represent standard deviation.

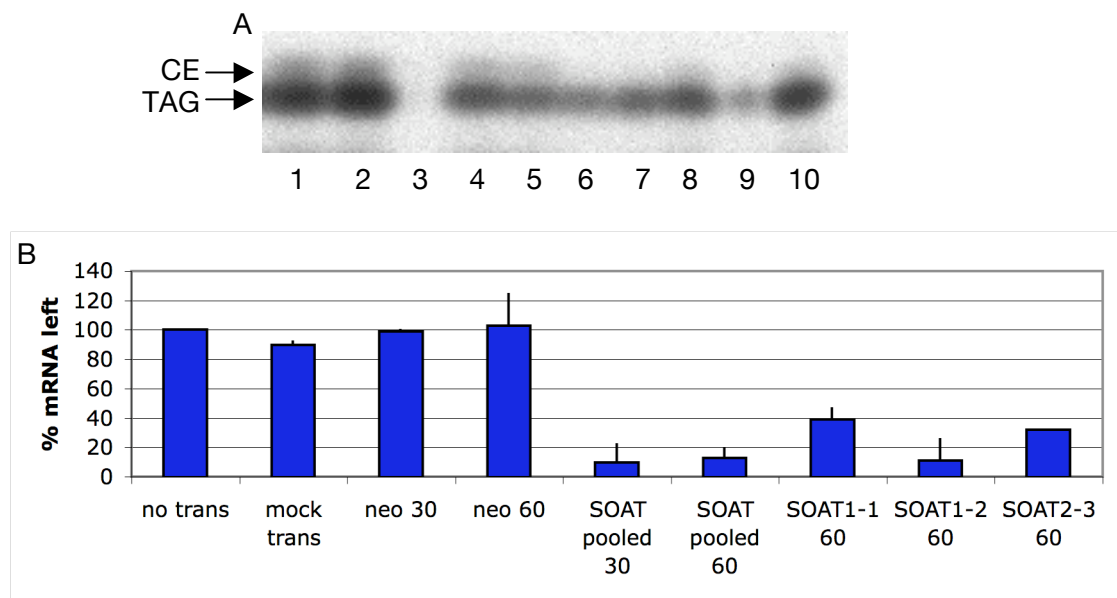


Figure 22: Decrease of cholesterol esters upon SOAT1 siRNA knock-down. (a) Close-up on the ^{14}C -labeled storage lipids on a TLC. Lipids were extracted 72h after transfection for the following samples: no transfection (1), mock transfection (2), or treatment with siRNA against eg5 (30nM) (3), neomycin (30nM) (4) or 60nM (5) and SOAT1 (pool (30nM) (6)), pool (60nM) (7), sequence 1 (60nM) (8), sequence 2 (60nM) (9) and sequence 3 (60nM) (10)). (b) Ratio between cholesterol ester and triglyceride levels after normalization to non-transfected samples. Error bars represent standard deviation.

The Screen

A screen targeting 600 human kinases was performed in Hela cells in duplicates using a pool of three siRNAs per gene. The screen was carried out in a 96 well-plate format, although only the 60 internal wells of the plates were used to avoid unspecific effects related to medium evaporation in the external wells.

The transfection was performed following the scheme shown in figure 23. Although most of the wells were transfected with siRNAs against kinases, each row contained either a well transfected with the pool of SOAT1 siRNAs, used as positive control, or a well mock-transfected as negative control. This ensures that each TLC plate contains a positive and a negative control. In addition, several wells dispersed in the plates were transfected either with the positive control eg5 or with the negative control S2.

In addition, the number of cells in each well was evaluated by fluorescent measurement using propidium iodide, in order to take into account cell death and variation in cell growth after the siRNA treatment.

Lipid extracts from the siRNA transfected cells were then separated by TLC. A sample TLC plate is shown in figure 24. Such plate contains both the positive control SOAT1 and the negative mock transfection control (figure 24, lane b and c respectively). The other samples are derived from the kinase knock-downs. Out of the 600 kinases, 35 were identified whose knock-down induces a modification of lipid composition readily visible on the TLC plate. Mostly, the level of cholesterol or triglyceride was affected in these knock-downs. Further analysis of the different knock-downs was achieved by comparison of the lipid profiles. This extended the number of gene knock-downs inducing a phenotype to 91.

Using the program CUPID, the kinases were clustered in function of the modifications of their lipid profiles (figure 25). Thereby, 10 phenotypic classes characterized by their lipid phenotype could be identified. It must be noted that no correlation was observed between the kinase groups generated by the clustering and the kinase families shown in the same color in figure 23. This suggests that different members of a same family of kinases are implicated in different biological processes, while several kinases from different families can act together or independently in a specific regulation process.

AGC-CAMK-R1

	1	2	3	4	5	6	7	8	9	10	11	12
A												
B		GPRK7	HSA250839	LATS1	LATS2	MAST205	MGC23665	CDC42BPA	PDPK1	pknbeta	SOAT	
C		PRKCA	PRKCB1	PRKCD	PRKCE	PRKCG	PRKCI	PRKCL1	PRKCL2	PRKCQ	mock	
D		PRKX	PRKY	RHOK	ROCK1	ROCK2	RPS6KA1	RPS6KA2	RPS6KA3	RPS6KA4	SOAT	
E		RPS6KB2	RPS6KC1	RPS6KL1	SGK	SGK2	SGKL	STK38	STK38L	PRKCH	mock	
F		ARK5	C20orf97	C8FW	CAMK1	CAMK1G	CAMK2A	CAMK2B	CAMK2D	CAMK2G	SOAT	
G		CKLIK	DAPK1	DAPK2	DAPK3	DCAMKL1	GS3955	HUNK	KIAA0999	KIAA1811	mock	
H												

AGC-CAMK-GO1-R2

	1	2	3	4	5	6	7	8	9	10	11	12
A												
B		GPRK6	ADRBK1	MAPKAPK3	CDC42BPP	MELK	PRKACA	PRKACB	CHK	ADK	SOAT	
C		PRKACG	ADRBK2	MAPKAPK5	DMPK	MGC42105	PRKCZ	PRKG1	DGKI	AK1	mock	
D		PRKG2	AKT1	MARK1	FLJ14813	MGC45428	RPS6KA5	RPS6KA6	FLJ13052	AK3	SOAT	
E		RPS6KB1	AKT2	MARK2	FLJ25006	MGC8407	NM_007174	eg-5	HK1	AK3L1	mock	
F		APEG1	AKT3	MARK3	GPRK2L	MKNK1	CAMK4	CASK	MGC26597	AK5	SOAT	
G		CHEK2	CDC42BPA	MARKL1	GPRK5	MKNK2	LOC283629	MAPKAPK2	NYD-SP15	C9orf12	mock	
H												

CMGC-CAMK-R3

	1	2	3	4	5	6	7	8	9	10	11	12
A												
B		CDK9	CDKL1	CDKL2	CDKL3	CDKL5	CLK1	CLK2	CLK3	CLK4	SOAT	
C		DYRK2	DYRK3	DYRK4	ERK8	FLJ32818	GSK3A	GSK3B	HIPK2	HIPK3	mock	
D		MAPK1	MAPK10	MAPK11	MAPK12	MAPK13	MAPK14	MAPK4	MAPK6	MAPK7	SOAT	
E		PCTK1	PCTK2	PFTK1	PRPF4B	RAGE	SRPK1	STK23	SRPK2	CDK11	mock	
F		MYLK2	PASK	PHKG1	PHKG2	PIM1	PIM2	PRKAA1	PRKAA2	PRKCM	SOAT	
G		PSKH2	SNARK	SNF1LK	SNRK	SSTK	STK17A	STK17B	STK22B	STK22C	mock	
H												

CMGC-CAMK-GO1-R4

	1	2	3	4	5	6	7	8	9	10	11	12
A												
B		CDK8	ALS2CR7	STK33	CDK2	MGC4796	CRK7	DYRK1A	DGKE	DGKG	SOAT	
C		DYRK1B	CCRK	TRAD	CDK3	LOC91807	ICK	LOC51701	FLJ12171	FLJ12476	mock	
D		MAK	CDC2	TRIO	CDK4	---	MAPK8	MAPK9	GENE	GUK1	SOAT	
E		Nbak2	CDC2L1	TTN	CDK5	S2	eg-5	---	KIAA0626	LCK	mock	
F		MYLK	CDC2L5	CHEK1	CDK6	S2	PRKCN	PRKD2	NME4	NME7	SOAT	
G		PSKH1	CDK10	STK11	CDK7	eg-5	STK22D	STK29	PFKFB3	PFKFB4	mock	
H												

GO1-R5

	1	2	3	4	5	6	7	8	9	10	11	12
A												
B		CKB	CKM	CKMT1	CKMT2	CSS3R	DCK	DGKA	DGKB	DGKD	SOAT	
C		DGKQ	DGKZ	DGUOK	KFZP586B16	DTYMK	EKI1	FLJ10761	FLJ10842	FLJ11149	mock	
D		FLJ22055	FLJ32704	FN3K	FUK	GALK1	GALK2	GCK	GK	GK2	SOAT	
E		HK2	HK3	IHPK1	IHPK3	ITPK1	ITPKA	ITPKB	ITPKC	KHK	mock	
F		MGC26954	MRC2	MVK	NAGK	NBP	NM23-H6	NME1	NME2	NME3	SOAT	
G		NYD-SP25	P15RS	PACSIN1	PANK1	PAPSS1	PAPSS2	PDXK	PFKFB1	PFKFB2	mock	
H												

Other-GO1-R6

	1	2	3	4	5	6	7	8	9	10	11	12
A												
B		EIF2AK3	ERN1	ERN2	FLJ10074	FLJ20335	FLJ20574	FLJ23356	FLJ32685	GAK	SOAT	
C		GUCY2F	HRI	IKBKE	KIS	LOC149420	MGC16169	MOS	NEK11	NEK2	mock	
D		NEK7	NEK9	NPR1	NPR2	NRBP	PAGE-1	PIK3R4	PINK1	PKMYT1	SOAT	
E		PRKWNK4	RNASEL	SCYL1	SDCCAG43	SNK	STK12	STK13	STK16	STK18	mock	
F		STK6	TBK1	TEX14	TLK1	TLK2	TOPK	TTK	ULK1	ULK2	SOAT	
G		CALM3	CARKL	CDK5R1	CDKN1A	CDKN3	CERK	S2	eg-5	eg-5	mock	
H												

Figure 23: Plate layout for the siRNA transfection of the kinase screen.

Kinases are depicted in different colors in function of protein families. Black and white wells are used for the controls.

Other-CK1-R7

	1	2	3	4	5	6	7	8	9	10	11	12
A												
B		CSNK2A2	AAK1	CSNK1A1	CAMKK1	LOC51231	GSG2	GUCY2C	S2	eg-5	SOAT	
C		GUCY2D	ASB10	CSNK1D	CAMKK2	MGC33182	NEK3	NEK4	---	---	mock	
D		NEK6	BIKE	CSNK1E	CDC7L1	TTBK	PLK	PRKR	S2	eg-5	SOAT	
E		PRKWNK1	BUB1	CSNK1G1	CHUK	VRK1	STK31	STK35	---	---	mock	
F		STK36	BUB1B	CSNK1G2	CNK	VRK2	WEE1	NEK8	S2	eg-5	SOAT	
G		PRKWNK3	C20orf64	CSNK1G3	CSNK2A1	---	---	---	---	---	mock	
H												

STE-Atyp-R8

	1	2	3	4	5	6	7	8	9	10	11	12
A												
B		MAP3K4	MAP3K5	MAP3K6	MAP3K8	MAP4K1	MAP4K2	MAP4K3	MAP4K4	MAP4K5	SOAT	
C		MYO3B	OSR1	PAK1	PAK2	PAK3	PAK4	PAK6	SLK	STK10	mock	
D		STK39	STK4	TAO1	PAK7	MAP2K7	S2	eg-5	S2	eg-5	SOAT	
E		ATM	ATR	BCKDK	BCR	BRD2	BRD3	BRD4	BRDT	CABC1	mock	
F		FLJ12229	FRAP1	H11	HAK	LAK	LOC203054	LOC57143	MGC20727	MIDORI	SOAT	
G		PDK4	PRKDC	PTK9	PTK9L	SMG1	STK19	SUDD	TAF1	TAF1L	mock	
H												

STE-Atyp-TK-R9

	1	2	3	4	5	6	7	8	9	10	11	12
A												
B		MAP3K3	ALS2CR2	TRIM33	MAP2K3	MINK	MST4	p761P1010	ABL1	S2	SOAT	
C		MYO3A	FLJ23074	TRPM6	MAP2K4	STK24	STK25	EPHB4	ABL2	eg-5	mock	
D		STK3	FLJ90524	TRPM7	MAP2K5	---	---	FLT3	ACK1	S2	SOAT	
E		AD034	JIK	TRRAP	MAP2K6	EEF2K	FASTK	KIT	ALK	eg-5	mock	
F		FLJ11159	MAP2K1	---	MAP3K14	PDK1	PDK2	PDGFRA	AXL	S2	SOAT	
G		PDK3	MAP2K2	---	MAP3K2	TIF1	TRIM28	SRMS	BLK	eg-5	mock	
H												

TK-R10

	1	2	3	4	5	6	7	8	9	10	11	12
A												
B		EGFR	EPHA1	EPHA2	EPHA3	EPHA4	EPHA5	EPHA7	EPHA8	EPHB1	SOAT	
C		EPHB6	ERBB2	ERBB3	ERBB4	FER	FGFR1	FGFR2	FGFR3	FGFR4	mock	
D		FLT4	FRK	FYN	HCK	IGF1R	INSR	ITK	JAK1	JAK2	SOAT	
E		KPI2	LTK	LYN	MATK	MERTK	MET	MST1R	MUSK	NTRK1	mock	
F		PDGFRB	PTK2	PTK2B	PTK6	PTK7	RET	ROR1	ROR2	ROS1	SOAT	
G		SYK	TEC	TEK	TIE	TNK1	TXK	TYK2	TYRO3	YES1	mock	
H												

TKL-GO2-R11

	1	2	3	4	5	6	7	8	9	10	11	12
A												
B		FLJ23119	FLJ25965	FLJ34389	ILK	IRAK1	IRAK2	IRAK3	IRAK4	KIAA1804	SOAT	
C		MAP3K10	MAP3K11	MAP3K12	MAP3K13	MAP3K7	MASL1	RAF1	RIPK1	RIPK2	mock	
D		TGFBR1	TGFBR2	ZAK	Ksr	ANKK1	S2	eg-5	S2	eg-5	SOAT	
E		PFKM	PFKP	PGK1	PGK2	PI4K2B	PI4KII	PIK4CA	PIK4CB	PIP5K1A	mock	
F		PKD2	PKLR	PKM2	PMVK	PNKP	PRKAR2A	PRKRA	PRP4	PRPS1	SOAT	
G		SPHK1	SPHK2	SPS	SPS2	TK1	TK2	TPK1	UCK1	UGP2	mock	
H												

TKL-GO2-TK-R12

	1	2	3	4	5	6	7	8	9	10	11	12
A												
B		BRAF	ACVR1	URKL1	AMHR2	LIMK1	LIMK2	BMX	EPHB2	EPHB3	SOAT	
C		LOC51086	ACVR1B	XYLB	ANKRD3	RIPK3	TESK1	BTK	FGR	FLT1	mock	
D		TESK2	ACVR2	ZAP70	ARAF1	S2	eg-5	CSF1R	JAK3	KDR	SOAT	
E		PFKL	ACVR2B	---	BMPR1A	PIP5K2A	PIP5K2B	CSK	NTRK2	NTRK3	mock	
F		PK428	ACVRL1	S2	BMPR1B	PRPS2	PYCS	DDR1	RYK	SRC	SOAT	
G		RBSK	ALK7	eg-5	BMPR2	UMP-CMPK	UMPK	DDR2	FES	INSRR	mock	
H												

Figure 23: Plate layout for the siRNA transfection of the kinase screen (continued).

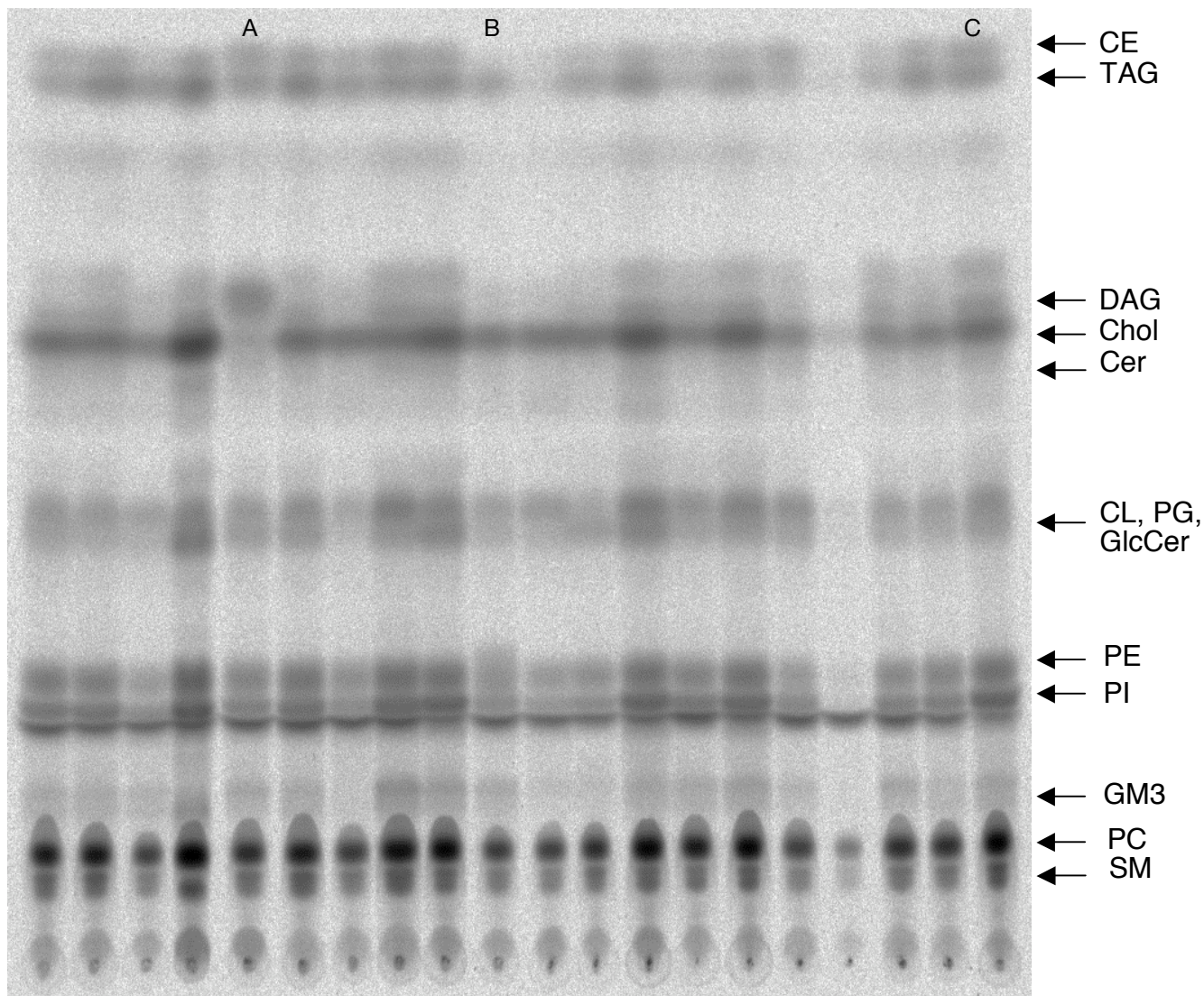


Figure 24: Typical TLC plate from the screen. This plate corresponds to the samples from rows B and C of the 5th 96 well-plate (see figure 23). Each vertical lane corresponds to the lipid extract of a kinase or control knock-down. Lipids were separated on the TLC and the positions of the different lipid classes on the plate are indicated on the right of the plate. ¹⁴C-labeled lipids were visualized upon exposure on a phosphorimager plate. Specific lanes are denominated with letters: (a) CSS3R knock-down, (b) SOAT1 knock-down, (c) mock transfection.

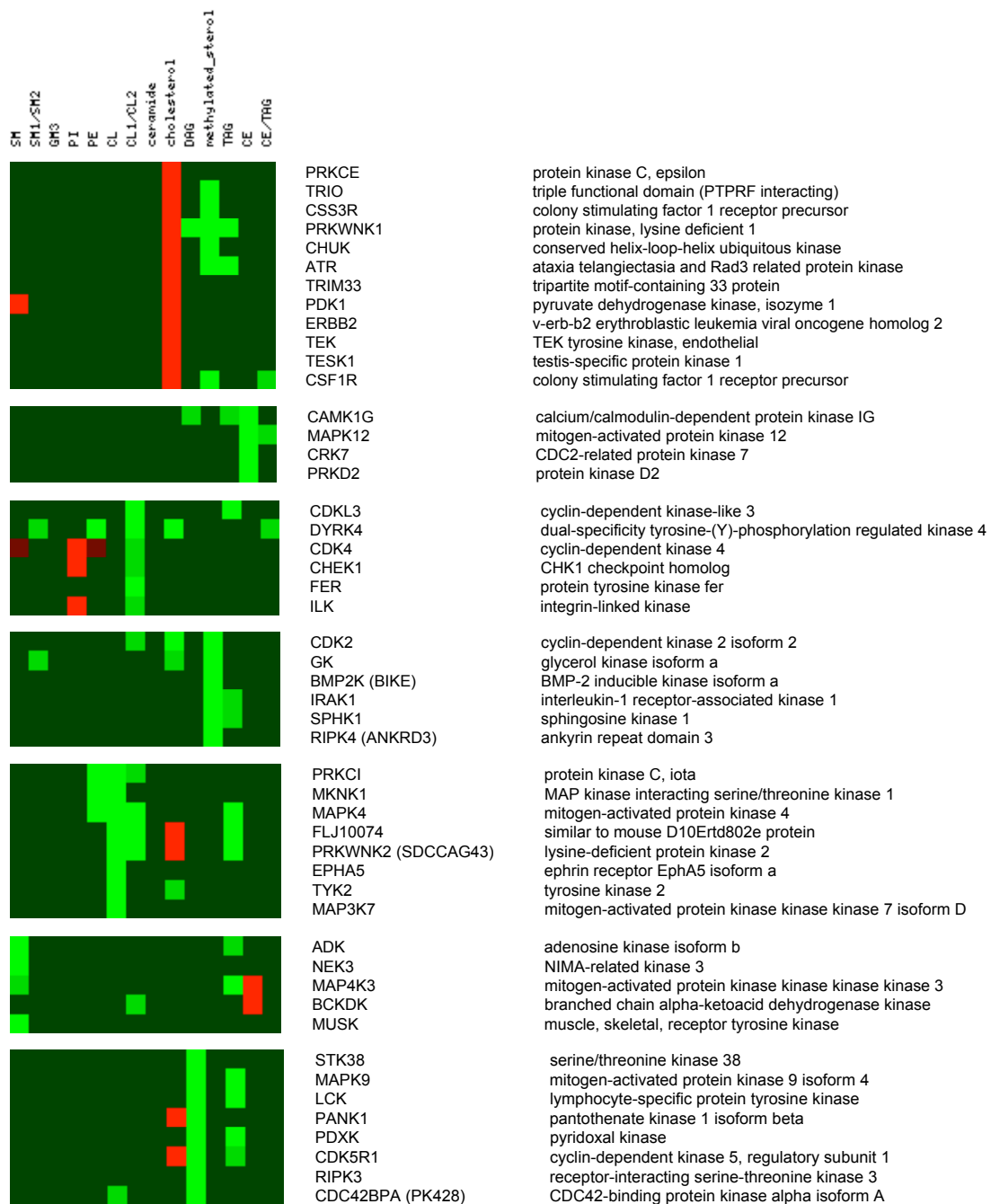


Figure 25: Clustering of the phenotypic lipid profiles generated by the screen of 600 human kinases. Clustering was performed with the program CUPID using Pearson correlation and generated 10 phenotypic clusters. Phenotypes were described as increase (green) or decrease (red) in specific lipids or lipid ratios. Annotation was performed using CUPID and corrected manually when needed.

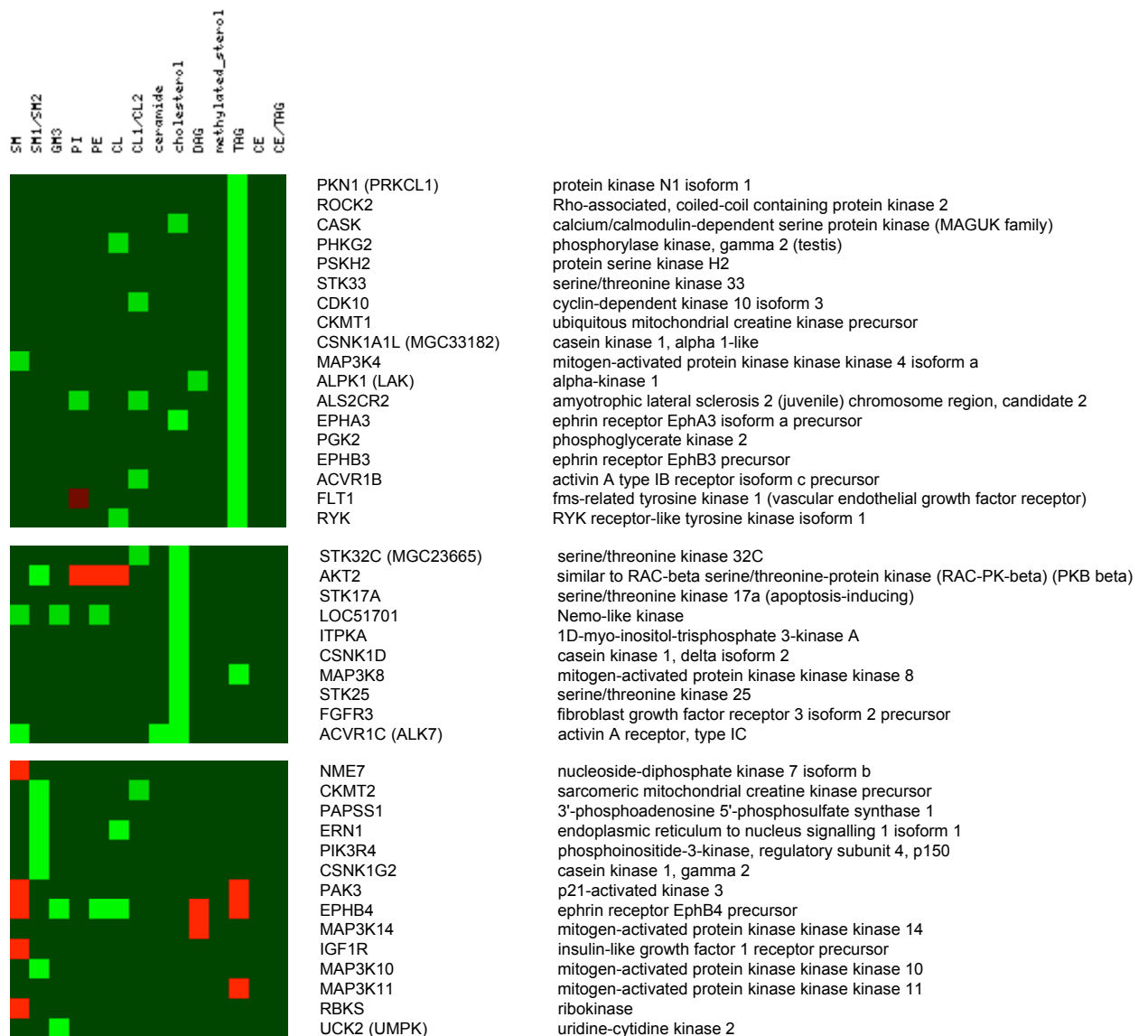


Figure 25: Clustering of the phenotypic lipid profiles (continued).

Among the phenotypes observed, several siRNAs induced a decrease in cholesterol and apparition of an additional lipid band running slightly further than cholesterol (figure 24, lane a). This band could be due to the accumulation of an intermediate of cholesterol biosynthesis. The running behavior of several sterols was then tested (figure 26). Among the sterols tested, the methylated sterols lanosterol and lophenol showed a similar running behavior as the new lipid band. On the basis of the biosynthetic pathway of cholesterol, this new band is likely to be due to the accumulation of the tri- or dimethylated precursors of cholesterol biosynthesis, lanosterol or demethyl lanosterol respectively. Unfortunately, the accumulation seems to be only transient and, therefore the low abundance of this intermediate didn't allow its direct identification by mass spectrometry.

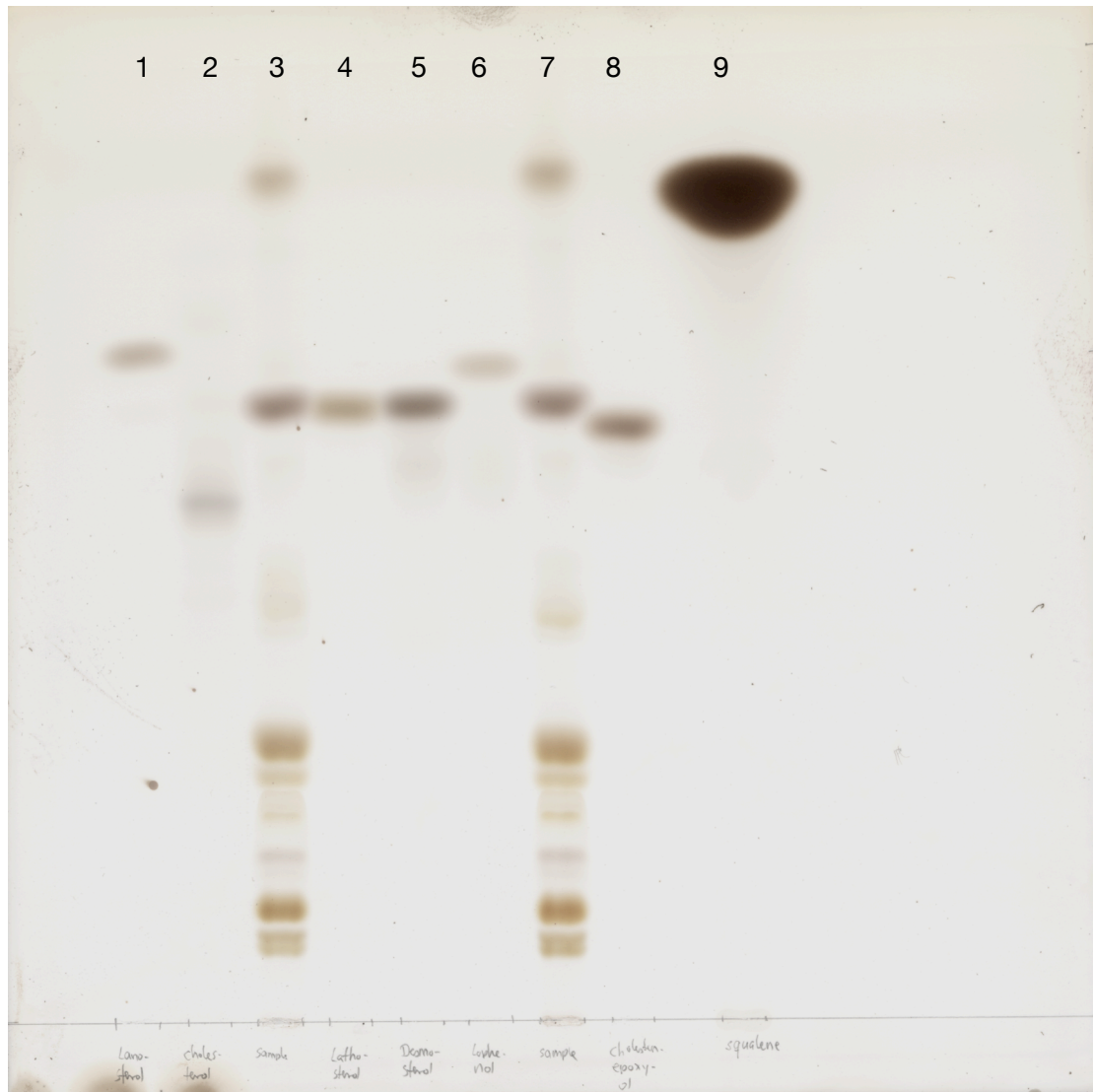


Figure 26: Running behaviour of cholesterol derivatives.

The lanes 3 and 7 have been loaded with HeLa lipid extracts while the other lanes were loaded with standards for the following sterol derivatives: lanosterol (lane 1), 7-dehydrocholesterol (lane 2), lathosterol (lane 4), desmosterol (lane 5), lophenol (lane 6), epoxycholesterol (lane 8) and squalene (lane 9). Lipids were visualized upon charring with H_2SO_4 .

Validation of the screen

Cholesterol is a major structural component of membranes and microdomains and has been implicated in several cellular processes. In addition, it is an important lipid in clinical studies because of its implication in several diseases like atherosclerosis and obesity. Therefore, the knock-downs that induce accumulation of a potential methylated cholesterol precursor, such as lanosterol, were further analyzed. Six kinases were selected because their depletion resulted in the strongest phenotypes. A new set of three siRNAs of different sequences was used to validate these results. However, although the phenotype could be reproduced using the pool of sequences

used during the screen, there was no new lipid accumulating after treatment with a pool of three new sequences (figure 27). This strongly suggested that the phenotype observed during the screen was sequence-dependent. To check if the difference in phenotypes could result from variation of silencing efficiency between the sequences, mRNA level of the corresponding gene was measured by Real-Time PCR after siRNA treatment (figure 28). However, for most of the genes tested, the new set of sequences was inducing a stronger decrease in mRNA level than the sequences used during the screen. Therefore, the loss of phenotype observed could not result from a decreased silencing efficiency. The phenotype and mRNA level were also analyzed after treatment with individual siRNA sequences. Results from this more detailed analysis are summarized in table 4. As an example, the lipid phenotypes obtained using siRNAs targeting IKK1 are shown in figure 29. Out of the six sequences tested, only two induced the accumulation of the new lipid band, confirming the sequence dependency of the phenotype.

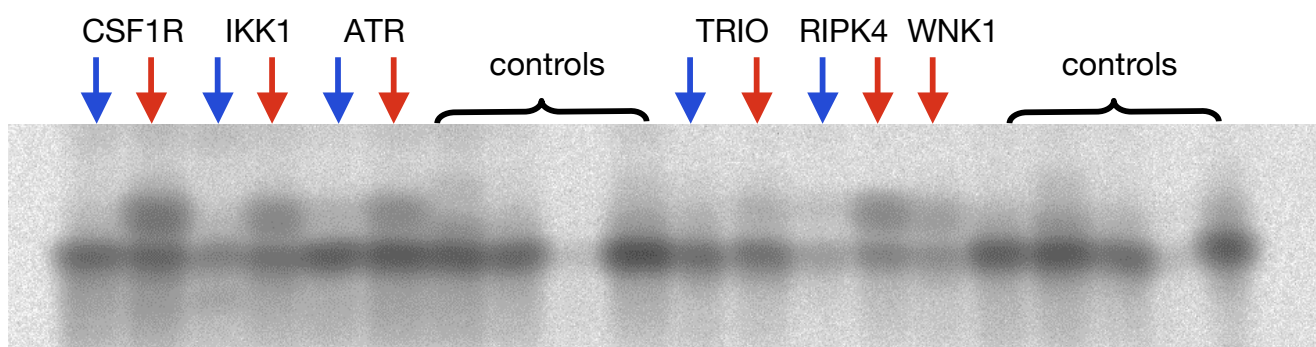


Figure 27: Lipid phenotype upon siRNA treatment.

Close-up of the cholesterol/lanosterol region of the TLC plate. Lipid extracts from HeLa cells treated with pools of three siRNAs from the screen (red arrows) or pools of three siRNAs of new sequences (blue arrows) were separated on TLC plates and compared to controls in the following order: mock transfection, SOAT1, eg5 and no transfection. ¹⁴C-labeled lipids were visualized upon exposure on phosphorimager plate.

IKK1 is a signaling kinase responsible for phosphorylation of the NF κ B inhibitor κ B (Hayden & Ghosh 2004). Upon phosphorylation, κ B is degraded by the proteasome, releasing and thereby activating NF κ B (Baldwin 1996, Hayden & Ghosh 2004). This protein was chosen to further analyze the sequence dependency of the lipid phenotype. The silencing efficiency of six siRNAs targeting this kinase was monitored both at the mRNA level by Real-Time PCR and at the protein level by western blotting (figure 30 a. and b.). At the mRNA level, the best knock-down was observed for the individual sequence 2, although this sequence didn't induce any lipid phenotype. By western blotting, no protein was detectable after treatment with any of the siRNAs against IKK1, suggesting a strong silencing potency of all the sequences against this protein, even if the silencing at the mRNA level was not complete. This suggests that a silencing mechanism other than mRNA cleavage may also take place. Furthermore, this rules out the possibility that the difference in lipid phenotype observed could be due to a variation in protein silencing. In addition, the effect of siRNAs targeting NF κ B1 and NF κ B2 was monitored, but no

lipid phenotype was observed in both cases (results not shown). Finally, HeLa cells were treated with parthenolide, a known inhibitor of IKK (Kwok et al 2001). Upon increasing concentration, parthenolide induces cell death, but no accumulation of a new lipid band or decrease in cholesterol is observed (figure 30 c.).

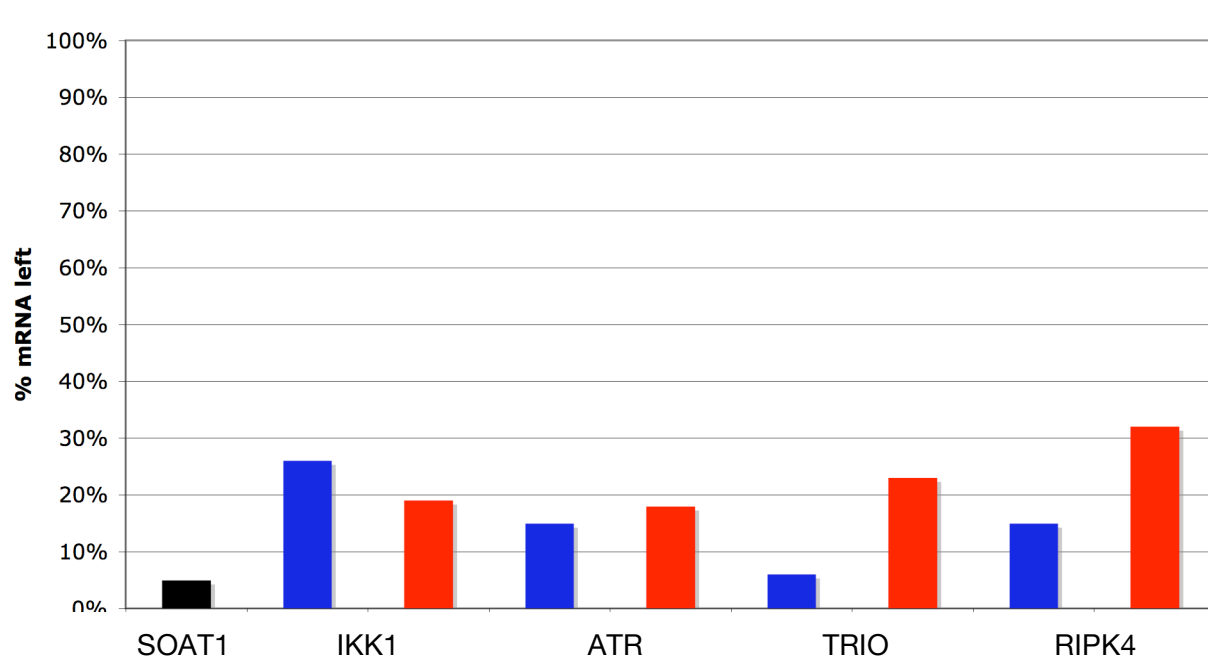


Figure 28: mRNA level upon siRNA treatment. RNA was extracted from HeLa cells treated with pools of three siRNAs from the screen (red) or pools of three siRNAs of new sequences (blue) targeting the genes mentioned below the graph. mRNA level of the targeted genes were measured by Real-Time PCR and normalized to GAPDH mRNA. Level of the corresponding mRNA for mock transfected samples was set to 100%.

This led to the conclusion that the lipid phenotype observed is not due to decrease in the targeted genes, but probably to the decrease of another, yet unidentified gene, a phenomenon known as off-target effect (Jackson et al 2003).

Analysis of a wider set of genes was then carried out. This set included two kinases whose knock-down induces a strong decrease in one SM band, and 12 kinases whose knock-down induces an increase in TAG. Results of this analysis can be found in table 4. As for the previous kinases, most of the time, only one or two siRNA sequences were responsible for the lipid phenotype observed, and, when tested, no correlation could be found between the phenotype observed and the decrease in mRNA level. Only three kinases show a phenotype using three independent siRNAs: CASK, PDXK and MAPK9, the strongest phenotype being observed for the latest.

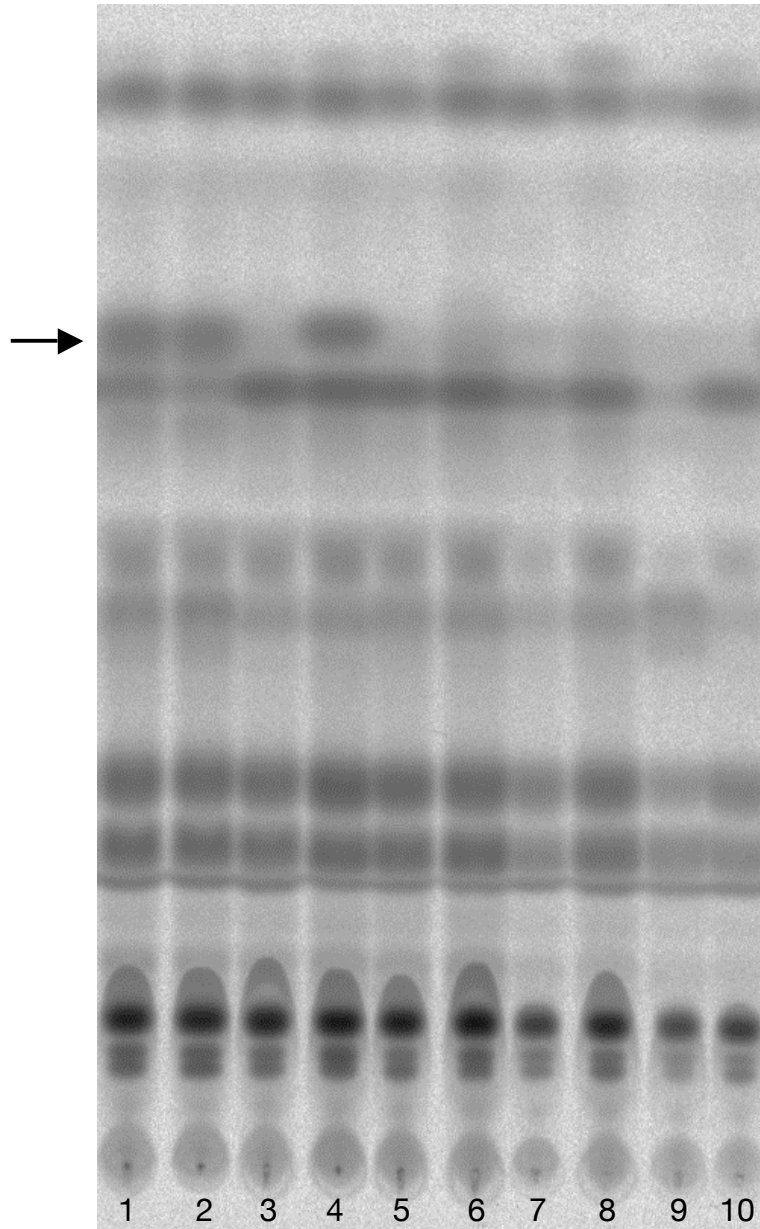


Figure 29: TLC of HeLa cells extracts upon IKK1 knock-down. Lipid extracts from HeLa cells treated with a pool of three siRNAs against IKK1 from the screen (lane 1) or the corresponding individual sequences (lane 2-4) or with a pool of three siRNAs of new sequences (lane 7) or the corresponding individual sequences (lane 8-10) were compared to the S2 treated-cells (lane 5) and mock transfected control (lane 6). ^{14}C -labeled lipids were visualized upon exposure on a phosphorimager plate. The position of the phenotypic band is indicated by the arrow.

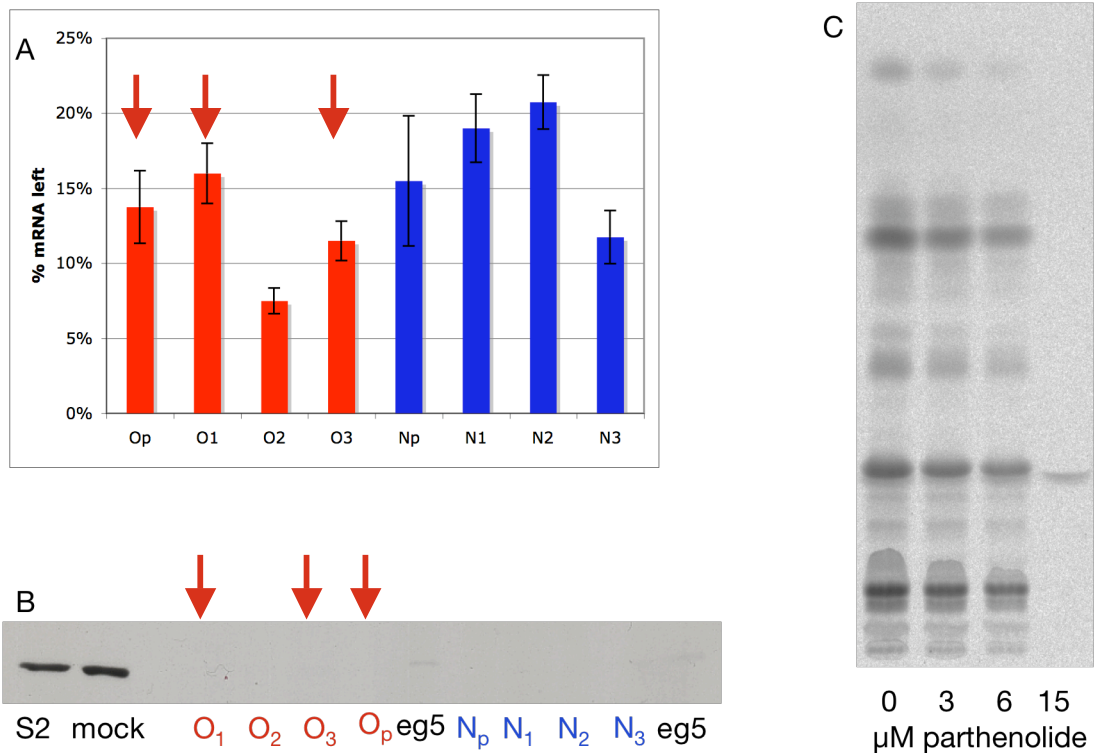


Figure 30: Effect of knock-down or inhibition of IKK1.

(a) IKK1 mRNA levels and (b) protein levels were measured from HeLa cells treated with a pool of three siRNAs from the screen (Op) or the corresponding individual sequences (O1, O2 and O3) or with a pool of three siRNAs of new sequences (Np) or the corresponding individual sequences (N1, N2 and N3). mRNA levels were measured by Real-Time PCR and normalized to GAPDH mRNA. Level of the corresponding mRNA for mock-transfected samples was set to 100%. (b) Protein levels were analyzed by western blotting and compared to the mock-transfected control and S2 treated-cells. Red arrows indicate the samples that give a lipid phenotype (c) Lipid extracts from HeLa cells treated with increasing amount of parthenolide were separated by TLC. ¹⁴C-labeled lipids were visualized upon exposure on a phosphorimager plate.

However the phenotype could not be reproduced using siRNAs from other companies neither for CASK nor for PDXK. Furthermore, the addition of pyridoxal phosphate, the enzymatic product of PDXK, didn't rescue the phenotype (data not shown). On the contrary, the phenotype could be reproduced for MAPK9 with an additional siRNA from another company.

All these data taken together, MAPK9 was selected to study its potential implication in triglyceride homeostasis.

Table 4: Lipid phenotype and RT-PCR data obtained for kinase knock-down.

	Screen sequences			New sequences			Invitrogen	Qiagen
	siRNA1	siRNA2	siRNA3	siRNA1	siRNA2	siRNA3		
Cholesterol								
CSF1R	x	o	x	o	o	o		
IKK1	x	o	x	o	o	o		
	16	8	12	19	21	24		
	14			16				
ATR	o	x	-	-	-	-		
		15						
	19							
RIPK4	x	o	x	o	o	o		
	24	27	28	67	33	31		
	32			15				
TRIO	o	o	o	o	-	-		
	23			6				
PRKWINK1	x	o	o	-	-	-		
	8							
SM								
CKMT2	o	x	o	-	-	-		
CSN1KG2	x	o	o	-	-	-		
TAG								
PRKCL1	o	o	x	-	-	-		
ROCK2	x	o	x	o	o	o	o	o
	20	54	26	11	22	10		
	20			31				
CASK	x	o	x	o	x	o	o	o
	7	4	18					
	5							
PHKG2	x	o	o	o	o	o		
MAPK9	o	x	x	o	x + CE	o		x
	27	23	22	23	20	24		
	15			24				
LCK	dead	x	x	dead	dead	dead		o
PDXK	x	o	x	o	x	o	o	o
	0.1	1	1					
	9							
LAK	o	TAG	CE	-	-	-		
MAP3K4	x	x	o	o	o	o		
	51	33	30	3	15	34		
	29			17				
ALS2CR2	o	o	x	-	-	-		
EPHB3	o	o	o	-	-	-		
FLT1	o	o	x	-	-	-		

x phenotype
 o no phenotype
 - no siRNA
 10 % mRNA left (individual siRNA)
 10 % mRNA left (pooled siRNA)

MAPK9: A potential regulator of triglyceride metabolism

MAPK9, also known as the c-jun N-terminal kinase 2 (JNK2) (Kallunki et al 1994), is a member of the mitogen-activated protein kinase (MAPK) family (Karin & Gallagher 2005, Manning & Davis 2003). There are three members in the JNK subfamily, termed JNK1, JNK2 and JNK3 (Bogoyevitch 2006). While JNK1 and JNK2 are ubiquitously expressed, JNK3 expression is restricted to the brain and testis. JNK proteins are activated through a typical MAPK cascade, through phosphorylation by the MAPK kinases MKK4 and MKK7 (Karin & Gallagher 2005, Manning & Davis 2003). There is a wide range of upstream mediators, allowing JNK activation upon diverse stimuli. In turn, JNK phosphorylates several transcription factors, such as c-jun or the activating transcription factor ATF2, as well as non-nuclear substrates, such as the B-cell leukemia associated oncogenes (Bcl) mitochondrial proteins (Bogoyevitch 2006). JNK proteins are strongly implicated in induction of apoptosis through the phosphorylation of the Bcl proteins that activate the apoptosis program (Putcha et al 2003, Yu et al 2004). Accordingly, the JNK1^{-/-} JNK2^{-/-} double knock-out mice (Kuan et al 1999, Sabapathy et al 1999) dies in utero because of dysregulation of apoptosis in several parts of the brain, leading to defective neural tube closure. The individual knock-outs however are viable and develop normally. Nevertheless, impaired late differentiation of T lymphocytes is observed in these mice, delineating a role for JNK in the immune response (Dong et al 2000, Karin & Gallagher 2005). In addition, JNK proteins have been shown to get activated upon various environmental stresses, such as UV light (Derijard et al 1994), osmotic stress (Bogoyevitch et al 1995) or glucose deprivation (Liu et al 1997).

Although these proteins, in particular JNK1 and JNK2, are partially redundant, they also have isoform-specific roles (Bogoyevitch 2006). Among these, of particular interest is the role of JNK2 in atherosclerosis (Sumara et al 2005). JNK2 is specifically activated in the aorta of high-cholesterol fed ApoE^{-/-} mice, animal models for atherosclerosis (Ricci et al 2004). Similarly, JNK activation has been observed in human atherosclerotic lesions (Nishio et al 2001). Furthermore, the double knock-out mice ApoE^{-/-} JNK2^{-/-}, but not ApoE^{-/-} JNK1^{-/-}, show decreased atherosclerotic lesions, compared to the ApoE^{-/-} mice. This is apparently due to a decreased phosphorylation of scavenger receptor A in macrophages of these double knock-out mice (Ricci et al 2004), resulting in impaired internalization of modified LDL, and thereby decrease in foam cells accumulation (Fong & Le 1999, Kosswig et al 2003).

On the other hand, JNK1 has been linked to obesity since the JNK1^{-/-} mice are partially resistant to high fat diet induced obesity and have an increased tolerance to high glucose or insulin level (Hirosumi et al 2002). Therefore, JNK1 is believed to be implicated in the development of insulin resistance and type II diabetes, via serine phosphorylation of the downstream effector of the insulin receptor, IRS1, leading to inhibition of the insulin response pathway (Aguirre et al 2000, Aguirre et al 2002).

Phenotypic characterization

As mentioned in the previous chapter, four siRNAs targeting MAPK9 induce the same phenotype and MAPK9 appears therefore as a potential regulator of lipid metabolism. Knock-down of the kinase was confirmed both by Real-Time PCR (table 4) and by western blot (figure 32). Although four siRNAs show a consistent increase in TAG, one of the siRNAs shows in addition an increase in the level of another storage lipid: cholesterol ester (figure 31). To date, no evidence allows the distinction between an off-target effect of this sequence or a physiological relevance for the concomitant increase of these two classes of storage lipids. Although the initial data were obtained in delipidated medium, the increase of TAG could be confirmed in a medium that was not lipid-depleted. The phenotype was also observed upon oleate feeding and radioactive oleate staining of the cells (figure 33).

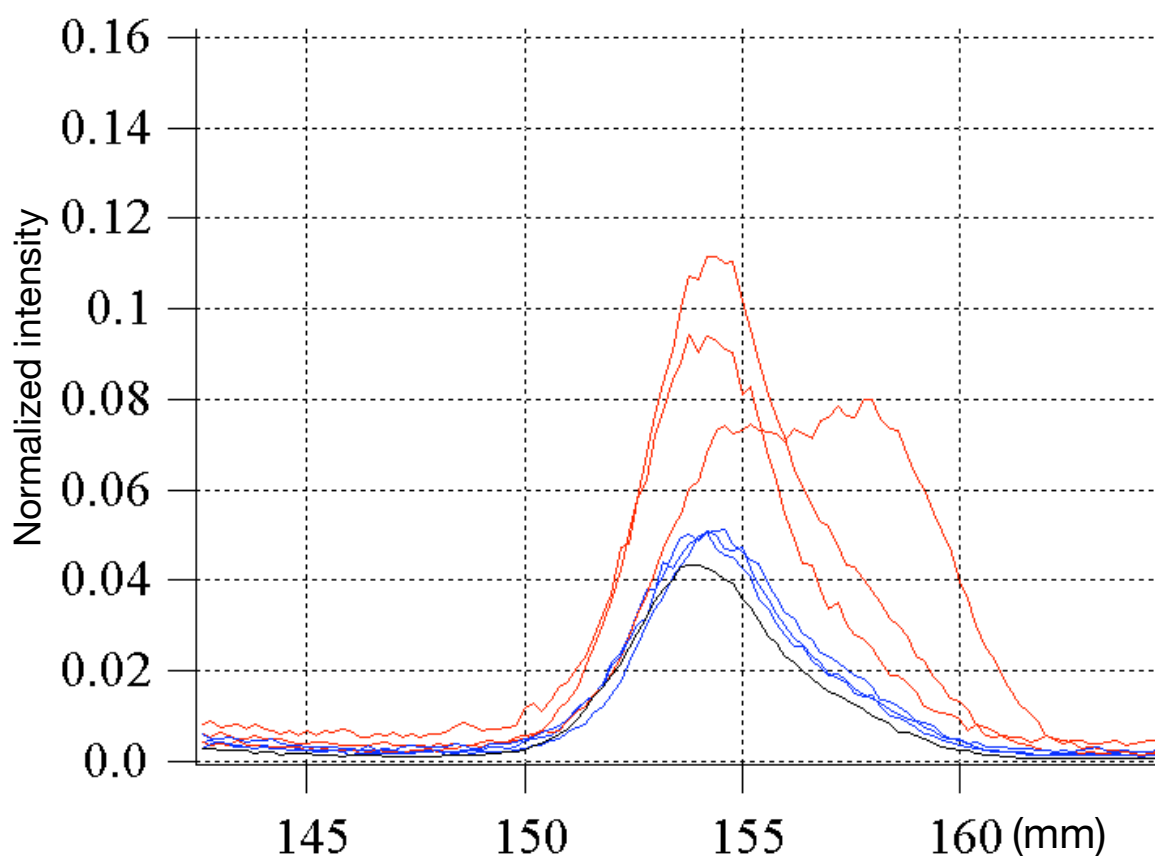


Figure 31: Increase of TAG upon MAPK9 knock-down.

The figure shows a close-up of the storage lipid region from the lipid profiles obtained after TLC. Intensities were normalized to the level of PC. The black profile represents the mock-transfected negative control, the blue profiles the effect of siRNA O1, N1 and N3 targeting MAPK9, showing no phenotype, and the red profiles the effects of siRNA O2, O3 and N2 targeting MAPK9, showing an increase in TAG level. The siRNA N2 shows in addition an increase in the signal corresponding to the upper band, cholesterol ester, visible here by the shoulder in the lipid peak.

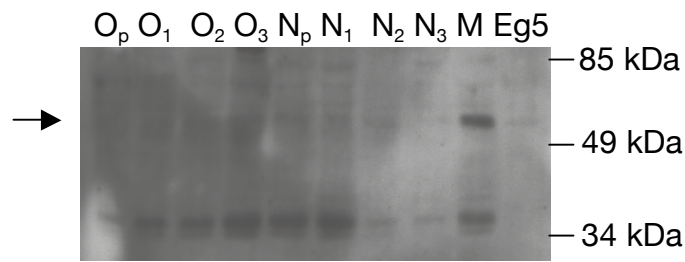


Figure 32: Knock-down of MAPK9 monitored by western blot. Hela cells were treated using a pool of 3 siRNAs targeting MAPK9 (Op and Np) or the corresponding individual sequences (O1, O2, O3, N1, N2 and N3) and the level of MAPK9 protein (55kDa) was compared for the different knock-downs and the mock transfection control (M). The unspecific band located around 35 kDa can be considered as a loading control.

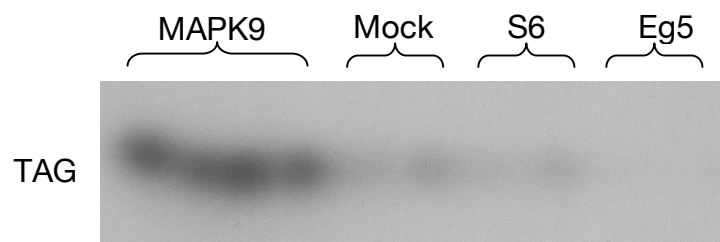


Figure 33: Radioactive labeling of TAG upon MAPK9 knock-down. Hela cells were fed with oleate and radioactive oleate 4h after siRNA transfection. Lipids were extracted 48h after transfection and separated by TLC. Radioactive signal was revealed by autoradiography. siRNA used for transfection are indicated on the figure. A pool of the three sequences from the screen was used for MAPK9.

The effect of SP600125, a specific JNK inhibitor (Bennett et al 2001) was also tested. Although this inhibitor induces some cell death at higher concentration, the ratio between TAG and the other lipids is increasing upon SP600125 treatment, further suggesting that this effect is specific for the down-regulation of MAPK9 (figure 34). Nevertheless, it should be noted that a concomitant decrease in cholesterol is observed upon inhibitor treatment. This effect could be due however to the inhibition of other kinases, considering the poor specificity of the compound (Bain et al 2003).

The phenotype was then confirmed using mass spectrometry. Lipid extracts from Hela cells treated with a pool of siRNAs targeting MAPK9 were analyzed by MS by Dominik Schwudke. There again, an increase in TAG was observed. Since MS analyzes the lipid composition of the cells as a whole, these data demonstrate that the phenotype reflects the status of the full TAG pool and not only an increase in newly synthesized TAG. Furthermore, mass spectrometry allows analysis of individual lipid species. The effect of MAPK9 knock-down on the level of individual TAG species was then analysed. As shown in figure 35, an increase was observed in all the TAG species monitored, suggesting no species specificity in the phenotype.

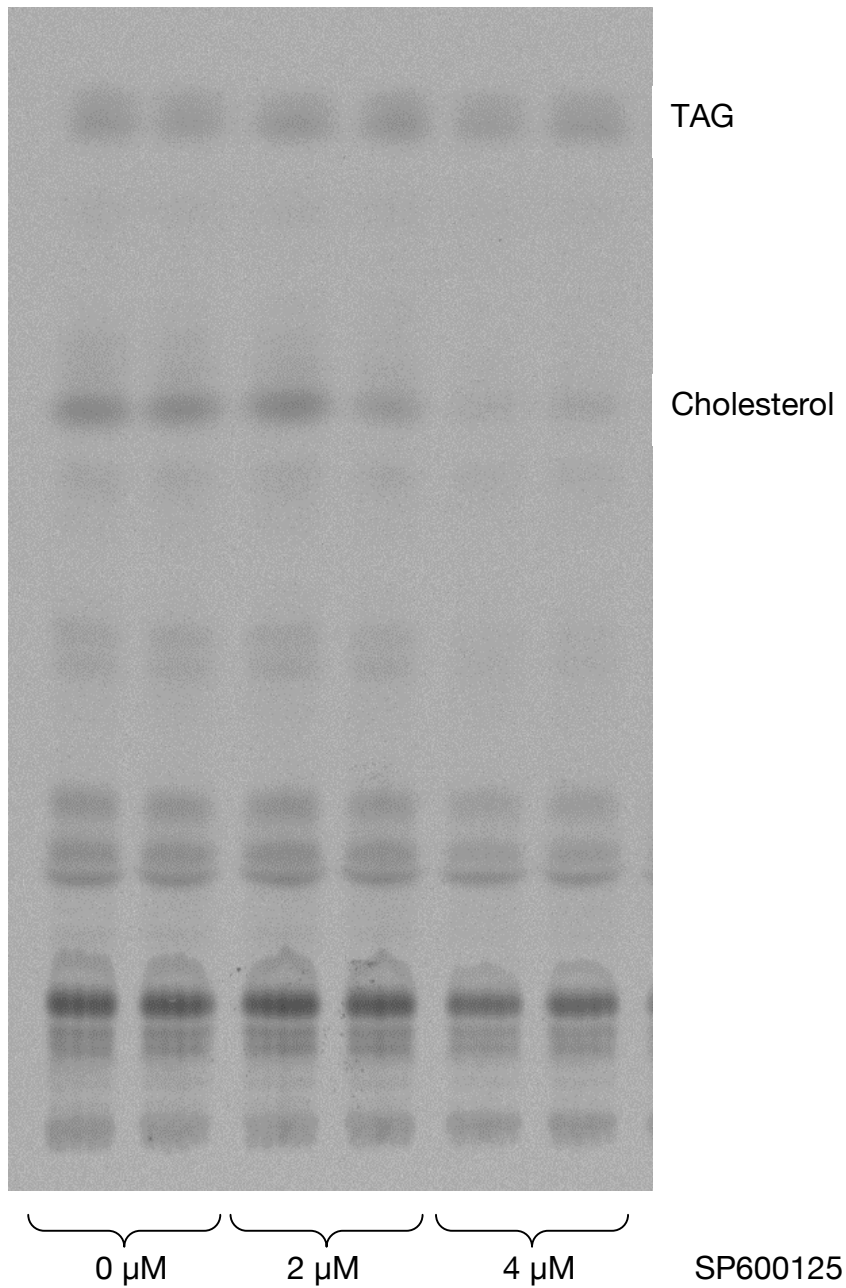


Figure 34: Effect of SP600125 on lipid composition. Hela cells were treated with various concentration of SP600125 as indicated on the figure. The lipid extracts from these cells were then separated by TLC. 14 C-labeled lipids were visualized upon exposure on phosphorimager plate.

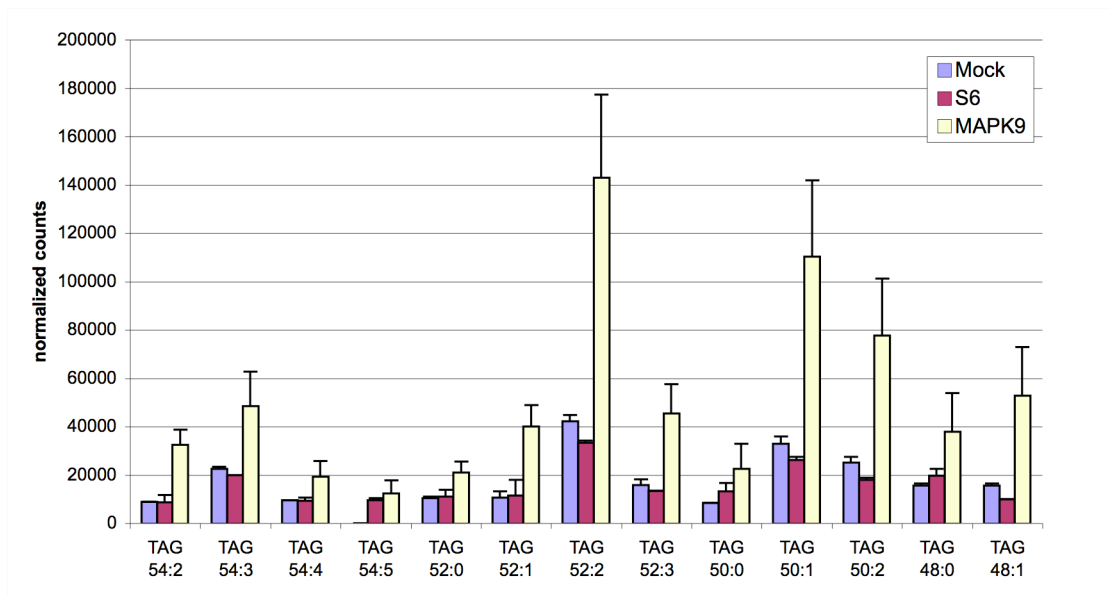


Figure 35: Effect of MAPK9 knock-down on individual TAG species monitored by LTQ-Orbitrap mass spectrometry. Values have been normalized on the level of the lipid species PC 34:1.

Inside the cell, TAG is found mainly in specialized organelles called lipid droplets. These organelles can be specifically labeled using BODIPY (Gocze & Freeman 1994). Cells were therefore stained with BODIPY upon MAPK9 knock-down. In delipidated conditions, almost no lipid droplets are detectable in wild-type cells. However, upon knock-down of MAPK9, BODIPY stains small round structures characteristic of lipid droplet staining (figure 36). When a high quantity of oleate is provided to the cells in order to favor lipid droplets accumulation, a small increase in BODIPY staining is still visible in the MAPK9 knock-down, although much less significant that in the absence of extracellular lipids (figure 36).

Taken together, these data strongly suggest a role of MAPK9 in the regulation of TAG homeostasis. As a MAP kinase, MAPK9 can act by direct phosphorylation of its cytoplasmic target, directly affecting the activity of the protein, or, most commonly, by activation of transcription factors that activate, or eventually inhibit, the expression of other genes. Therefore, the expression of genes of the TAG biosynthetic or degradation pathways was monitored to check if they were affected in the MAPK9 knock-down.

TAG can be synthesized via different pathways (Coleman & Lee 2004). The major one originates from glycerol-3-phosphate, which is combined with a fatty acid by the glycerol-phosphate acyltransferase (GPAT) to form lysophosphatidic acid (LPA). LPA is first acylated by the acylglycerol-phosphate acyltransferase (AGPAT) to form PA. Then PA is dephosphorylated by lipin1 to form DAG, which in turn is acylated by diacylglycerol acyltransferase (DGAT) proteins to yield TAG (Coleman & Lee 2004). To test the effect of the MAPK9 knock-down on TAG biosynthesis, the expression of the enzymes AGPAT and lipin1 was monitored by RT-PCR, but no increase in the expression of these genes was observed. On the contrary, a small decrease in expression was observed for lipin1, which could be a compensatory effect due to the increase in TAG. Then, the expression of the hormone-sensitive lipase (HSL) and

the adipose triglyceride lipase (ATGL) was also monitored both by RT-PCR and WB. These two lipases are known to hydrolyze the TAG from lipid droplets (Haemmerle et al 2006, Holm et al 2000, Zimmermann et al 2004). However, no variation in expression of these genes was observed, neither using RT-PCR, nor WB (figure 37). Similarly, no change in ATGL expression was observed upon UV (Derijard et al 1994) or anisomycin (Iordanov et al 1997) activation of JNK (figure 38).

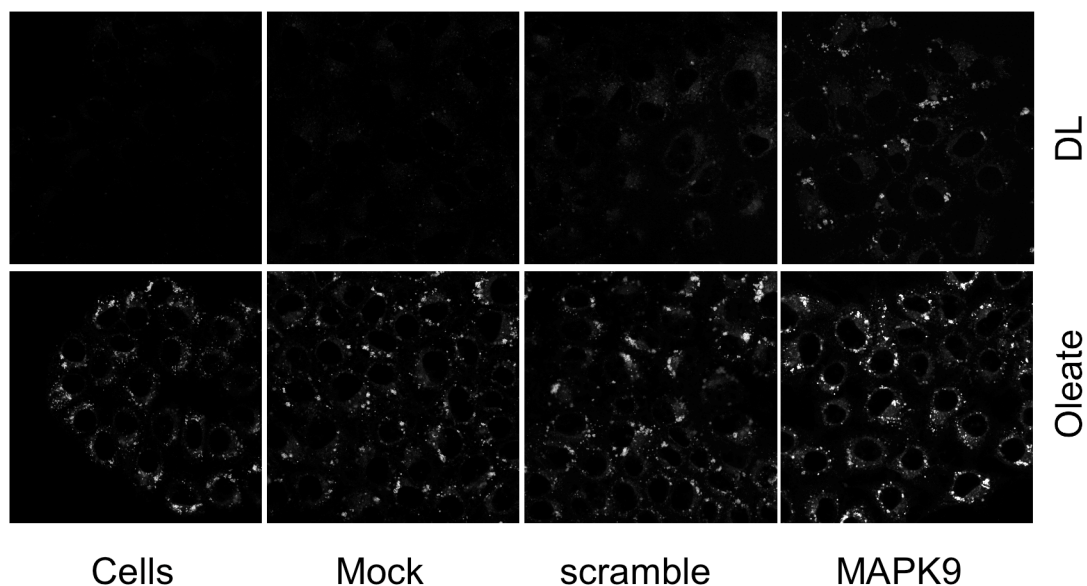


Figure 36: Effect of MAPK9 knock-down on BODIPY staining. Untransfected A431, mock-transfected A431 and A431 cells transfected with scramble or MAPK9 siRNA were transferred to a medium containing delipidated serum or a medium supplemented with oleate 24h before fixation. Lipid droplets were stained using the lipid dye Bodipy493/503. Images were taken by Julia Massier.

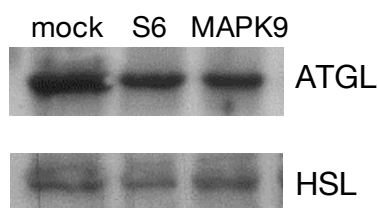


Figure 37: ATGL and HSL levels monitored by WB upon MAPK9 knock-down. Hela cells were transfected with the siRNA indicated at the top of the picture (a pool of the three sequences from the screen was used for MAPK9). Cells were harvested 72h after transfection and analyzed by western blot using ATGL and HSL primary antibodies.

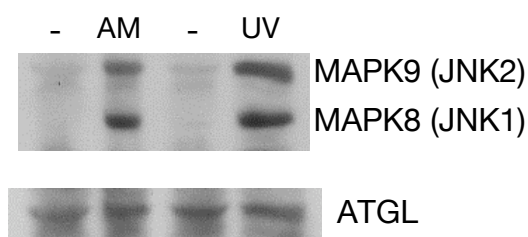


Figure 38: ATGL levels monitored by WB upon JNK activation. The level of ATGL was monitored by western blot upon JNK activation by 2h anisomycin (AM) treatment or 10' UV excitation (200W). Activation of JNK was verified using a phospho-specific JNK antibody.

However, other genes implicated in these processes may be the targets of MAPK9 signaling. Moreover, variation in their activity may be regulated at the post-transcriptional rather than at the transcriptional level. Therefore, more general assay may be necessary to evaluate MAPK9 influence on TAG metabolism.

Sty1: A potential homolog of MAPK9 in *S. pombe*

To further confirm the specificity of the phenotype and the role of MAPK9 in the regulation of TAG metabolism, a MAPK9 homolog in yeast was also analyzed. Gene deletion in yeast is a much better established technique and it is therefore possible to study the effect of gene knock-out in that organism, a system much less prone to off-target effects.

The JNK and p38 subfamilies of MAP kinases are often referred to as the stress-activated kinases, because of their role in response to several external stress stimuli (Bogoyevitch 2006, Tibbles & Woodgett 1999). In yeast, both *S. cerevisiae* and *S. pombe* contain one stress-activated kinase, named High osmolarity glycerol kinase 1 (Hog1) and Suppressor of tyrosine phosphatase 1 (Sty1) respectively (O'Rourke et al 2002, Toone & Jones 1998). While Hog1 is activated upon osmotic stress only (O'Rourke et al 2002), Sty1 is activated upon a wide-range of stimuli, like the mammalian kinases (Chen et al 2003, Degols et al 1996). Furthermore, Sty1 is activated upon glucose deprivation such as MAPK9 (Stettler et al 1996) and appear therefore as a potential homolog of that kinase in yeast.

To test this hypothesis, the accumulation of lipid droplets in the Sty1 deletion strain JM1160 was visualized. For this purpose, cells were labeled with the hydrophobic dye Nile Red (Greenspan et al 1985, Tong et al 2006). As shown in figure 39 (upper panels), there is a strong increase in lipid droplet staining by Nile Red in the Sty1 deletion strain compared to the wild-type strain PR109, confirming the homology between the mammalian and the yeast protein. Consistent with this observation, an increase in TAG upon labeling with radioactive oleate was visible in the Sty1 deletion mutant (figure 40, lane 1 and 3).

The same yeast strains were then analyzed upon glucose depletion. In this case, the glucose present in the medium was replaced by sorbitol to maintain the osmolarity of the growth medium (Madrid et al 2004). Sorbitol however can't be used as a carbon source by *S. pombe*. In these conditions, yeast arrest in G2 phase till glucose is added again to the medium. Interestingly, Nile Red staining of wild-type cells shifts from the lipid droplet structures to a more diffuse staining of the nuclear membrane and some other undefined structure in the cytoplasm (figure 39 (lower panels)). Comparatively, in the Sty1 mutant strain, although some more diffuse staining is observed, there is still a prominent lipid droplet staining (figure 39 (lower panels)). One could hypothesize that this shift in labeling observed in wild-type yeast was due to the loss of lipid droplets resulting from the use of TAG as an alternative energy source. However, oleate labeling of these yeasts shows an increase in TAG level upon glucose depletion, both for the wild type and the mutant yeasts (figure 40, lane 2 and 4). This implies that upon glucose depletion, TAG accumulates in another organelle rather than in lipid droplets and that this process is at least partially impaired in the Sty1 deletion strain.

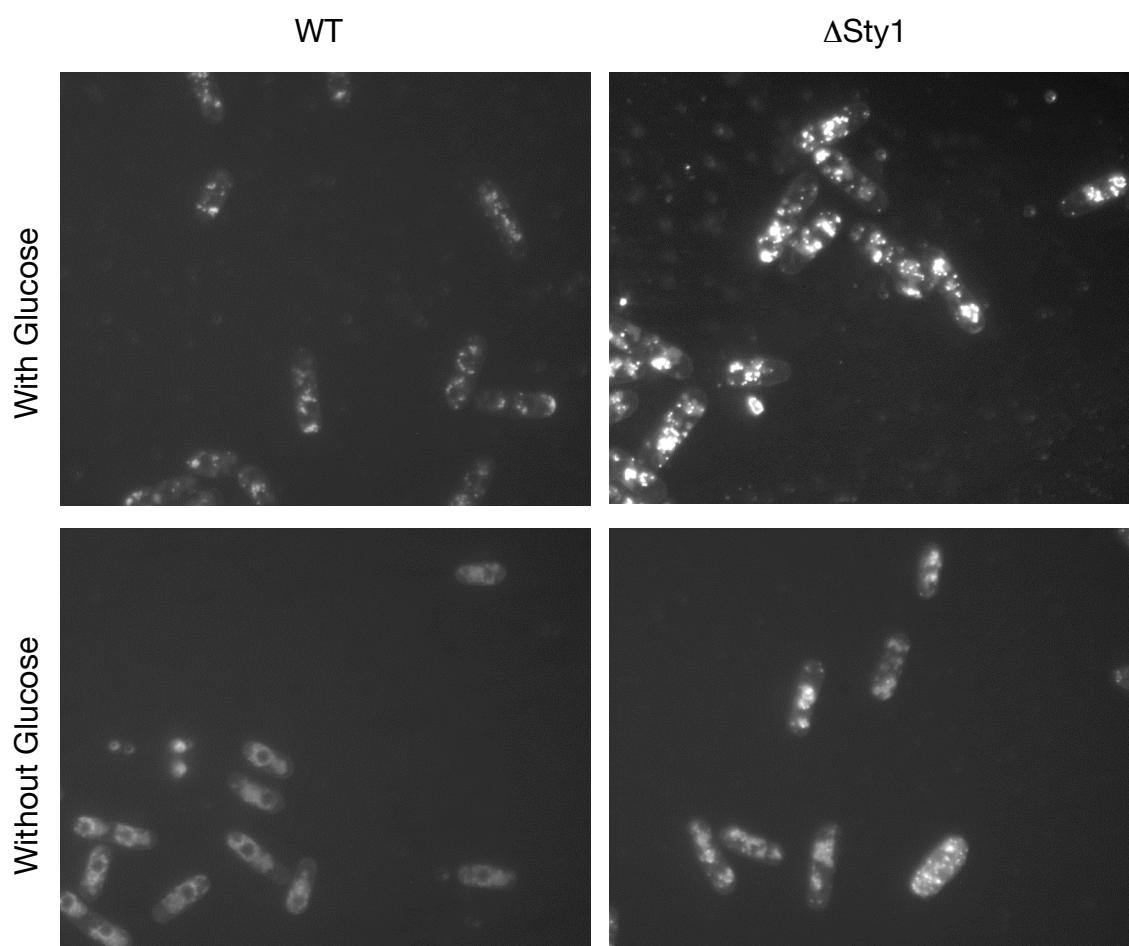


Figure 39: Nile Red staining with or without glucose depletion. The wild-type strain PR109 (left panels) and the Sty1 deletion strain JM1160 (right panels) have been stained with Nile Red after 1 hour growth in glucose-containing EMM2 (upper panels) or glucose-free EMM2 (lower panels).

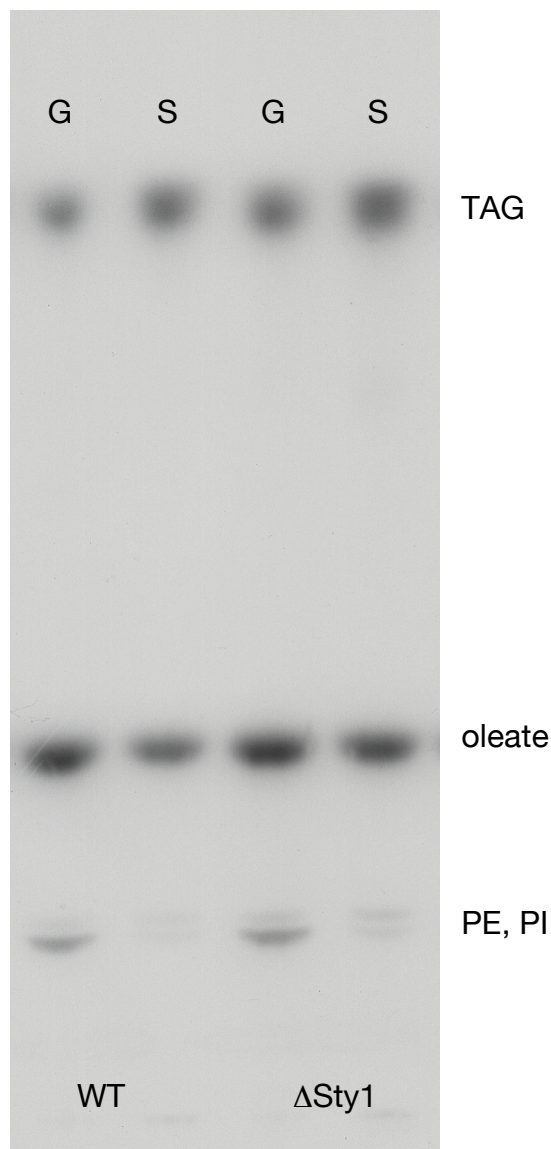


Figure 40: Radioactive oleate staining of yeast lipid extracts separated by TLC. Lipid extracts from the wild type strain PR109 (lane 1,2) and the Sty1 deletion strain JM1160 (lane 3,4) were separated on TLC plate and the radioactive signal was obtained by autoradiography. Yeast cells were either grown in glucose containing (G: lane 1 and 3) or in glucose-free EMM2 for 1h (S: lane 2 and 4).

TAG differs in structure from the phospholipids and harbors a conical shape due to the third fatty acid. Therefore this lipid is not well suited for lipid bilayer structure. However, in vitro studies showed that a small amount, namely 3% of TAG can accumulate in artificial membranes (Hamilton 1989). Because of the nuclear membrane staining of Nile Red, the accumulation of TAG could occur in the endoplasmic reticulum (ER). To test this possibility, the PG2747 yeast strain was used. This strain encodes for a GFP-tagged truncated ER resident protein, the NADPH-P450 reductase (Ding et al 2000). A nice staining of the nuclear membrane and the cortical ER, which locates just below the plasma membrane, is observed in normal growth conditions (figure 41). However, upon glucose depletion, a similar

staining is observed, which differs from the Nile red staining observed in these conditions. This suggests that the structure in which the dye accumulates is distinct from the ER. Furthermore, by bright-field microscopy, less internal structures are visible in the yeasts upon glucose depletion (figure 42). This difference can be partially explained by the decrease in lipid droplets under these conditions. However, since not all these internal structures co-localize with the Nile Red staining in wild-type cells, it suggests that some other internal structures are disturbed under glucose-free conditions, potentially the vacuoles.

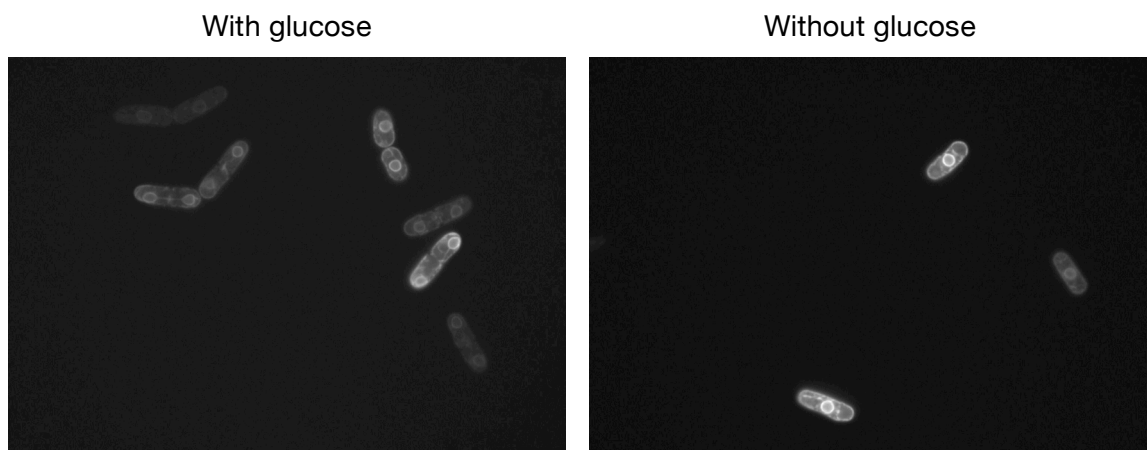


Figure 41: No effect of glucose depletion on ER structure. Yeast cells from the PG2747 strain, coding for the GFP-tagged truncated NADPH-P450 reductase were grown for 1h in glucose containing (left panel) or in glucose-free EMM2 (right panel).

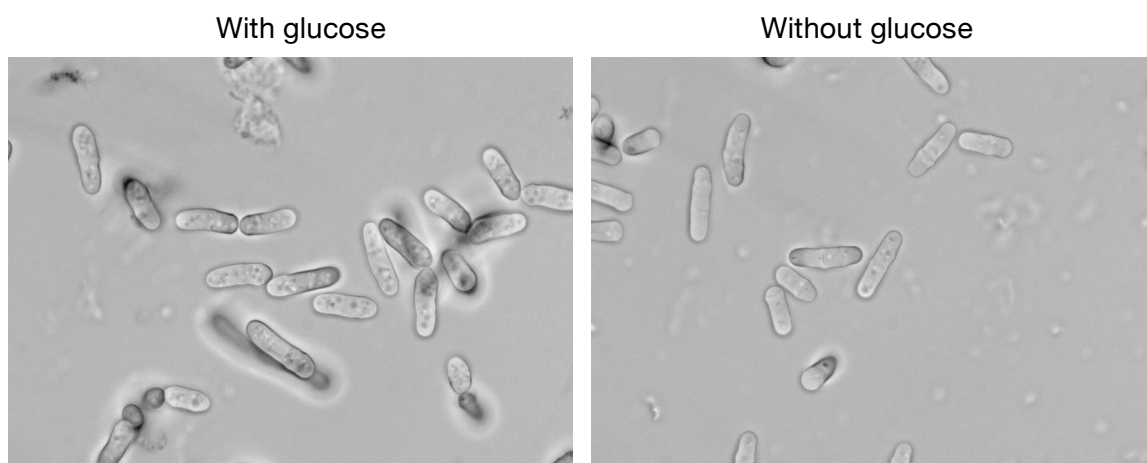


Figure 42: Decrease in visible internal structure upon glucose depletion observed by bright-field microscopy. Yeasts from the PG2747 strain were grown for 1h in glucose containing (left panel) or glucose-free EMM2 (right panel).

In yeast, nutrient depletion induces growth arrest. In *S. cerevisiae*, it is known that upon glucose depletion, cells accumulate glycogen and triglycerides (Francois & Parrou 2001, Werner-Washburne et al 1993). These are then used upon stress release to leave the arrested state. The accumulation of TAG could have a similar purpose in *S. pombe*. Therefore, the growth recovery of both the mutant strain and

the wild-type strain were monitored after a growth arrest due to nutrient stress. Cells were maintained for 20h under glucose-free conditions. Then, the medium was replaced for a classical EMM2 medium containing glucose. The Sty1 deletion strain JM1160 shows a slight impairment in growth compared to the wild-type strains PR109 and L972 (figure 43). However, a similar growth impairment is observed when the cells are always maintained in glucose-containing medium. This suggests that either the recovery after glucose depletion is not impaired in the Sty1 deletion strain, or that the glucose present in the recovery medium is sufficient to provide the energy necessary for the recovery.

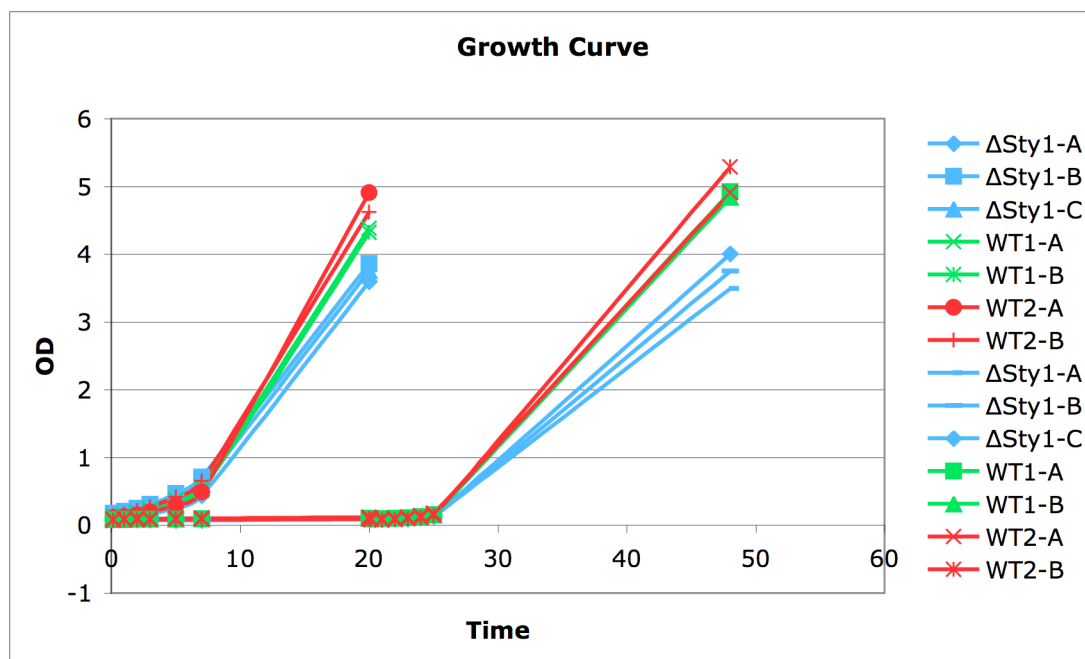


Figure 43: Growth curve upon recovery from glucose depletion.

The growth of the Sty1 deletion strain JM1160 was compared with the growth of the wild-type strains PR109 (WT1) and L972 (WT2) in supplemented EMM2 (left) or in supplemented EMM2 after 20h growth arrest in glucose-free conditions (right). Optical Density (OD) was measured at 600 nm. When OD was above 1, yeast cultures were diluted 5x and the measured OD was then multiplied 5x to ensure linearity of the measurement.

Discussion

Dysregulation of lipid metabolism is a major cause of some of the most common diseases in our societies. Understanding its molecular basis and identifying the players of this process are therefore major challenges for the identification of new potential drug targets. In the context of this thesis, a screening procedure was developed, which allows to delineate the implication of some genes in the maintenance of lipid homeostasis. This method is based on a combination of RNA interference and lipid analysis by TLC and has proved to be successful for observing alterations of lipid composition upon specific siRNA treatment. Using TLC as a read-out system, modifications can be observed in all lipid classes. However, most phenotypes were affecting cholesterol, cholesterol esters and triglycerides. These lipids, being more subject to variation in the human body upon changes in diet or health status, may be similarly more subject to variation in cells, while the pool of glycerophospholipids, which have a more structural role, is more constant.

In parallel, the potency of mass spectrometry as a lipid analysis tool in the context of large-scale studies was investigated. MS extends the analysis to individual lipid species and not only classes, thereby giving rise to a more complete overview of the lipid status of a cell. In particular, changes in saturation of the fatty acyl chains of glycerophospholipids and sphingolipids, which is a major factor for membrane fluidity or membrane microdomains (Simons97), can be assessed by MS and not by TLC. In addition, its high sensitivity allows analysis of lipid extracts without any need for labeling. Thereby, the analysis is not limited to the study of newly synthesized lipids but really gives an overview of the lipid status of the cell as a whole. MS appears therefore as a powerful tool to study lipid composition.

For sample injection, the robotic nanoflow ion source Nanomate, which allows automatic injection of samples from a 96 well-plate, increases the potential of MS for larger-scale analysis (Schultz et al 2000). However, a major drawback of the use of MS for lipid analysis is the fact that it requires lipid extracts of high quality. One phase lipid extracts such as the ones used for TLC analysis contain too many contaminating molecules that impair injection of the samples and induce significant background, limiting the detection of less abundant lipid species. However, several methods could overcome this problem. First, labeling of the lipids using radioactive precursors or precursors containing non radioactive isotopes, such as deuterium or ^{13}C , could allow better identification of the lipids relative to the background. However, while the radioactive isotopes will radioactively contaminate the mass spectrometers, the non-radioactive isotopic precursors are most of the time not commercially available. Furthermore, the presence of non-labeled contaminants in the sample can still impair the sample injection and induce suppression of the ions of interest. Another alternative is the use of automated two-phases extraction. Schwudke et al. are currently developing a two-phases system based on methyl-tert-butylether. In this system, the organic phase has a lower density, and is then above the aqueous phase and more accessible for direct injection by the Nanomate. This would generate easily accessible high quality lipid extracts suitable for large-scale analysis (personal communication). Moreover, Schwudke et al. developed with our collaboration a method, based on PCA, which allows easy identification of lipid

modifications despite the large amount of data produced by MS analysis (Schwudke et al 2007). It therefore appears that only minor improvements are still necessary to use MS as a lipid analysis tool for large-scale analysis.

Off-target Effects

Although several siRNA knock-downs gave rise to modifications in lipid composition, most of these phenotypes appeared to be due to potential off-target effects. When it was initially discovered, RNA interference was considered as a revolutionary tool, both because of its ease and of its specificity. It was suggested that only genes that show a perfect complementation to a siRNA would be targeted, and mismatches of just one nucleotide would be sufficient to disrupt this effect (Elbashir et al 2001a). However, more recently, several reports suggested that this rule is not always applying and that expression of several unintended genes is also affected by the use of a given siRNA (Birmingham et al 2006, Jackson et al 2003, Lin et al 2005, Ma et al 2006). One possibility could be that siRNA molecules can be processed in the cells like the endogenous miRNAs. The human genome, as well as the genome of other organisms, encodes small genes generating RNA stem loop structures (Bartel 2004, Kim & Nam 2006). These molecules are then successively processed by Drosha and Dicer, two RNaseIII-like enzymes generating an imperfect siRNA-like duplex (Lee et al 2003b). Conversely to siRNAs that induce cleavage of their mRNA targets (Elbashir et al 2001b, Hammond et al 2000), miRNAs are mainly responsible for translational repression (Bartel 2004, Kim & Nam 2006). Only partial complementarity is sufficient, which results in down-regulation of multiple genes by a single miRNA. The off-target effects observed upon siRNA treatment could therefore arise from partial complementarity to untargeted genes and subsequent inhibition of translation (Doench et al 2003, Saxena et al 2003, Scacheri et al 2004, Zeng et al 2003). However, since some miRNAs have also been shown to regulate their targets at the mRNA level (Lim et al 2005), similar unintended mRNA down-regulation could also occur upon siRNA treatment (Jackson et al 2003, Lin et al 2005).

Among the screens that have been previously carried out, although some of them didn't seem to suffer from off-target effects (Kittler et al 2004, MacKeigan et al 2005, Pelkmans et al 2005), others also concluded that their major phenotypes were actually due to the down-regulation of unintended genes (Lin et al 2005, Ma et al 2006). In particular, Lin et al. showed that a partial complementation of only 7 nucleotides was sufficient to induce mRNA down-regulation of an unintended gene (Lin et al 2005). These 7 nucleotides correspond to the seed region of miRNA, which is also necessary for miRNA-induced down-regulation (Birmingham et al 2006, Jackson et al 2006, Lin et al 2005).

The difference in off-target occurrence between these various screens could arise from several causes. First, in the screens that don't show off-targets, only a small subset of genes has been tested. It is therefore not unlikely that other phenotypes

are due to off-target effects. Furthermore, it is possible that some cellular processes would be more sensitive to off-target effects than others. In the case of lipid metabolism, several miRNAs have been implicated in its regulation (Esau et al 2006, Esau et al 2004, Krutzfeldt et al 2005, Krutzfeldt & Stoffel 2006, Teleman et al 2006, Xu et al 2003). It is possible that several genes implicated in lipid homeostasis are targets of miRNAs and would therefore be more sensitive to unintended down-regulation by siRNA (Jackson et al 2006, Stark et al 2005). Supporting this hypothesis, a high proportion of genes implicated in lipid metabolism have long 3' untranslated region (UTR), the part of the gene that is preferentially targeted by miRNAs. However, no homology has been found between the siRNAs from this screen believed to generate off-target effects and the already identified miRNAs. Nevertheless, some miRNAs still wait to be discovered and other sequences in the 3'UTR could be responsible for the off-targeting. Unfortunately, considering the high number of genes that contain a 7nt complementarity to a given siRNA in their 3'UTR, such homology can't be used to identify the potential off-targets (Birmingham et al 2006).

Another astonishing feature of the potential off-target effects observed in the screen is the fact that several targeted genes show the same potential off-target phenotypes upon treatment with two independent siRNAs although other siRNAs inducing a similar or stronger knock-down of the targeted gene do not induce any phenotype. Statistically, it seems very unlikely that several siRNAs would induce the same off-target effect. A potential explanation of that phenomenon could be that the down-regulation of both the target and an off-target would be responsible for the phenotype. In a system such as the regulation of lipid metabolism, redundancy is to be expected, and down-regulation of two independent pathways may be necessary for induction of a lipid phenotype. This hypothesis is however difficult to test without knowing the potential off-targeted genes.

Several suggestions have been made to decrease the occurrence of off-target effects. One of them is the use of lower siRNA concentration. It has been suggested that decreasing the siRNA concentration would not impair down-regulation of the targeted gene, but decrease the occurrence of off-target effects (Persengiev et al 2004). But, if this may be true for very efficient siRNAs, down-regulation of the target may be affected upon use of a less potent siRNA, thereby increasing the occurrence of false negatives in a screen. For this reason, high siRNA concentrations were also used in previous screens (MacKeigan et al 2005, Pelkmans et al 2005). Furthermore, decreasing the siRNA concentration most of the time didn't disrupt the potential off-target phenotypes (results not shown). Similar conclusions were also reached by others (Jackson et al 2003). Similarly, esiRNAs have been suggested to generate less off-target effects due to the low concentration of any individual sequence (Kittler et al 2007). However, although some esiRNAs were very potent in knocking-down their targets, some others showed only minor down-regulation, thereby also increasing the occurrence of false negatives in a screen. However, these two methods are a sensible compromise to limit off-target effects.

Another possibility is to directly compare the effect of several individual sequences targeting the same gene in the primary screen. Although difference in efficiency may result in different phenotypes, it again appears as a sensible way to directly select potential real targets. In addition, nowadays, most suppliers have improved their siRNA design to reduce off-target effects. Yannis Kalaidzidis has developed a method that allows evaluation of the quality of a library. Following this multi-parametric method, an old library against motor proteins (generated using the same algorithm as the kinase library used in this screen) led to approximately 75% non-correlating phenotypes, while the last generation of kinase library from the same company only generates around 25% non-correlating phenotypes (personal communication). Further understanding of the RNA interference process and further improvement of the siRNA design accordingly may therefore be sufficient to generate meaningful screening results.

Regulation of Cholesterol Metabolism

Despite the prominent off-target problems encountered in the screen, some interesting observations could be made. The first one is the fact that several siRNAs induce a decrease in cholesterol and a simultaneous accumulation of a potential methylated sterol precursor. Interestingly, some of these siRNAs were also reported to inhibit endocytosis in a previous screen (Pelkmans et al 2005), suggesting an important role for cholesterol in this process.

So far, regulation of HMG-CoA reductase was believed to be the major regulation step in the synthesis of cholesterol (Goldstein & Brown 1990). However, the accumulation of methylated sterols suggests that an additional important regulatory step exists downstream in the cholesterol biosynthetic pathway. In humans, two cholesterol precursors are methylated, namely lanosterol and demethyllanosterol. They appear therefore as potential regulatory species. Lanosterol has been shown to be instrumental in down-regulation of HMG-CoA reductase by promoting its Insig-dependent ubiquitination and degradation (Song et al 2005a). Furthermore, lanosterol proved to be toxic when added to CHO-7 cells in delipidated medium, although other natural sterols didn't impair cell growth (Xu et al 2005). Viability could be recovered by addition of cholesterol suggesting a role of lanosterol in inhibiting cholesterol synthesis. In addition, the downstream enzyme, CYP51, which catalyzes the lanosterol demethylation to form demethyllanosterol, is the most evolutionarily conserved cytochrome P450 enzyme and the only one found both in prokaryotes and eukaryotes (Debeljak et al 2003, Waterman & Lipesheva 2005). As the other enzymes of the cholesterol biosynthetic pathway, it is activated upon SREBP activation (Rawson 2003). However, since additional sequences are highly conserved in the CYP51 promoter, other regulation systems are to be expected (Debeljak et al 2003). On the other hand, demethyllanosterol, also called follicular fluid meiosis-activating sterol (FF-MAS), has been identified as a signaling molecule responsible for the induction of meiosis in germ cells (Byskov et al 1995). Furthermore, the increase in FF-MAS in these cells is coupled to a decrease of free

cholesterol (Baltsen et al 2001). Therefore, accumulation of this molecule may also be tightly regulated in cells.

Unfortunately, at this stage, the gene that is responsible for the methylated sterol accumulation is not yet identified and therefore these hypotheses can't be confirmed.

Regulation of Triglyceride Metabolism via MAPK9

One of the phenotypes frequently observed within the screen was the increase of triglycerides. Triglycerides represent the most condensed form of energy in the cell and are therefore essential lipids for energy storage. They are found mostly in lipid droplets, specific organelles specialized in lipid storage.

Although most of the siRNAs inducing TAG increase seem to do so via off-target effects, four siRNAs targeting MAPK9 showed a consistent phenotype without obvious off-target effects. This leads to the identification of MAPK9 as an essential regulator of lipid droplet metabolism. The increase in TAG could be confirmed both by TLC and by mass spectrometry. Furthermore, a similar phenotype was observed using an inhibitor of MAPK9. In addition, this effect was coupled to an increase in lipid droplets, as could be observed by BODIPY staining upon MAPK9 knock-down.

To further confirm the specificity of the phenotype, the potential homolog of MAPK9 in *S. pombe*, Sty1, was also analyzed. Although Sty1 is more closely related to the p38 subfamily of MAP kinases, both the JNK MAP kinases, from which MAPK9 belongs, and Sty1 are activated upon glucose depletion (Liu et al 1997, Stettler et al 1996). Furthermore, both are cytoplasmic proteins that translocate to the nucleus upon activation, while p38 kinases localization is not altered upon activation (Toone & Jones 1998). In addition, complementation studies with the *S. cerevisiae* homolog of Sty1, Hog1, showed that both JNK and p38 kinases could partially substitute for the loss of Hog1 (Galcheva-Gargova et al 1994, Han et al 1994). All these data taken together suggest that Sty1 could be a functional homolog of MAPK9. Accordingly, it is shown in this work that deletion of this gene induces both an increase in TAG and an increase in lipid droplets.

Taken together, these data suggest that both MAPK9 and its *S. pombe* homolog Sty1 are implicated in the regulation of TAG metabolism and lipid droplets.

Previously, MAPK9 has already been implicated in atherosclerosis, a major disease arising from dysregulation of lipid metabolism. Activation of MAPK9 was observed in atherosclerotic lesions both in mice and humans (Nishio et al 2001, Ricci et al 2004). Deletion of MAPK9 in atherosclerosis mouse model decreased the occurrence of the lesions (Ricci et al 2004). This appeared to be due to a decrease in LDL internalization by macrophages, following defective phosphorylation of scavenger receptor A, one of the main receptors for modified LDL, and concomitant decrease

in foam cell formation (Ricci et al 2004). This confirms the implication of MAPK9 in lipid-related processes.

However, since in this assay the strongest phenotype was observed in delipidated conditions, MAPK9 must influence TAG metabolism directly at the intracellular level. Therefore, the phenotype observed could arise both from an increase in lipid synthesis or a decrease in lipolysis (figure 44). As it was previously shown, PPAR γ is down-regulated by JNK activation (Camp et al 1999). Knock-down of MAPK9 would therefore release the inhibition of PPAR γ . Since PPAR γ is stimulating fatty acid uptake and synthesis (Beaven & Tontonoz 2006, Chawla et al 2001b), this could account for the increase in TAG observed in the MAPK9 knock-down. However, several lines of evidence would rather favor a decrease in lipolysis. In adipocytes, TNF α has been shown to induce lipolysis in a JNK-dependent fashion (Ryden et al 2004). This happens via down-regulation of perilipin expression, a lipid droplet associated protein thought to modulate the access of the lipases to the lipid droplet surface (Souza et al 1998). Perilipin is not expressed in non-adipose tissues, but a similar mechanism could take place with a yet unidentified lipid droplet protein. Furthermore, JNK proteins are activated upon glucose depletion (Liu et al 1997). In these conditions, cells need to obtain their energy from other sources, such as TAG. MAPK9 could therefore be implicated in that process. Interestingly, upon activation of Sty1, several genes involved in peroxisomal β -oxidation are up-regulated (Chen et al 2003), further favoring the lipolysis hypothesis. To test this possibility, the level of mRNA of several genes implicated in biosynthesis or degradation of TAG was monitored upon MAPK9 knock-down and activation, but no significant variation could be observed. But, since other genes than the ones tested could be implicated and since regulation could occur at the post-transcriptional level, a more general assay will be required to delineate the mechanism of TAG regulation by MAPK9.

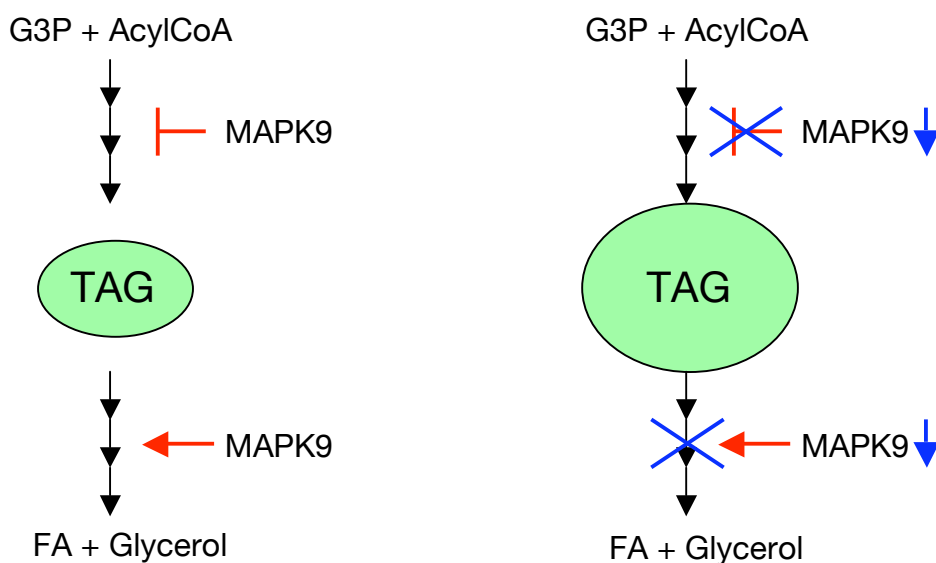


Figure 44: Model of MAPK9 actions. MAPK9 would inhibit TAG synthesis and/or favor TAG mobilization. Upon MAPK9 knock-down, these processes would be reversed inducing accumulation of TAG.

List of abbreviations

ABC	ATP Binding Cassette
ACAT	Acyl-CoA:Cholesterol Acyltransferase
AGPAT	Acylglycerol-Phosphate Acyltransferase
AM	Anisomycin
Apo	Apolipoprotein
ATF	Activating Transcription Factor
ATGL	Adipose Triglyceride Lipase
ATP	Adenosine Triphosphate
Bcl	B-cell leukemia associated oncogenes
BSA	Bovine Serum Albumin
CASK	Calcium/Calmodulin dependent Serine protein Kinase
cDNA	Complementary DNA
<i>C. elegans</i>	<i>Caenorhabditis elegans</i>
CE	Cholesterol Ester
Cer	Ceramide
CETP	Cholesteryl Ester Transfer Protein
Chol	Cholesterol
CL	Cardiolipin
CoA	CoenzymeA
COP	Coat Protein
CTP	Cytidine Triphosphate
CUPID	Cluster analysis and Pathway Information for HTS Data
CYP	Cytochrome P450
DAG	Diacylglycerol
DGAT	Diacylglycerol Acyl Transferase
DMEM	Dulbecco's Modified Eagle's Medium
DNA	Deoxyribonucleic Acid
dsRNA	Double-strand RNA
<i>E. coli</i>	<i>Escherichia coli</i>
EMM	Edinburgh Minimal Medium
ER	Endoplasmic Reticulum
Esi-QqTof	Electrospray-double Quadrupole-Time of flight
esiRNA	Endonuclease-prepared siRNA
EtOH	Ethanol
FATP	Fatty Acid Transporter
FBS	Fetal Bovine Serum
FF-MAS	Follicular Fluid Meiosis-Activating Sterol
Fig.	Figure
F-luc	Firefly Luciferase
GalCer	Galactosyl Ceramide
GAPDH	Glyceraldehyde-3-Phosphate Dehydrogenase
GlcCer	Glucosyl Ceramide
GLUT4	Glucose Transporter 4
GPAT	Glycerol-Phosphate Acyltransferase

HDL	High Density Lipoprotein
HMG-CoA	3-Hydroxy-3-Methylglutaryl-CoA
Hog	High osmolarity glycerol
HPTLC	High Performance Thin Layer Chromatography
HRP	Horseradish Peroxidase
HSL	Hormone-Sensitive Lipase
IDL	Intermediate Density Lipoprotein
IgG	Immunoglobulin G
ikB	Inhibitor of kappa B
IKK	Inhibitor of kappa B Kinase
Insig	Insulin induced genes
IRS	Insulin Receptor Substrate
JNK	c-jun N-terminal Kinase
LCAT	Lecithin-Cholesterol-Acyltransferase
LDL	Low Density Lipoprotein
LPA	Lysophosphatidic Acid
LXR	Liver X Receptor
MKK	MAP Kinase Kinase
MAP	Mitogen Activated protein
MAPK	MAP Kinase
Mdr	Multidrug resistance protein
MeOH	Methanol
miR	MicroRNA
miRNA	MicroRNA
mRNA	Messenger RNA
MS	Mass Spectrometry
NFκB	Nuclear Factor kappa B
nt	Nucleotide
OD	Optical Density
PA	Phosphatidic Acid
PBS	Phosphate Buffered Saline
PC	Phosphatidylcholine
PCA	Principal Component Analysis
PCR	Polymerase Chain Reaction
PDXK	Pyridoxal Kinase
PE	Phosphatidylethanolamine
PI	Phosphatidylinositol
PPAR	Peroxisome Proliferator-Activated Receptor
PS	Phosphatidylserine
RISC	RNA-Induced Silencing Complex
R-luc	Renilla luciferase
RNA	Ribonucleic Acid
RNAi	RNA interference
RT	Reverse Transcriptase
S2	Silencer 2 siRNA
S5	Silencer 5 siRNA

S6	Silencer 6 siRNA
S1P	Site-1 protease
S2P	Site-2 protease
SCAP	SREBP-Cleavage-Activating Protein
<i>S. cerevisiae</i>	<i>Saccharomyces cerevisiae</i>
SDS	Sodium Dodecyl Sulfate
siRNA	Small interfering RNA
SM	Sphingomyelin
SOAT	Sterol O-Acyl Transferase
<i>S. Pombe</i>	<i>Schizosaccharomyces Pombe</i>
SPT	Serine Palmitoyl Transferase
SRE	Sterol Regulatory Element
SREBP	Sterol Regulatory Element Binding Protein
Sty	Suppressor of tyrosine phosphatase
TAG	Triacylglycerol
TDS	Technology Development Studio
TLC	Thin Layer Chromatography
TNF α	Tumor Necrosis Factor alpha
UTR	Untranslated Region
UV	Ultraviolet
VCAM-1	Vascular Cell Adhesion Molecule-1
VLDL	Very Low Density Lipoprotein
YES	Yeast Extract + Supplements

List of figures

Fig. 1: Increase of overweight population in least developing countries	07
Fig. 2: Obesity in the US in 2004	09
Fig. 3: The early steps of atherosclerosis	11
Fig. 4: Example of a fatty acid structure: palmitic acid	12
Fig. 5: Example of a triacylglycerol structure: tripalmitoylglycerol	13
Fig. 6: Example of a phospholipids structure: dipalmitoylphosphatidylcholine	14
Fig. 7: Example of a sphingolipid structure: palmitoylsphingomyelin	15
Fig. 8: Example of a sterol structure: cholesterol	16
Fig. 9: Two-steps processing of SREBP	20
Fig. 10: Decrease in fatty acid synthesis and cholesterol levels upon miR-122 depletion	23
Fig. 11: Schematic representation of the method	41
Fig. 12: Incorporation of acetate into cholesterol	42
Fig. 13: Test of extraction and labeling conditions	43
Fig. 14: TLC with standard lipids	45
Fig. 15: Effect of oligofectamine on lipid composition as determined by MS	46
Fig. 16: TLC analysis of lipid extracts of esiRNA knock-downs	48
Fig. 17: Decrease of PI levels in the PI knock-down	49
Fig. 18: Propidium iodide fluorescence intensity in function of cell numbers	50
Fig. 19: Esi-MS analysis of lipid extracts from HeLa cells	52
Fig. 20: Principal Component Analysis (PCA) of 262 individual mass detected in HeLa cells feeding experiments	53
Fig. 21: Decrease in SOAT1 mRNA level upon siRNA treatment	56
Fig. 22: Decrease of cholesterol esters upon SOAT1 siRNA knock-down	56
Fig. 23: Plate layout for the siRNA transfection of the kinase screen	58
Fig. 24: Typical TLC plate from the screen	60
Fig. 25: Clustering of the phenotypic lipid profiles	61
Fig. 26: Running behaviour of cholesterol derivatives	63
Fig. 27: Lipid phenotype upon siRNA treatment	64
Fig. 28: mRNA level upon siRNA treatment	65
Fig. 29: TLC of HeLa cells extracts upon IKK1 knock-down	66
Fig. 30: Effect of knock-down or inhibition of IKK1	67
Fig. 31: Increase of TAG upon MAPK9 knock-down	70
Fig. 32: Knock-down of MAPK9 monitored by western blot	71
Fig. 33: Radioactive labeling of TAG upon MAPK9 knock-down	71
Fig. 34: Effect of SP600125 on lipid composition	72
Fig. 35: Effect of MAPK9 knock-down on individual TAG species monitored by LTQ-Orbitrap mass spectrometry	73
Fig. 36: Effect of MAPK9 knock-down on BODIPY staining	74
Fig. 37: ATGL and HSL levels monitored by WB upon MAPK9 knock-down	74
Fig. 38: ATGL levels monitored by WB upon JNK activation	75
Fig. 39: Nile Red staining with or without glucose depletion	76
Fig. 40: Radioactive oleate staining of yeast lipid extracts separated by TLC	77
Fig. 41: No effect of glucose depletion on ER structure	78

Fig. 42: Decrease in internal structure upon glucose depletion observed by bright-field microscopy	78
Fig. 43: Growth curve upon recovery from glucose depletion	79
Fig. 44: Model of MAPK9 actions	86

List of tables

Table 1: List of siRNA used in this work	28
Table 2: List of RT-PCR primers used in this work	31
Table 3: Lipid species whose abundance was specifically increased by spiking fatty acids	54
Table 4: Lipid phenotype and RT-PCR data obtained for kinase knock-down	68

Bibliography

- Aguirre V, Uchida T, Yenush L, Davis R, White MF. 2000. The c-Jun NH(2)-terminal kinase promotes insulin resistance during association with insulin receptor substrate-1 and phosphorylation of Ser(307). *J Biol Chem* 275: 9047-54
- Aguirre V, Werner ED, Giraud J, Lee YH, Shoelson SE, White MF. 2002. Phosphorylation of Ser307 in insulin receptor substrate-1 blocks interactions with the insulin receptor and inhibits insulin action. *J Biol Chem* 277: 1531-7
- Avramoglu RK, Basciano H, Adeli K. 2006. Lipid and lipoprotein dysregulation in insulin resistant states. *Clin Chim Acta* 368: 1-19
- Bain J, McLauchlan H, Elliott M, Cohen P. 2003. The specificities of protein kinase inhibitors: an update. *Biochem J* 371: 199-204
- Baldwin AS, Jr. 1996. The NF-kappa B and I kappa B proteins: new discoveries and insights. *Annu Rev Immunol* 14: 649-83
- Baltsen M, Bogh IB, Byskov AG. 2001. Content of meiosis activating sterols in equine follicular fluids: correlation to follicular size and dominance. *Theriogenology* 56: 133-45
- Bartel DP. 2004. MicroRNAs: genomics, biogenesis, mechanism, and function. *Cell* 116: 281-97
- Beaven SW, Tontonoz P. 2006. Nuclear receptors in lipid metabolism: targeting the heart of dyslipidemia. *Annu Rev Med* 57: 313-29
- Bell RM, Hannun YA, Loomis CR. 1986. Mechanism of regulation of protein kinase C by lipid second messengers. *Symp Fundam Cancer Res* 39: 145-56
- Bennett BL, Sasaki DT, Murray BW, O'Leary EC, Sakata ST, et al. 2001. SP600125, an anthrapyrazolone inhibitor of Jun N-terminal kinase. *Proc Natl Acad Sci U S A* 98: 13681-6
- Berger J, Moller DE. 2002. The mechanisms of action of PPARs. *Annu Rev Med* 53: 409-35
- Bernstein E, Caudy AA, Hammond SM, Hannon GJ. 2001. Role for a bidentate ribonuclease in the initiation step of RNA interference. *Nature* 409: 363-6
- Birmingham A, Anderson EM, Reynolds A, Ilsley-Tyree D, Leake D, et al. 2006. 3' UTR seed matches, but not overall identity, are associated with RNAi off-targets. *Nat Methods* 3: 199-204
- Bligh EG, Dyer WJ. 1959. A rapid method of total lipid extraction and purification. *Can J Biochem Physiol* 37: 911-7
- Bogdanov M, Heacock PN, Dowhan W. 2002. A polytopic membrane protein displays a reversible topology dependent on membrane lipid composition. *Embo J* 21: 2107-16
- Bogoyevitch MA. 2006. The isoform-specific functions of the c-Jun N-terminal Kinases (JNKs): differences revealed by gene targeting. *Bioessays* 28: 923-34
- Bogoyevitch MA, Ketterman AJ, Sugden PH. 1995. Cellular stresses differentially activate c-Jun N-terminal protein kinases and extracellular signal-regulated protein kinases in cultured ventricular myocytes. *J Biol Chem* 270: 29710-7
- Briggs MR, Yokoyama C, Wang X, Brown MS, Goldstein JL. 1993. Nuclear protein that binds sterol regulatory element of low density lipoprotein receptor

- promoter. I. Identification of the protein and delineation of its target nucleotide sequence. *J Biol Chem* 268: 14490-6
- Brown AJ, Sun L, Feramisco JD, Brown MS, Goldstein JL. 2002. Cholesterol addition to ER membranes alters conformation of SCAP, the SREBP escort protein that regulates cholesterol metabolism. *Mol Cell* 10: 237-45
- Brown DA. 2001. Lipid droplets: proteins floating on a pool of fat. *Curr Biol* 11: R446-9
- Brugger B, Erben G, Sandhoff R, Wieland FT, Lehmann WD. 1997. Quantitative analysis of biological membrane lipids at the low picomole level by nano-electrospray ionization tandem mass spectrometry. *Proc Natl Acad Sci U S A* 94: 2339-44
- Bussolino F, Camussi G. 1995. Platelet-activating factor produced by endothelial cells. A molecule with autocrine and paracrine properties. *Eur J Biochem* 229: 327-37
- Byskov AG, Andersen CY, Nordholm L, Thogersen H, Xia G, et al. 1995. Chemical structure of sterols that activate oocyte meiosis. *Nature* 374: 559-62
- Caballero B. 2005. A nutrition paradox--underweight and obesity in developing countries. *N Engl J Med* 352: 1514-6
- Camp HS, Tafuri SR, Leff T. 1999. c-Jun N-terminal kinase phosphorylates peroxisome proliferator-activated receptor-gamma1 and negatively regulates its transcriptional activity. *Endocrinology* 140: 392-7
- Campfield LA, Smith FJ, Guisez Y, Devos R, Burn P. 1995. Recombinant mouse OB protein: evidence for a peripheral signal linking adiposity and central neural networks. *Science* 269: 546-9
- Carpenter AE, Sabatini DM. 2004. Systematic genome-wide screens of gene function. *Nat Rev Genet* 5: 11-22
- Chawla A, Boisvert WA, Lee CH, Laffitte BA, Barak Y, et al. 2001a. A PPAR gamma-LXR-ABCA1 pathway in macrophages is involved in cholesterol efflux and atherogenesis. *Mol Cell* 7: 161-71
- Chawla A, Repa JJ, Evans RM, Mangelsdorf DJ. 2001b. Nuclear receptors and lipid physiology: opening the X-files. *Science* 294: 1866-70
- Chen D, Toone WM, Mata J, Lyne R, Burns G, et al. 2003. Global transcriptional responses of fission yeast to environmental stress. *Mol Biol Cell* 14: 214-29
- Chernushevich IV, Loboda AV, Thomson BA. 2001. An introduction to quadrupole-time-of-flight mass spectrometry. *J Mass Spectrom* 36: 849-65
- Chiang JY, Kimmel R, Stroup D. 2001. Regulation of cholesterol 7alpha-hydroxylase gene (CYP7A1) transcription by the liver orphan receptor (LXRalpha). *Gene* 262: 257-65
- Chinetti G, Lestavel S, Bocher V, Remaley AT, Neve B, et al. 2001. PPAR-alpha and PPAR-gamma activators induce cholesterol removal from human macrophage foam cells through stimulation of the ABCA1 pathway. *Nat Med* 7: 53-8
- Coleman RA, Lee DP. 2004. Enzymes of triacylglycerol synthesis and their regulation. *Prog Lipid Res* 43: 134-76
- Dansky HM, Barlow CB, Lominska C, Sikes JL, Kao C, et al. 2001. Adhesion of monocytes to arterial endothelium and initiation of atherosclerosis are

- critically dependent on vascular cell adhesion molecule-1 gene dosage. *Arterioscler Thromb Vasc Biol* 21: 1662-7
- De Matteis M, Godi A, Corda D. 2002. Phosphoinositides and the golgi complex. *Curr Opin Cell Biol* 14: 434-47
- Debeljak N, Fink M, Rozman D. 2003. Many facets of mammalian lanosterol 14alpha-demethylase from the evolutionarily conserved cytochrome P450 family CYP51. *Arch Biochem Biophys* 409: 159-71
- Degols G, Shiozaki K, Russell P. 1996. Activation and regulation of the Spc1 stress-activated protein kinase in *Schizosaccharomyces pombe*. *Mol Cell Biol* 16: 2870-7
- Derijard B, Hibi M, Wu IH, Barrett T, Su B, et al. 1994. JNK1: a protein kinase stimulated by UV light and Ha-Ras that binds and phosphorylates the c-Jun activation domain. *Cell* 76: 1025-37
- Ding DQ, Tomita Y, Yamamoto A, Chikashige Y, Haraguchi T, Hiraoka Y. 2000. Large-scale screening of intracellular protein localization in living fission yeast cells by the use of a GFP-fusion genomic DNA library. *Genes Cells* 5: 169-90
- Dobrosotskaya IY, Seegmiller AC, Brown MS, Goldstein JL, Rawson RB. 2002. Regulation of SREBP processing and membrane lipid production by phospholipids in *Drosophila*. *Science* 296: 879-83
- Doench JG, Petersen CP, Sharp PA. 2003. siRNAs can function as miRNAs. *Genes Dev* 17: 438-42
- Dong C, Yang DD, Tournier C, Whitmarsh AJ, Xu J, et al. 2000. JNK is required for effector T-cell function but not for T-cell activation. *Nature* 405: 91-4
- Dorsett Y, Tuschl T. 2004. siRNAs: applications in functional genomics and potential as therapeutics. *Nat Rev Drug Discov* 3: 318-29
- Duncan EA, Brown MS, Goldstein JL, Sakai J. 1997. Cleavage site for sterol-regulated protease localized to a leu-Ser bond in the luminal loop of sterol regulatory element-binding protein-2. *J Biol Chem* 272: 12778-85
- Elbashir SM, Harborth J, Lendeckel W, Yalcin A, Weber K, Tuschl T. 2001a. Duplexes of 21-nucleotide RNAs mediate RNA interference in cultured mammalian cells. *Nature* 411: 494-8
- Elbashir SM, Harborth J, Weber K, Tuschl T. 2002. Analysis of gene function in somatic mammalian cells using small interfering RNAs. *Methods* 26: 199-213
- Elbashir SM, Lendeckel W, Tuschl T. 2001b. RNA interference is mediated by 21- and 22-nucleotide RNAs. *Genes Dev* 15: 188-200
- Esau C, Davis S, Murray SF, Yu XX, Pandey SK, et al. 2006. miR-122 regulation of lipid metabolism revealed by in vivo antisense targeting. *Cell Metab* 3: 87-98
- Esau C, Kang X, Peralta E, Hanson E, Marcusson EG, et al. 2004. MicroRNA-143 regulates adipocyte differentiation. *J Biol Chem* 279: 52361-5
- Espenshade PJ, Li WP, Yabe D. 2002. Sterols block binding of COPII proteins to SCAP, thereby controlling SCAP sorting in ER. *Proc Natl Acad Sci U S A* 99: 11694-9
- Fahy E, Subramaniam S, Brown HA, Glass CK, Merrill AH, Jr., et al. 2005. A comprehensive classification system for lipids. *J Lipid Res* 46: 839-61

- Fire A, Xu S, Montgomery MK, Kostas SA, Driver SE, Mello CC. 1998. Potent and specific genetic interference by double-stranded RNA in *Caenorhabditis elegans*. *Nature* 391: 806-11
- Fong LG, Le D. 1999. The processing of ligands by the class A scavenger receptor is dependent on signal information located in the cytoplasmic domain. *J Biol Chem* 274: 36808-16
- Forsburg SL, Rhind N. 2006. Basic methods for fission yeast. *Yeast* 23: 173-83
- Fourcade S, Savary S, Albet S, Gauthe D, Gondcaille C, et al. 2001. Fibrate induction of the adrenoleukodystrophy-related gene (ABCD2): promoter analysis and role of the peroxisome proliferator-activated receptor PPARalpha. *Eur J Biochem* 268: 3490-500
- Francois J, Parrou JL. 2001. Reserve carbohydrates metabolism in the yeast *Saccharomyces cerevisiae*. *FEMS Microbiol Rev* 25: 125-45
- Fu H, Tie Y, Xu C, Zhang Z, Zhu J, et al. 2005. Identification of human fetal liver miRNAs by a novel method. *FEBS Lett* 579: 3849-54
- Galcheva-Gargova Z, Derijard B, Wu IH, Davis RJ. 1994. An osmosensing signal transduction pathway in mammalian cells. *Science* 265: 806-8
- Gil J, Esteban M. 2000. Induction of apoptosis by the dsRNA-dependent protein kinase (PKR): mechanism of action. *Apoptosis* 5: 107-14
- Gocze PM, Freeman DA. 1994. Factors underlying the variability of lipid droplet fluorescence in MA-10 Leydig tumor cells. *Cytometry* 17: 151-8
- Goldstein JL, Brown MS. 1990. Regulation of the mevalonate pathway. *Nature* 343: 425-30
- Goldstein JL, DeBose-Boyd RA, Brown MS. 2006. Protein sensors for membrane sterols. *Cell* 124: 35-46
- Greenspan P, Mayer EP, Fowler SD. 1985. Nile red: a selective fluorescent stain for intracellular lipid droplets. *J Cell Biol* 100: 965-73
- Haemmerle G, Lass A, Zimmermann R, Gorkiewicz G, Meyer C, et al. 2006. Defective lipolysis and altered energy metabolism in mice lacking adipose triglyceride lipase. *Science* 312: 734-7
- Hamilton JA. 1989. Interactions of triglycerides with phospholipids: incorporation into the bilayer structure and formation of emulsions. *Biochemistry* 28: 2514-20
- Hammond SM, Bernstein E, Beach D, Hannon GJ. 2000. An RNA-directed nuclease mediates post-transcriptional gene silencing in *Drosophila* cells. *Nature* 404: 293-6
- Han J, Lee JD, Bibbs L, Ulevitch RJ. 1994. A MAP kinase targeted by endotoxin and hyperosmolarity in mammalian cells. *Science* 265: 808-11
- Han X, Gross RW. 2003. Global analyses of cellular lipidomes directly from crude extracts of biological samples by ESI mass spectrometry: a bridge to lipidomics. *J Lipid Res* 44: 1071-9
- Harborth J, Elbashir SM, Bechert K, Tuschl T, Weber K. 2001. Identification of essential genes in cultured mammalian cells using small interfering RNAs. *J Cell Sci* 114: 4557-65
- Harborth J, Elbashir SM, Vandenburgh K, Manninga H, Scaringe SA, et al. 2003. Sequence, chemical, and structural variation of small interfering RNAs and

- short hairpin RNAs and the effect on mammalian gene silencing. *Antisense Nucleic Acid Drug Dev* 13: 83-105
- Hayden MS, Ghosh S. 2004. Signaling to NF-kappaB. *Genes Dev* 18: 2195-224
- Hirosumi J, Tuncman G, Chang L, Gorgun CZ, Uysal KT, et al. 2002. A central role for JNK in obesity and insulin resistance. *Nature* 420: 333-6
- Holen T, Amarzguioui M, Wiiger MT, Babaie E, Prydz H. 2002. Positional effects of short interfering RNAs targeting the human coagulation trigger Tissue Factor. *Nucleic Acids Res* 30: 1757-66
- Holm C, Osterlund T, Laurell H, Contreras JA. 2000. Molecular mechanisms regulating hormone-sensitive lipase and lipolysis. *Annu Rev Nutr* 20: 365-93
- Hu Q, Noll RJ, Li H, Makarov A, Hardman M, Graham Cooks R. 2005. The Orbitrap: a new mass spectrometer. *J Mass Spectrom* 40: 430-43
- Hua X, Nohturfft A, Goldstein JL, Brown MS. 1996. Sterol resistance in CHO cells traced to point mutation in SREBP cleavage-activating protein. *Cell* 87: 415-26
- Iordanov MS, Pribnow D, Magun JL, Dinh TH, Pearson JA, et al. 1997. Ribotoxic stress response: activation of the stress-activated protein kinase JNK1 by inhibitors of the peptidyl transferase reaction and by sequence-specific RNA damage to the alpha-sarcin/ricin loop in the 28S rRNA. *Mol Cell Biol* 17: 3373-81
- Jackson AL, Bartz SR, Schelter J, Kobayashi SV, Burchard J, et al. 2003. Expression profiling reveals off-target gene regulation by RNAi. *Nat Biotechnol* 21: 635-7
- Jackson AL, Burchard J, Schelter J, Chau BN, Cleary M, et al. 2006. Widespread siRNA "off-target" transcript silencing mediated by seed region sequence complementarity. *Rna* 12: 1179-87
- Ji Y, Jian B, Wang N, Sun Y, Moya ML, et al. 1997. Scavenger receptor BI promotes high density lipoprotein-mediated cellular cholesterol efflux. *J Biol Chem* 272: 20982-5
- Kahn SE, Hull RL, Utzschneider KM. 2006. Mechanisms linking obesity to insulin resistance and type 2 diabetes. *Nature* 444: 840-6
- Kajimoto K, Naraba H, Iwai N. 2006. MicroRNA and 3T3-L1 pre-adipocyte differentiation. *Rna* 12: 1626-32
- Kalaany NY, Mangelsdorf DJ. 2006. LXRS and FXR: the yin and yang of cholesterol and fat metabolism. *Annu Rev Physiol* 68: 159-91
- Kalaidzidis YL, Gavrilov AV, Zaitsev PV, Kalaidzidis AL, Korolev EV. 1997. PLUK-An Environment for Software Development. *Programming and Computer Software* 23: 206-12
- Kallunki T, Su B, Tsigelny I, Sluss HK, Derijard B, et al. 1994. JNK2 contains a specificity-determining region responsible for efficient c-Jun binding and phosphorylation. *Genes Dev* 8: 2996-3007
- Karin M, Gallagher E. 2005. From JNK to pay dirt: jun kinases, their biochemistry, physiology and clinical importance. *IUBMB Life* 57: 283-95
- Kawasaki H, Suyama E, Iyo M, Taira K. 2003. siRNAs generated by recombinant human Dicer induce specific and significant but target site-independent gene silencing in human cells. *Nucleic Acids Res* 31: 981-7

- Kim VN, Nam JW. 2006. Genomics of microRNA. *Trends Genet* 22: 165-73
- Kittler R, Buchholz F. 2003. RNA interference: gene silencing in the fast lane. *Semin Cancer Biol* 13: 259-65
- Kittler R, Putz G, Pelletier L, Poser I, Heninger AK, et al. 2004. An endoribonuclease-prepared siRNA screen in human cells identifies genes essential for cell division. *Nature* 432: 1036-40
- Kittler R, Surendranath V, Heninger AK, Slabicki M, Theis M, et al. 2007. Genome-wide resources of endoribonuclease-prepared short interfering RNAs for specific loss-of-function studies. *Nat Methods* 4: 337-44
- Kliwer SA, Sundseth SS, Jones SA, Brown PJ, Wisely GB, et al. 1997. Fatty acids and eicosanoids regulate gene expression through direct interactions with peroxisome proliferator-activated receptors alpha and gamma. *Proc Natl Acad Sci U S A* 94: 4318-23
- Kosswig N, Rice S, Daugherty A, Post SR. 2003. Class A scavenger receptor-mediated adhesion and internalization require distinct cytoplasmic domains. *J Biol Chem* 278: 34219-25
- Krutzfeldt J, Rajewsky N, Braich R, Rajeev KG, Tuschl T, et al. 2005. Silencing of microRNAs in vivo with 'antagomirs'. *Nature* 438: 685-9
- Krutzfeldt J, Stoffel M. 2006. MicroRNAs: a new class of regulatory genes affecting metabolism. *Cell Metab* 4: 9-12
- Kuan CY, Yang DD, Samanta Roy DR, Davis RJ, Rakic P, Flavell RA. 1999. The Jnk1 and Jnk2 protein kinases are required for regional specific apoptosis during early brain development. *Neuron* 22: 667-76
- Kuerschner L, Ejsing CS, Ekroos K, Shevchenko A, Anderson KI, Thiele C. 2005. Polyene-lipids: a new tool to image lipids. *Nat Methods* 2: 39-45
- Kunjathoor VV, Febbraio M, Podrez EA, Moore KJ, Andersson L, et al. 2002. Scavenger receptors class A-I/II and CD36 are the principal receptors responsible for the uptake of modified low density lipoprotein leading to lipid loading in macrophages. *J Biol Chem* 277: 49982-8
- Kwok BH, Koh B, Ndubuisi MI, Elofsson M, Crews CM. 2001. The anti-inflammatory natural product parthenolide from the medicinal herb Feverfew directly binds to and inhibits I κ B kinase. *Chem Biol* 8: 759-66
- Lakics V, Vogel SN. 1998. Lipopolysaccharide and ceramide use divergent signaling pathways to induce cell death in murine macrophages. *J Immunol* 161: 2490-500
- Lee MH, Lu K, Patel SB. 2001. Genetic basis of sitosterolemia. *Curr Opin Lipidol* 12: 141-9
- Lee SJ, Sekimoto T, Yamashita E, Nagoshi E, Nakagawa A, et al. 2003a. The structure of importin-beta bound to SREBP-2: nuclear import of a transcription factor. *Science* 302: 1571-5
- Lee Y, Ahn C, Han J, Choi H, Kim J, et al. 2003b. The nuclear RNase III Drosha initiates microRNA processing. *Nature* 425: 415-9
- Lehmann JM, Kliwer SA, Moore LB, Smith-Oliver TA, Oliver BB, et al. 1997. Activation of the nuclear receptor LXR by oxysterols defines a new hormone response pathway. *J Biol Chem* 272: 3137-40

- Lewis GF, Rader DJ. 2005. New insights into the regulation of HDL metabolism and reverse cholesterol transport. *Circ Res* 96: 1221-32
- Li AC, Glass CK. 2002. The macrophage foam cell as a target for therapeutic intervention. *Nat Med* 8: 1235-42
- Li AC, Glass CK. 2004. PPAR- and LXR-dependent pathways controlling lipid metabolism and the development of atherosclerosis. *J Lipid Res* 45: 2161-73
- Libby P. 2002. Inflammation in atherosclerosis. *Nature* 420: 868-74
- Liebisch G, Binder M, Schifferer R, Langmann T, Schulz B, Schmitz G. 2006. High throughput quantification of cholesterol and cholesteryl ester by electrospray ionization tandem mass spectrometry (ESI-MS/MS). *Biochim Biophys Acta* 1761: 121-8
- Lim LP, Lau NC, Garrett-Engele P, Grimson A, Schelter JM, et al. 2005. Microarray analysis shows that some microRNAs downregulate large numbers of target mRNAs. *Nature* 433: 769-73
- Lin X, Ruan X, Anderson MG, McDowell JA, Kroeger PE, et al. 2005. siRNA-mediated off-target gene silencing triggered by a 7 nt complementation. *Nucleic Acids Res* 33: 4527-35
- Linder ME, Deschenes RJ. 2007. Palmitoylation: policing protein stability and traffic. *Nat Rev Mol Cell Biol* 8: 74-84
- Liu X, Gupta AK, Corry PM, Lee YJ. 1997. Hypoglycemia-induced c-Jun phosphorylation is mediated by c-Jun N-terminal kinase 1 and Lyn kinase in drug-resistant human breast carcinoma MCF-7/ADR cells. *J Biol Chem* 272: 11690-3
- Loeb-Hennard C, McIntyre JO. 2000. (R)-3-hydroxybutyrate dehydrogenase: selective phosphatidylcholine binding by the C-terminal domain. *Biochemistry* 39: 11928-38
- Ma JB, Ye K, Patel DJ. 2004. Structural basis for overhang-specific small interfering RNA recognition by the PAZ domain. *Nature* 429: 318-22
- Ma JB, Yuan YR, Meister G, Pei Y, Tuschl T, Patel DJ. 2005. Structural basis for 5'-end-specific recognition of guide RNA by the *A. fulgidus* Piwi protein. *Nature* 434: 666-70
- Ma Y, Creanga A, Lum L, Beachy PA. 2006. Prevalence of off-target effects in *Drosophila* RNA interference screens. *Nature* 443: 359-63
- Maceyka M, Payne SG, Milstien S, Spiegel S. 2002. Sphingosine kinase, sphingosine-1-phosphate, and apoptosis. *Biochim Biophys Acta* 1585: 193-201
- MacKeigan JP, Murphy LO, Blenis J. 2005. Sensitized RNAi screen of human kinases and phosphatases identifies new regulators of apoptosis and chemoresistance. *Nat Cell Biol* 7: 591-600
- Madrid M, Soto T, Franco A, Paredes V, Vicente J, et al. 2004. A cooperative role for Atf1 and Pap1 in the detoxification of the oxidative stress induced by glucose deprivation in *Schizosaccharomyces pombe*. *J Biol Chem* 279: 41594-602
- Manning AM, Davis RJ. 2003. Targeting JNK for therapeutic benefit: from junk to gold? *Nat Rev Drug Discov* 2: 554-65

- Mittal V. 2004. Improving the efficiency of RNA interference in mammals. *Nat Rev Genet* 5: 355-65
- Mol JN, van der Krol AR, van Tunen AJ, van Blokland R, de Lange P, Stuitje AR. 1990. Regulation of plant gene expression by antisense RNA. *FEBS Lett* 268: 427-30
- Murray CJ, Lopez AD. 1997. Global mortality, disability, and the contribution of risk factors: Global Burden of Disease Study. *Lancet* 349: 1436-42
- Myers JW, Jones JT, Meyer T, Ferrell JE, Jr. 2003. Recombinant Dicer efficiently converts large dsRNAs into siRNAs suitable for gene silencing. *Nat Biotechnol* 21: 324-8
- Nishio H, Matsui K, Tsuji H, Tamura A, Suzuki K. 2001. Immunohistochemical study of the phosphorylated and activated form of c-Jun NH2-terminal kinase in human aorta. *Histochem J* 33: 167-71
- Nohturfft A, Yabe D, Goldstein JL, Brown MS, Espenshade PJ. 2000. Regulated step in cholesterol feedback localized to budding of SCAP from ER membranes. *Cell* 102: 315-23
- O'Rourke SM, Herskowitz I, O'Shea EK. 2002. Yeast go the whole HOG for the hyperosmotic response. *Trends Genet* 18: 405-12
- Olkkonen VM, Levine TP. 2004. Oxysterol binding proteins: in more than one place at one time? *Biochem Cell Biol* 82: 87-98
- Olofsson SO, Boren J. 2005. Apolipoprotein B: a clinically important apolipoprotein which assembles atherogenic lipoproteins and promotes the development of atherosclerosis. *J Intern Med* 258: 395-410
- Parker JS, Roe SM, Barford D. 2005. Structural insights into mRNA recognition from a PIWI domain-siRNA guide complex. *Nature* 434: 663-6
- Peet DJ, Turley SD, Ma W, Janowski BA, Lobaccaro JM, et al. 1998. Cholesterol and bile acid metabolism are impaired in mice lacking the nuclear oxysterol receptor LXR alpha. *Cell* 93: 693-704
- Pelkmans L, Fava E, Grabner H, Hannus M, Habermann B, et al. 2005. Genome-wide analysis of human kinases in clathrin- and caveolae/raft-mediated endocytosis. *Nature* 436: 78-86
- Pelleymounter MA, Cullen MJ, Baker MB, Hecht R, Winters D, et al. 1995. Effects of the obese gene product on body weight regulation in ob/ob mice. *Science* 269: 540-3
- Peng J, Gygi SP. 2001. Proteomics: the move to mixtures. *J Mass Spectrom* 36: 1083-91
- Persengiev SP, Zhu X, Green MR. 2004. Nonspecific, concentration-dependent stimulation and repression of mammalian gene expression by small interfering RNAs (siRNAs). *Rna* 10: 12-8
- Porter JA, Young KE, Beachy PA. 1996. Cholesterol modification of hedgehog signaling proteins in animal development. *Science* 274: 255-9
- Putcha GV, Le S, Frank S, Besirli CG, Clark K, et al. 2003. JNK-mediated BIM phosphorylation potentiates BAX-dependent apoptosis. *Neuron* 38: 899-914
- Rawson RB. 2003. The SREBP pathway--insights from Insigs and insects. *Nat Rev Mol Cell Biol* 4: 631-40

- Rawson RB, Zelenski NG, Nijhawan D, Ye J, Sakai J, et al. 1997. Complementation cloning of S2P, a gene encoding a putative metalloprotease required for intramembrane cleavage of SREBPs. *Mol Cell* 1: 47-57
- Reaven GM. 1988. Banting lecture 1988. Role of insulin resistance in human disease. *Diabetes* 37: 1595-607
- Repa JJ, Berge KE, Pomajzl C, Richardson JA, Hobbs H, Mangelsdorf DJ. 2002. Regulation of ATP-binding cassette sterol transporters ABCG5 and ABCG8 by the liver X receptors alpha and beta. *J Biol Chem* 277: 18793-800
- Repa JJ, Liang G, Ou J, Bashmakov Y, Lobaccaro JM, et al. 2000a. Regulation of mouse sterol regulatory element-binding protein-1c gene (SREBP-1c) by oxysterol receptors, LXRalpha and LXRbeta. *Genes Dev* 14: 2819-30
- Repa JJ, Mangelsdorf DJ. 2000. The role of orphan nuclear receptors in the regulation of cholesterol homeostasis. *Annu Rev Cell Dev Biol* 16: 459-81
- Repa JJ, Turley SD, Lobaccaro JA, Medina J, Li L, et al. 2000b. Regulation of absorption and ABC1-mediated efflux of cholesterol by RXR heterodimers. *Science* 289: 1524-9
- Reynolds A, Leake D, Boese Q, Scaringe S, Marshall WS, Khvorova A. 2004. Rational siRNA design for RNA interference. *Nat Biotechnol* 22: 326-30
- Ricci R, Sumara G, Sumara I, Rozenberg I, Kurrer M, et al. 2004. Requirement of JNK2 for scavenger receptor A-mediated foam cell formation in atherogenesis. *Science* 306: 1558-61
- Robinson NC. 1993. Functional binding of cardiolipin to cytochrome c oxidase. *J Bioenerg Biomembr* 25: 153-63
- Romano N, Macino G. 1992. Quelling: transient inactivation of gene expression in *Neurospora crassa* by transformation with homologous sequences. *Mol Microbiol* 6: 3343-53
- Ryden M, Arvidsson E, Blomqvist L, Perbeck L, Dicker A, Arner P. 2004. Targets for TNF-alpha-induced lipolysis in human adipocytes. *Biochem Biophys Res Commun* 318: 168-75
- Sabapathy K, Jochum W, Hochedlinger K, Chang L, Karin M, Wagner EF. 1999. Defective neural tube morphogenesis and altered apoptosis in the absence of both JNK1 and JNK2. *Mech Dev* 89: 115-24
- Saxena S, Jonsson ZO, Dutta A. 2003. Small RNAs with imperfect match to endogenous mRNA repress translation. Implications for off-target activity of small inhibitory RNA in mammalian cells. *J Biol Chem* 278: 44312-9
- Scacheri PC, Rozenblatt-Rosen O, Caplen NJ, Wolfsberg TG, Umayam L, et al. 2004. Short interfering RNAs can induce unexpected and divergent changes in the levels of untargeted proteins in mammalian cells. *Proc Natl Acad Sci U S A* 101: 1892-7
- Schlegel RA, Callahan M, Krahling S, Pradhan D, Williamson P. 1996. Mechanisms for recognition and phagocytosis of apoptotic lymphocytes by macrophages. *Adv Exp Med Biol* 406: 21-8
- Schneiter R, Brugger B, Sandhoff R, Zellnig G, Leber A, et al. 1999. Electrospray ionization tandem mass spectrometry (ESI-MS/MS) analysis of the lipid molecular species composition of yeast subcellular membranes reveals acyl

- chain-based sorting/remodeling of distinct molecular species en route to the plasma membrane. *J Cell Biol* 146: 741-54
- Schultz GA, Corso TN, Prosser SJ, Zhang S. 2000. A fully integrated monolithic microchip electrospray device for mass spectrometry. *Anal Chem* 72: 4058-63
- Schwudke D, Hannich JT, Surendranath V, Grimard V, Moehring T, et al. 2007. Top-down lipidomic screens by multivariate analysis of high-resolution survey mass spectra. *Anal Chem* 79: 4083-93
- Sever N, Yang T, Brown MS, Goldstein JL, DeBose-Boyd RA. 2003. Accelerated degradation of HMG CoA reductase mediated by binding of insig-1 to its sterol-sensing domain. *Mol Cell* 11: 25-33
- Simons K, Ikonen E. 1997. Functional rafts in cell membranes. *Nature* 387: 569-72
- Song BL, Javitt NB, DeBose-Boyd RA. 2005a. Insig-mediated degradation of HMG CoA reductase stimulated by lanosterol, an intermediate in the synthesis of cholesterol. *Cell Metab* 1: 179-89
- Song BL, Sever N, DeBose-Boyd RA. 2005b. Gp78, a membrane-anchored ubiquitin ligase, associates with Insig-1 and couples sterol-regulated ubiquitination to degradation of HMG CoA reductase. *Mol Cell* 19: 829-40
- Souza SC, de Vargas LM, Yamamoto MT, Lien P, Franciosa MD, et al. 1998. Overexpression of perilipin A and B blocks the ability of tumor necrosis factor alpha to increase lipolysis in 3T3-L1 adipocytes. *J Biol Chem* 273: 24665-9
- Stark A, Brennecke J, Bushati N, Russell RB, Cohen SM. 2005. Animal MicroRNAs confer robustness to gene expression and have a significant impact on 3'UTR evolution. *Cell* 123: 1133-46
- Stein CJ, Colditz GA. 2004. The epidemic of obesity. *J Clin Endocrinol Metab* 89: 2522-5
- Stettler S, Warbrick E, Prochnik S, Mackie S, Fantes P. 1996. The wis1 signal transduction pathway is required for expression of cAMP-repressed genes in fission yeast. *J Cell Sci* 109 (Pt 7): 1927-35
- Sumara G, Belwal M, Ricci R. 2005. "Jnking" atherosclerosis. *Cell Mol Life Sci* 62: 2487-94
- Tartaglia LA, Dembski M, Weng X, Deng N, Culpepper J, et al. 1995. Identification and expression cloning of a leptin receptor, OB-R. *Cell* 83: 1263-71
- Tauchi-Sato K, Ozeki S, Houjou T, Taguchi R, Fujimoto T. 2002. The surface of lipid droplets is a phospholipid monolayer with a unique Fatty Acid composition. *J Biol Chem* 277: 44507-12
- Teleman AA, Maitra S, Cohen SM. 2006. Drosophila lacking microRNA miR-278 are defective in energy homeostasis. *Genes Dev* 20: 417-22
- Thiele C, Hannah MJ, Fahrenholz F, Huttner WB. 2000. Cholesterol binds to synaptophysin and is required for biogenesis of synaptic vesicles. *Nat Cell Biol* 2: 42-9
- Tibbles LA, Woodgett JR. 1999. The stress-activated protein kinase pathways. *Cell Mol Life Sci* 55: 1230-54
- Tong F, Black PN, Bivins L, Quackenbush S, Ctrnacta V, DiRusso CC. 2006. Direct interaction of *Saccharomyces cerevisiae* Faa1p with the Omi/HtrA protease

- orthologue Ynm3p alters lipid homeostasis. *Mol Genet Genomics* 275: 330-43
- Toone WM, Jones N. 1998. Stress-activated signalling pathways in yeast. *Genes Cells* 3: 485-98
- Topper JN, Gimbrone MA, Jr. 1999. Blood flow and vascular gene expression: fluid shear stress as a modulator of endothelial phenotype. *Mol Med Today* 5: 40-6
- Unger RH. 2003. The physiology of cellular liporegulation. *Annu Rev Physiol* 65: 333-47
- Unger RH, Orci L. 2002. Lipoapoptosis: its mechanism and its diseases. *Biochim Biophys Acta* 1585: 202-12
- Venkateswaran A, Repa JJ, Lobaccaro JM, Bronson A, Mangelsdorf DJ, Edwards PA. 2000. Human white/murine ABC8 mRNA levels are highly induced in lipid-loaded macrophages. A transcriptional role for specific oxysterols. *J Biol Chem* 275: 14700-7
- Verges B. 2005. New insight into the pathophysiology of lipid abnormalities in type 2 diabetes. *Diabetes Metab* 31: 429-39
- Wang N, Lan D, Chen W, Matsuura F, Tall AR. 2004. ATP-binding cassette transporters G1 and G4 mediate cellular cholesterol efflux to high-density lipoproteins. *Proc Natl Acad Sci U S A* 101: 9774-9
- Wang X, Briggs MR, Hua X, Yokoyama C, Goldstein JL, Brown MS. 1993. Nuclear protein that binds sterol regulatory element of low density lipoprotein receptor promoter. II. Purification and characterization. *J Biol Chem* 268: 14497-504
- Wang YX, Lee CH, Tjep S, Yu RT, Ham J, et al. 2003. Peroxisome-proliferator-activated receptor delta activates fat metabolism to prevent obesity. *Cell* 113: 159-70
- Wassenegger M, Heimes S, Riedel L, Sanger HL. 1994. RNA-directed de novo methylation of genomic sequences in plants. *Cell* 76: 567-76
- Waterman MR, Lepesheva GI. 2005. Sterol 14 alpha-demethylase, an abundant and essential mixed-function oxidase. *Biochem Biophys Res Commun* 338: 418-22
- Weil D, Garcon L, Harper M, Dumenil D, Dautry F, Kress M. 2002. Targeting the kinesin Eg5 to monitor siRNA transfection in mammalian cells. *Biotechniques* 33: 1244-8
- Werner-Washburne M, Braun E, Johnston GC, Singer RA. 1993. Stationary phase in the yeast *Saccharomyces cerevisiae*. *Microbiol Rev* 57: 383-401
- Whitfield GK, Jurutka PW, Haussler CA, Haussler MR. 1999. Steroid hormone receptors: evolution, ligands, and molecular basis of biologic function. *J Cell Biochem Suppl* 32-33: 110-22
- Wu Z, Xie Y, Morrison RF, Bucher NL, Farmer SR. 1998. PPARgamma induces the insulin-dependent glucose transporter GLUT4 in the absence of C/EBPalpha during the conversion of 3T3 fibroblasts into adipocytes. *J Clin Invest* 101: 22-32

- Xu F, Rychnovsky SD, Belani JD, Hobbs HH, Cohen JC, Rawson RB. 2005. Dual roles for cholesterol in mammalian cells. *Proc Natl Acad Sci U S A* 102: 14551-6
- Xu P, Vernooy SY, Guo M, Hay BA. 2003. The *Drosophila* microRNA Mir-14 suppresses cell death and is required for normal fat metabolism. *Curr Biol* 13: 790-5
- Yang D, Buchholz F, Huang Z, Goga A, Chen CY, et al. 2002a. Short RNA duplexes produced by hydrolysis with *Escherichia coli* RNase III mediate effective RNA interference in mammalian cells. *Proc Natl Acad Sci U S A* 99: 9942-7
- Yang T, Espenshade PJ, Wright ME, Yabe D, Gong Y, et al. 2002b. Crucial step in cholesterol homeostasis: sterols promote binding of SCAP to INSIG-1, a membrane protein that facilitates retention of SREBPs in ER. *Cell* 110: 489-500
- Yu C, Minemoto Y, Zhang J, Liu J, Tang F, et al. 2004. JNK suppresses apoptosis via phosphorylation of the proapoptotic Bcl-2 family protein BAD. *Mol Cell* 13: 329-40
- Yu L, Hammer RE, Li-Hawkins J, Von Bergmann K, Lutjohann D, et al. 2002. Disruption of *Abcg5* and *Abcg8* in mice reveals their crucial role in biliary cholesterol secretion. *Proc Natl Acad Sci U S A* 99: 16237-42
- Zelcer N, Tontonoz P. 2006. Liver X receptors as integrators of metabolic and inflammatory signaling. *J Clin Invest* 116: 607-14
- Zeng Y, Yi R, Cullen BR. 2003. MicroRNAs and small interfering RNAs can inhibit mRNA expression by similar mechanisms. *Proc Natl Acad Sci U S A* 100: 9779-84
- Zhang Y, Proenca R, Maffei M, Barone M, Leopold L, Friedman JM. 1994. Positional cloning of the mouse obese gene and its human homologue. *Nature* 372: 425-32
- Zimmermann R, Strauss JG, Haemmerle G, Schoiswohl G, Birner-Gruenberger R, et al. 2004. Fat mobilization in adipose tissue is promoted by adipose triglyceride lipase. *Science* 306: 1383-6

Thank You so much!

So many people to thanks...

First of all, I would like to thank all the people that have been directly and indirectly implicated in this work:

- Christoph Thiele, my supervisor, for this project, for all his great technical advices that made some experiments possible and for his comprehension.*
- All the past and present members of the Fatlab for the great atmosphere in which I have spent these last four years, and in particular to Monika Suchanek and Julia Massier for their guidance, their help and the so many long discussions, and Christine Mössinger for her thorough reading of this manuscript. I also would like to thank Doris Richter for her magnificent help and her permanent smile that makes everyday life in the lab so much nicer.*
- Ralf Kittler and Anne Heninger for providing esiRNAs or for helping producing esiRNAs, as well as for their knowledge in the field.*
- Eugenio Fava and the members of the TDS for their help in setting up and performing the kinase screen.*
- Yannis Kalaidzidis for providing me with computer tools to analyze my data.*
- Christer Ejising and in particular Dominik Schwudke for the mass spectrometry analysis.*
- Isabel Raabe and Iva Tolic for providing yeast strains and for their help in discovering this new model organism.*
- Dr. Millar for providing the Sty1 deletion strain.*
- Charles Ferguson for the EM pictures that unfortunately didn't make their way to this manuscript.*
- Frank Buchholz, Denis Corbeil and Petra Schwille, as members of my IAC committee, for their interesting advices and Gerhard Rödel for accepting at the last minute to officially supervise this thesis.*

And to all the other people that help me at one point or another during this work and that I can not mention because of the lack of space.

But of course, I would like to thank all my friends and family, here and abroad, that made these four years in Dresden a pleasure. For all the fun I had with them, the support they gave me, the friendship we share...

I herewith declare that I have produced this paper without the prohibited assistance of third parties and without making use of aids other than those specified; notions taken over directly or indirectly from other sources have been identified as such. This paper has not previously been presented in identical or similar form to any other German or foreign examination board.

The thesis work was conducted from 01.09.2003 to 15.06.2007 under the supervision of Dr. Christoph Thiele at the Max Planck Institute of Molecular Cell Biology and Genetics in Dresden.

I declare that I have not undertaken any previous unsuccessful doctorate proceedings.

I declare that I recognize the doctorate regulations of the Faculty of Sciences of the Dresden University of Technology.

Vinciane Grimard